CHEMICAL REVIEWS

REVIEW

pubs.acs.org/CR

Genetically Encodable Fluorescent Biosensors for Tracking Signaling Dynamics in Living Cells

Robert H. Newman,[†] Matthew D. Fosbrink,[†] and Jin Zhang[†,‡,*]

[†]Department of Pharmacology and Molecular Sciences

[‡]Solomon H. Snyder Department of Neuroscience, Johns Hopkins University School of Medicine, Baltimore, Maryland 21205, United States

CONTENTS

1. INTRODUCTION

Fluorescence has long been recognized as a powerful tool for probing biological structure and function. Nearly sixty-five years ago, Coons and colleagues introduced the first fluorescent-antibody techniques as a means of detecting pneumococcal antigens in mouse tissue.[1] In the years that followed, studies have been conducted in hundreds of cellular contexts using immunofluorescence and related techniques such as fluorescence in situ hybridization.[2] Together, these studies have provided cell biologists with a unique glimpse into the molecular organization of cells and tissues. However, because such approaches typically require fixation prior to detection, they provide only a snapshot of the highly dynamic cellular processes that govern cell physiology at the molecular level. To add a crucial temporal component to the study of cell biology, researchers have developed a diverse set of genetically encodable biosensors designed to probe dynamic cellular events in living cells with high spatial and temporal resolution. These sensors, which generally involve the incorporation of a fluorescent tag into a protein or a selected protein domain, have enabled researchers to track various components of intracellular signaling networks in real time within the native cellular environment. In this review, we will first explore the molecular basis of several genetically targetable fluorescent tags amenable to live cell imaging. We will then turn our attention to the development and use of fluorescent biosensors for studying dynamic signaling processes in living cells.

2. GENETICALLY TARGETABLE FLUORESCENT TAGS

A revolution in the field of live cell imaging occurred following the development of genetically encodable fluorescent tags to specifically label a protein-of-interest within the cellular milieu. Together, these labeling methods have allowed researchers to develop fluorescent biosensors that are able to track cellular proteins and other signaling molecules within their endogenous environment, providing unprecedented insights into the dynamic regulation of signaling networks in living cells. This "enlightenment" in the field of cell biology was sparked by the discovery, and subsequent cloning, of the green fluorescent protein (GFP) from the jellyfish *Aequorea victoria* (reviewed in

Received: January 4, 2010
Published: April 01, 2011

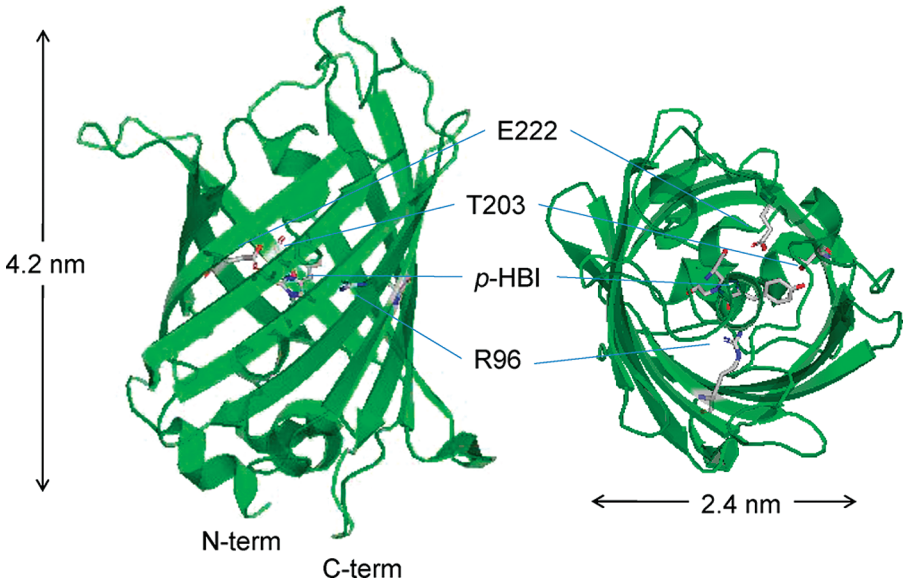

Figure 1. Structure of *A. victoria* GFP. *A. victoria* GFP showing the dimensions of the protein, the intrinsically derived *p*-HBI chromophore and several key residues surrounding the chromophore (image generated using PyMOL open access and PDB ID 1w7s).

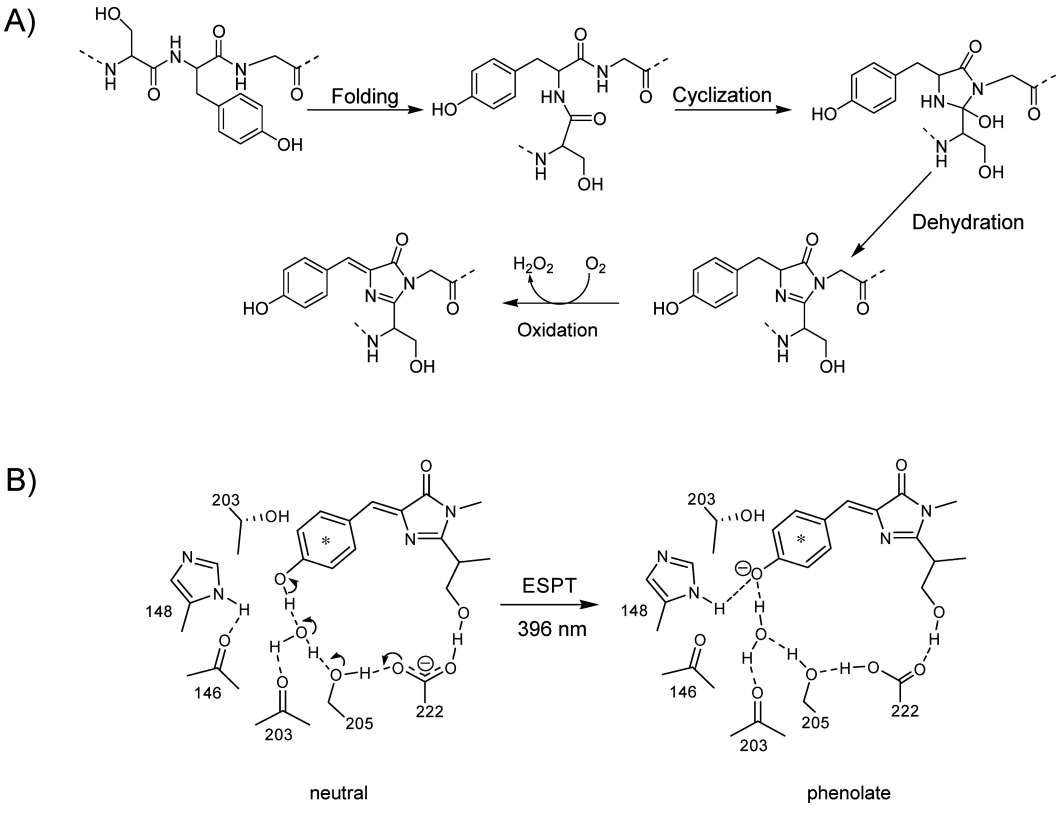

Figure 2. Chromophore formation and excited state proton transfer (ESPT). (A) The most widely accepted mechanism of *A. victoria* GFP chromophore formation. (B) Proposed mechanism of ESPT for *A. victoria* GFP (based on ref 25). Both the weakly fluorescent neutral species and the highly fluorescent phenolate anion are shown.

refs 3 and 4). As will be discussed in detail below, GFP and its relatives generate their chromophores autocatalytically by post-translational modification of their primary amino acid sequence.[3,5,6] This property, coupled with several desirable biophysical characteristics,[4] has made fluorescent proteins (FPs) a popular fusion tag for live cell imaging applications. In addition, several other protein labeling techniques have recently been developed to complement or extend the scope of FP-based methods. However, unlike the intrinsically derived fluorophores utilized by FPs, each of these systems relies upon the binding of exogenous small-molecule fluorescent dyes to engineered proteins or short polypeptide sequences, which, like FPs, can be

dx.doi.org/10.1021/cr100002u |*Chem. Rev.* 2011, 111, 3614–3666

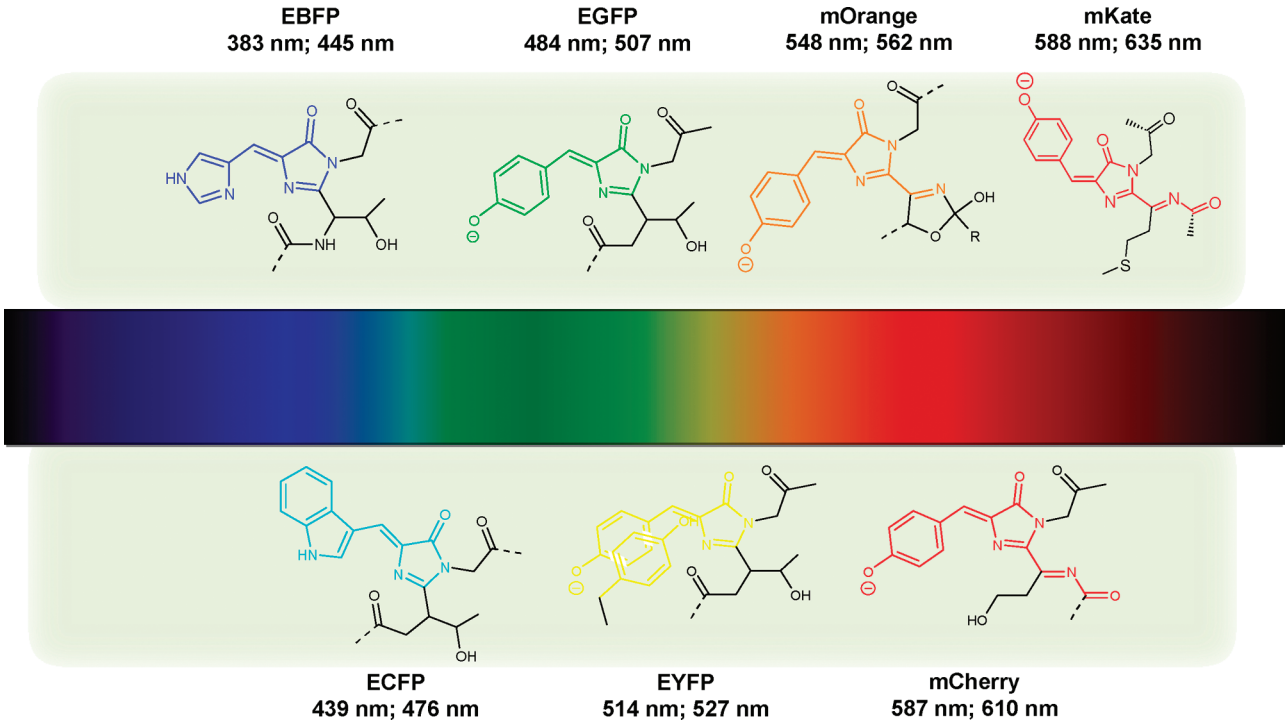

Figure 3. Chromophore structures of representative FP color variants within each spectral class. The conjugated ring structure of each chromophore is colored according to its emission profile. Excitation and emission maxima are indicated as in Figure 2b.

specifically targeted to a protein-of-interest located in various subcellular locations. Below we summarize FPs and several other genetically targetable fluorescent tags, focusing on both their benefits and limitations for tracking signaling dynamics in living cells.

2.1. Fusion to Fluorescent Proteins

By far, the most popular means of adding a fluorescent tag to a protein-of-interest is to express the target protein as a chimera with *A. victoria* GFP or one of its relatives. The power of this approach derives from its versatility and the relative ease with which it can be employed. This is because, under aerobic conditions, the FP fusion tag undergoes autocatalytic conversion to a highly fluorescent species, providing an easily detectible means of tracking tagged molecules in real-time with no further manipulation of the system.

Despite the manifold benefits of GFP-like proteins, several factors may influence their utility under cellular conditions. Therefore, to achieve success during a given imaging experiment involving FP-based biosensors, it is important to understand the molecular factors governing FP fluorescence. Since the fluorescent properties of GFP family members are highly dependent upon the protein microenvironment surrounding their intrinsically derived chromophore, we will begin by highlighting some of the structural characteristics that govern the spectral properties of FPs and their chromophores.

2.1.1. Fluorescent Protein Basics. *A. victoria* GFP is the founding member of a family of fluorescent (and nonfluorescent) proteins derived from several bioluminescent marine organisms including hydrozoa and reef-building corals of the class Anthozoa (Table 1).[7] Members of this family are characterized by a highly stable 11-stranded β-barrel structure[8,9] whose unique architecture aids in both the formation[10−12] and stabilization[4] of the conjugated ring systems that are responsible for their spectral properties (Figure 1). Although the extent of π-orbital conjugation and the specific microenvironment surrounding the chromophore differs among FP color variants, in each case chromophore maturation proceeds in a manner similar to that first described for *A. victoria* GFP.[6,10] Therefore, it is instructive to examine the formation of the fluorescent moiety of GFP to illustrate some of the general principles associated with FP chromophore maturation.

It has long been known that wild-type *A. victoria* GFP generates a highly fluorescent *p*-hydroxybenzylidene-5-imidizolinone (*p*-HBI) species from the tripeptide, Ser65-Tyr66-Gly67.[13] The most widely accepted mechanism of chromophore formation was proposed almost fifteen years ago based upon several experimental observations (reviewed in[3,6]). According to this theory, once the polypeptide chain has folded into a near-native conformation, it undergoes a series of autocatalytic post-translational modifications to generate the mature chromophore (Figure 2a). This process is generally described by a three step mechanism consisting of (1) internal cyclization of Ser65 and Gly67, (2) dehydration to form an imidizolin-5-one intermediate, and (3) dehydrogenation along the Cα-Cβ bond of Tyr66 to conjugate the ring systems.[14] Dehydrogenation is mediated by molecular oxygen and constitutes the rate limiting step during chromophore formation. Interestingly, the Wachter group recently proposed an alternative mechanism of chromophore formation based upon kinetic isotope effects at the Cβ position of several GFP variants. According to their model, oxidation of the condensed α-enolate heterocycle leads to the formation of a hydroxylated cyclic imine that is then converted to the mature chromophore by C−H bond scission at the benzylic carbon via general base catalysis.[15,16]

In addition to the above post-translational modifications, orange- and red-emitting FPs undergo a second oxidation step along the Cα-N bond of residue 65 (according to the GFP

dx.doi.org/10.1021/cr100002u |*Chem. Rev.* 2011, 111, 3614–3666

Table 1. Select Fluorescent Proteins Useful for Live Cell Imaging and Biosensor Development

Protein	Source	Ex (nm)	Em (nm)	ε ($M^{-1}cm^{-1}$)	QY	ε x QY	Quaternary structure	Ref.
Sirius	*A. victoria*	355	424	15,000	0.24	3,600	monomer	472
EBFP	*A. victoria*	383	445	29,900	0.31	9,269	monomer	473
SBFP2	*A. victoria*	380	446	34,000	0.47	15,980	monomer	38
EBFP2	*A. victoria*	383	448	32,000	0.56	17,920	monomer	49
Azurite	*A. victoria*	384	450	26,200	0.55	14,410	monomer	48
mKalama1	*A. victoria*	385	456	36,000	0.45	16,200	monomer	49
TagBFP	*E. quadricolor*	399	456	52,000	0.63	32,760	monomer	50
mBlueberry2	*D. striata*	402	467	51,000	0.48	24,480	monomer	49
SCFP3A	*A. victoria*	433	474	30,000	0.56	16,800	monomer	474
mTurquoise	*A. victoria*	434	474	30,000	0.84	25,200	monomer	**475**
mseCFP	*A. victoria*	434	474	30,000	0.4	12,000	monomer	476
Cerulean	*A. victoria*	433	475	43,000	0.62	26,660	monomer	41
ECFP	*A. victoria*	439	476	32,500	0.4	13,000	monomer	6
CyPet	*A. victoria*	435	477	35,000	0.51	17,850	monomer	477
TagCFP	*E. quadricolor*	458	480	37,000	0.57	21,090	monomer	478
mTFP1	*Clavularia* coral	462	492	64,000	0.85	54,400	monomer	43
Midori-ishi Cyan	*Acropara* sp	472	495	27,300	0.9	24,570	dimer	479
mUKG	*Sarcophyton* sp	483	499	66,000	0.73	48,180	monomer	276
TurboGFP	*Copepoda* sp	482	502	70,000	0.53	37,100	monomer	480
AceGFP	*A. coerulescens*	480	505	50,000	0.55	27,500	monomer	481
Azami Green	*Galaxeidae*	492	505	55,000	0.74	40,700	monomer	482
ZsGreen	*Zoanthus* sp	493	505	43,000	0.91	39,130	tetramer	44
TagGFP2	*E. quadricolor*	483	506	56,500	0.6	33,900	monomer	50
EGFP	*A. victoria*	484	507	56,000	0.6	33,600	monomer	34;36
mWasabi	*Clavularia* coral	493	509	70,000	0.8	56,000	monomer	483
Emerald	*A. victoria*	487	509	57,500	0.68	39,100	monomer	484
Superfolder GFP	*A. victoria*	488	510	83,300	0.65	54,145	monomer	37
Sapphire	*A. victoria*	399	511	29,000	0.64	18,560	monomer	3;105
T-Sapphire	*A. victoria*	399	511	44,000	0.6	26,400	monomer	485
SGFP2	*A. victoria*	495	512	46,000	0.7	32,200	monomer	38
TagYFP	*E. quadricolor*	508	524	64,000	0.6	38,400	monomer	478
mAmetrine	*A. victoria*	406	526	45,000	0.58	26,100	monomer	95
EYFP	*A. victoria*	514	527	83,400	0.61	50,874	monomer	57
Topaz	*A. victoria*	514	527	94,500	0.6	56,700	monomer	484
SYFP2	*A. victoria*	515	527	101,000	0.68	68,680	monomer	474
Venus	*A. victoria*	515	528	92,200	0.57	52,554	monomer	59
mCitrine	*A. victoria*	516	529	77,000	0.76	58,520	monomer	58
Ypet	*A. victoria*	517	530	104,000	0.77	80,080	monomer	477
PhiYFP	*Hydrozoa* sp	525	537	124,000	0.39	48,360	monomer	480
ZsYellow1	*Zoanthus* sp	529	539	20,200	0.42	8,484	tetramer	44
mBanana	*D. striata*	540	553	6,000	0.7	4,200	monomer	96
mOrange	*D. striata*	548	562	71,000	0.69	48,990	monomer	96
mKOκ	*Cerianthus* sp	551	563	105,000	0.61	64,050	monomer	276
Kusabira Orange2	*Cerianthus* sp	551	565	63,800	0.62	39,556	monomer	393
mOrange2	*D. striata*	549	565	58,000	0.6	34,800	monomer	54
OFP	*Cerianthus* sp	548	573	60,000	0.64	38,400	tetramer	486
TurboRFP	*E. quadricolor*	553	574	92,000	0.67	61,640	dimer	22
tdTomato	*D. striata*	554	581	138,000	0.69	95,220	tandem dimer	96
DsRed2	*D. striata*	563	582	43,800	0.55	24,090	tetramer	487
DsRed	*D. striata*	558	583	75,000	0.79	59,250	tetramer	44
DsRed-Express	*D. striata*	555	584	38,000	0.51	19,380	tetramer	487
TagRFP	*E. quadricolor*	555	584	100,000	0.48	48,000	monomer	22
TagRFP-T	*E. quadricolor*	555	584	81,000	0.41	33,210	monomer	54
mTangerine	*D. striata*	568	585	38,000	0.3	11,400	monomer	96
DsRed-Express2	*D. striata*	554	586	35,600	0.42	14,950	tetramer	165
DsRed-Max	*D. striata*	560	589	48,000	0.41	19,680	tetramer	165
AsRed2	*A. sulcata*	576	592	56,200	0.05	2,810	tetramer	44

dx.doi.org/10.1021/cr100002u |*Chem. Rev.* 2011, 111, 3614–3666

Table 1. Continued

Protein	Source	Ex (nm)	Em (nm)	ε ($M^{-1}cm^{-1}$)	QY	ε x QY	Quaternary structure	Ref.
mApple	*D. striata*	568	592	75,000	0.49	36,750	monomer	54
mStrawberry	*D. striata*	574	596	90,000	0.29	26,100	monomer	96
mRuby	*E. quadricolor*	558	605	112,000	0.35	39,200	monomer	488
mRFP1	*D. striata*	584	607	50,000	0.25	12,500	monomer	76
tdRFP611	*E. quadricolor*	558	609	70,000	0.47	32,900	tandem dimer	489
mCherry	*D. striata*	587	610	72,000	0.22	15,840	monomer	96
eqFP611	*E. quadricolor*	559	611	78,000	0.45	35,100	tetramer	489
tdKeima	*Montipora*	440	620	n.d.	n.d.	20,590	tandem dimer	490
mKeima	*Montipora*	440	620	14,400	0.24	3,456	monomer	490
mRaspberry	*D. striata*	598	625	86,000	0.15	12,900	monomer	491
tdRFP639	*E. quadricolor*	589	631	90,400	0.16	14,464	tandem dimer	489
tdKatushka2	*E. quadricolor*	588	633	132,500	0.37	49,025	tandem dimer	66
mKate	*E. quadricolor*	588	635	45,000	0.33	14,850	monomer	23
mKate2	*E. quadricolor*	588	635	62,500	0.4	25,000	monomer	66
mPlum	*D. striata*	590	649	41,000	0.1	4,100	monomer	491;492
eqFP650	*E. quadricolor*	592	650	65,000	0.24	15,600	dimer	515
mNeptune	*E. quadricolor*	600	650	67,000	0.2	13,400	monomer	67
AQ143	*A. equina*	595	655	90,000	0.04	3,600	tetramer	493
eqFP670	*E. quadricolor*	605	670	70,000	0.06	4,200	dimer	515

numbering system) to form an acylimine linkage with the polypeptide backbone (Figure 3).[17,18] Importantly, acylimine formation extends the conjugated π-system over a greater distance.[8] This serves to lower the energy barrier separating the ground (S_0) and excited states (S_1) of the fluorophore leading to red-shifted excitation and emission spectra.

Once formed, the mature chromophore lies along a highly distorted (~80°) α-helical segment nestled deep within the core of the protein[19] where it is likely shielded from attack by oxygen[20] or hydronium ions (Figure 1).[21] With a few notable exceptions related to eqFP611 from *Entacmaea quadricolor*,[17,22,23] all known fluorogenic GFP-like chromophores adopt a cis [Z−] configuration.[8,9] An extensive hydrogen bonding network within the central cavity helps maintain the coplanarity of the conjugated 5- and 6-membered ring systems. Structural analysis of the FPs and related nonfluorescent chromoproteins from Anthozoa suggests that the planarity of the chromophore is essential to the fluorescent properties of GFP family members.[17] Indeed, examination of numerous 4-hydroxybenzylidene-2,3-dimethyl-imidazolidinone derivatives revealed that an "avoided crossing" occurs between the S_1 and S_0 states when the rings were twisted, resulting in nonradiative decay back to S_0.[24] Such deviations from planarity can have a dramatic impact on the brightness of the FPs because of a reduction in the quantum yield (ϕ) of their fluorophore.[18,24]

In addition to helping hold the chromophore in the proper orientation, the protein microenvironment also impacts the spectral properties of the chromophore in other ways. For instance, in wild-type *A. victoria* GFP, the *p*-HBI chromophore alternates between two ionization states, a weakly fluorescent, neutral form dubbed the A state (ex = 396 nm, em = 508 nm) and a highly fluorescent phenolate species termed the B state (ex = 475 nm, em = 503 nm). Under physiological conditions, A predominates over B, exhibiting a magnitude ratio of nearly six to one. Structural analysis suggests that this distribution is maintained by an extensive hydrogen bonding network, consisting of E222, S205, and an immobilized water molecule, which preferentially stabilizes the A state (Figure 2b).[25] Interestingly, following excitation, A is converted to the phenolate anion, causing the fluorophore to emit light at a much longer wavelength (508 nm) than would be expected otherwise. This curious behavior is the result of a phenomenon known as excited state proton transfer (ESPT).[26] During ESPT, E222 abstracts a high-energy proton from the phenol moiety of Tyr66.[25] Not only does E222 serve as a general base during this reaction, but its conversion to a neutral acid also relieves the electrostatic repulsion that destabilizes the phenolate of B prior to excitation.[25] Importantly, this conversion is also accompanied by structural rearrangements in the protein core that further stabilize the B state via an extensive hydrogen-bonding network.

Though the photoisomerization of the GFP chromophore is intriguing from both a biological and a photochemical perspective, this behavior is not ideal for many live cell imaging applications. For instance, the existence of two isomerization states with distinct excitation/emission profiles can complicate the interpretation of experimental data. Moreover, as will be discussed in section 2.1.2.5, the ultraviolet (UV) light required to excite the predominant A state not only induces cellular autofluorescence, but it could also adversely affect the cellular environment under study. Therefore, to simplify the emission spectra and to improve the spectral properties of *A. victoria* GFP for live cell imaging applications, the wild-type protein has been mutated in several important ways. One of the most pronounced changes in the photophysical characteristics of GFP is caused by the substitution of a Thr residue for Ser at position 65 (S65T).[9,27] This mutation, which introduces a single methyl group into the chromophore structure, induces local conformational changes in the protein core that disrupt the ground state hydrogen bonding network.[25] As a result, the chromophore of the resultant variant, termed GFP(S65T), is converted almost exclusively to the phenolate species, simplifying its excitation/emission spectra and making it more well-suited for live cell imaging.

In addition, subtle alterations to the protein microenvironment surrounding the chromophore can also induce red- and blue-shifted spectra in GFP-like proteins. In fact, the excitation

and emission maxima of FP fluorophores can be shifted by nearly 20 nm due to local environmental effects such as $\pi-\pi$ stacking[9] or the position of charged groups within the protein core.[18,28,29] These effects, coupled with direct chemical modifications to the chromophore discussed above, have resulted in the development of FP color variants that span the rainbow (Figure 3). GFP-family members are generally divided into seven spectral classes based upon their emission maxima. These include GFP-like proteins emitting in the blue (BFPs; 440−470 nm), cyan (CFPs; 471−500 nm), green (GFPs; 501−520 nm), yellow (YFPs; 521−550 nm), orange (OFPs; 551−575 nm), red (RFPs: 576−610 nm), and far-red (FRFPs; 611−660 nm) (Table 1, reviewed in refs 30−32). Importantly, by facilitating multicolor imaging experiments and resonance energy transfer (RET)-based studies, the development of spectrally distinct FP derivatives has expanded the range of intracellular activities that can be monitored using genetically encodable FP tags.

2.1.2. Considerations When Utilizing Fluorescent Proteins to Build Biosensors. There are several important factors that must be considered when employing GFP family members as genetically encodable fluorescent tags. These include both physical and biological parameters, each of which can profoundly impact the success of a given experiment. Below, we discuss those properties that are most important when designing fluorescent biosensors for live cell imaging. Although all GFP-like proteins can be influenced to varying degrees by the factors outlined below, here we will discuss each factor in the context of a particular spectral class to help illustrate how it can affect the fluorescent properties of FPs, in general. When possible, we will also highlight how certain obstacles have been overcome to make FPs better-suited for imaging applications.

2.1.2.1. Protein Expression, Folding Efficiency, and Stability. One of the most important parameters when conducting any fluorescence imaging experiment is the brightness of the fluorogenic species. Since GFP-like proteins must achieve a near-native conformation prior to chromophore formation, their protein folding efficiency can impact their fluorescence intensity by affecting the rate of fluorophore maturation. For example, because of its low translation efficiency and poor stability at 37 °C, wild-type *A. victoria* GFP exhibits relatively weak fluorescence intensity when expressed in higher eukaryotes. Therefore, to improve the expression and folding efficiency of *A. victoria* GFP in plant and mammalian cell lines, researchers have modified its DNA sequence in several important ways. First, to increase its translation efficiency, over 190 humanized codon sequences[33,34] and a Kozak translation initiation site[3,35] have been incorporated into the wild-type GFP sequence. Likewise, a point mutation (F64L) that improves the folding efficiency of GFP at 37 °C has been introduced to speed chromophore maturation and thereby increase total fluorescence.[27] Along with the spectra-simplifying S65T point mutation discussed above,[9,27,36] these genetic modifications result in an enhanced version of GFP (EGFP) that is nearly 20 times brighter than the wild-type species when expressed in mammalian cells and excited at 490 nm.[34] Due to its improved fluorescence properties and increased stability at 37 °C, EGFP has become a favorite fusion tag in many live cell imaging applications. Similar modifications have also been incorporated into each of the *A. victoria* GFP color variants currently in use today.

Despite its widespread use, several mutations have recently been described that may further improve upon the utility of EGFP for cell imaging studies.[37,38] For instance, using DNA shuffling methodologies, Pedelacq et al. developed a superfolder GFP with substantially faster folding kinetics and enhanced solubility at 37 °C compared to EGFP.[37] Superfolder GFP contains nine point mutations (S30R, Y39N, F99S, N105T, Y145F, M153T, V163A, I171V, A206V) in addition to those present in EGFP.[37] Structural analysis suggests that the S30R mutation may account for the enhanced stability of superfolder GFP. Indeed, substitution of arginine for serine at this position promotes the formation of an extensive five-residue ionic network which is believed to increase the global stability of the protein's β-barrel architecture.[37] Importantly, aside from improved stability, superfolder GFP is also more amenable to circular permutation than the parent species. As we will see in section 2.2., circular permutation is particularly important for the development of several types of biosensors. Indeed, by altering the orientation or local environment of the chromophore through the rearrangement of the N- and C-terminal portions of the protein, circular permutation has been shown to impact the dynamic range of many fluorescent biosensors.[39] Thus, though its use in biosensors has not yet been reported, superfolder GFP represents an excellent candidate for the development of future sensors.

2.1.2.2. Intrinsic Brightness. To be reliably detected and imaged within the cellular environment, it is essential that a FP possesses sufficient brightness above the autofluorescence of the cell. As we have seen above, the relative brightness of a FP is dependent upon several biochemical factors, including its folding efficiency and maturation time.[40] In addition to these factors, several photophysical parameters can also impact the brightness of a FP inside the cell. Chief among these is the intrinsic brightness of its fluorophore. Intrinsic brightness is defined as the product of the molar extinction coefficient (ε) and the fluorescence quantum yield (ϕ) of a chromophore. Each of these parameters, which describe the efficiency with which a fluorophore absorbs and emits light, respectively, can be impacted by the protein microenvironment. This concept is illustrated by the development of Cerulean, an improved version of enhanced CFP (ECFP).[36,41]

Though it is commonly used as a fluorescence resonance energy transfer (FRET) donor in genetically encoded biosensors, ECFP[36] suffers from several shortcomings that limit its utility in live cell imaging applications.[41] Perhaps the most serious of these is its relatively low fluorescence intensity compared to other enhanced FP color variants.[36,41,42] The weak fluorescence intensity exhibited by ECFP can be attributed to both a low ε (26,000 M^{-1} cm^{-1}) and a poor ϕ (0.40). This often results in a low signal-to-noise ratio when ECFP is used for imaging experiments. To address this issue, Rizzo et al. employed both site-directed and random mutagenesis to generate the ECFP variant Cerulean (ECFP/S72A/Y145A/H148D).[41] While S72A is a common folding mutation engineered into many GFP variants, Y145A and H148D are largely responsible for the advantageous properties of Cerulean. For instance, substitution of Asp for His at position 148 improves the fluorescence lifetime characteristics of Cerulean by stabilizing one of two conformational isomers of the protein.[41,41] Meanwhile, Y145A is believed to minimize thermal deactivation of the photoexcited state of the fluorophore, thereby enhancing its fluorescence intensity. Indeed, due to 48% and 67% increases in ε and ϕ, respectively, Cerulean exhibits a 2.5-fold increase in fluorescence intensity relative to ECFP.[41] Together, these properties make Cerulean better-suited for many FRET-based applications than its predecessor.

In addition to Cerulean, a recently described monomeric teal fluorescent protein (mTFP1) derived from the cyan protein cFP484 may provide another useful alternative to ECFP.[43,44] Like Cerulean, mTFP1 exhibits single exponential lifetime decay kinetics.[43] However, because of its relatively high ε (64,000 $M^{-1}cm^{-1}$) and exceptional ϕ (0.85), mTFP1 is twice as bright as Cerulean, putting it on par with many of the commonly used YFP variants.[43] Moreover, the photostability of mTFP1 is also comparable to that of the most stable color variants available today (Table S1). Together, these attributes make mTFP1 a promising donor FP for many FRET-based biosensors.

2.1.2.3. Photostability. Like most fluorescent molecules, GFP family members are susceptible to irreversible photobleaching by reactive oxygen species (ROS) generated in the excited state.[45] Though the protection provided by their β-barrel architecture confers FPs with relatively good photostability compared to many small molecule fluorescent dyes, photodegradation can still significantly affect the observed fluorescence of many FP species. Studies suggest that FP photobleaching is likely the result of irreversible modification of the chromophore by self-generated singlet oxygen ($^1O_2$) species, which are known to attack aromatic residues similar to those comprising GFP-like chromophores.[45−47] Like many of the photophysical parameters associated with FPs, the extent of photobleaching can be impacted by the microenvironment surrounding the chromophore. This is exemplified by three recently described BFP family members: Azurite,[48] EBFP2,[49] and mTagBFP.[50]

Because of its low fluorescence intensity and rapid photobleaching under standard imaging conditions, EBFP (EGFP/Y66H/Y145F) is not suitable for many quantitative cell-based applications.[36] This is not the case for Azurite, an EBFP derivative with 1.6-fold brighter fluorescence and dramatically improved (40-fold) photostability relative to the parent protein.[48] The key mutations in Azurite, V105I and V224R, partially fill a cavity created when histidine is substituted for tyrosine in the original BFP isoforms.[48] By increasing packing interactions within the Azurite core, it is believed that the mobility of its chromophore is significantly reduced. The increased rigidity of the chromophore enhances its photostability while at the same time reducing the energy loss via internal conversion, the major cause of the low ϕ traditionally associated with EBFP.[51,52] Building upon these findings, Ai et al. recently developed an improved version of EBFP, termed EBFP2, which contains both superfolder and Azurite mutations.[49] EBFP2 exhibits a 4-fold increase in its fluorescence intensity and an astonishing 550-fold increase in its photostability relative to EBFP, putting it on par with other EGFP derivatives currently used for cellular imaging studies.[49] Though the molecular basis for the dramatically improved photostability exhibited by EBFP2 is not completely clear, it is likely that effects similar to those responsible for Azurite's resistance to photobleaching are at play.

Finally, rather than attempting to improve the photophysical properties of existing EBFP species, Subach and colleagues recently engineered a new class of BFPs whose chromophores contain the wild-type Y66 residue.[50] Using the RFP variant TagRFP as a starting point, the authors introduced several point mutations that incorporated aliphatic or aromatic residues in and around the chromophore. Recent structural and mutational analyses of a related blue FP, termed Blue102, suggest that these modifications may impede the oxidation of the Cα−Cβ bond required to bring the tyrosine ring and imidazolone ring/acylimine group into conjugation in the red chromophore.[53] As a consequence, the TagRFP chromophore becomes trapped at a blue-emitting intermediate stage, generating a new type of BFP. After several rounds of random mutagenesis to increase brightness and photostability, the authors arrived at monomeric TagBFP (mTagBFP). mTagBFP is nearly twice as bright as EBFP2, while exhibiting improved maturation kinetics (13 vs 25 min) and pH stability (pK_a 2.7 vs 5.0).[50] Moreover, when photostability was measured under laser scanning confocal illumination, mTagBFP was over twice as photostable as EBFP2 (over 1,100-times more stable than the original EBFP species).[50] Presumably, the presence of a neutral Tyr residue at position 66 confers mTagBFP with greater photostability than other BFP family members.

It should be noted that, despite recent improvements in the photostability of BFP and other GFP-like proteins, many of the molecular principles underlying FP photobleaching still remain a mystery. The recent development of a medium throughput assay designed to improve the photostability of GFP family members promises not only to generate new FP variants with enhanced photostability, but it is also likely to provide important insights into the molecular determinants affecting FP photobleaching.[54]

2.1.2.4. Environmental Sensitivity. Until this point, we have looked at some of the intrinsic properties of FPs that influence their brightness. However, environmental factors can also greatly impact the fluorescence properties of GFP family members. This is best illustrated by examining a series of YFPs derived from *A. victoria* GFP.[9] Though YFP family members each generate a *p*-HBI chromophore identical to that of GFP, their excitation and emission spectra are red-shifted by up to 20 nm relative to GFP.[9] The observed hyperchromic shifts are primarily because of π stacking interactions between the phenolate ion of the chromophore and a tyrosine residue substituted for T203.[9,55] Despite the fact that many of the early YFP variants, including EYFP (EGFP/S65G/S72A/T203Y), exhibit exceptionally high ε values and excellent ϕ values, their apparent fluorescence intensity is markedly reduced within certain cellular environments because of their pH-sensitivity (pK_a > 7.0) and an acute sensitivity to halide ions.[56] While these properties have been exploited for specific applications (for instance, see section 3.2.2. below), they are not beneficial for most live cell imaging applications.

The pronounced environmental sensitivity of early YFP derivatives can be attributed to inefficient fluorescence emission by the neutral form of the chromophore.[55] Since first generation YFPs exhibited pK_a values between 7.0 and 8.0,[55] the weakly fluorescent neutral chromophore is significantly populated at physiological pH, leading to reduced fluorescence intensity inside many subcellular compartments. This problem is compounded by salt effects which further increase the pK_a of the fluorophore by destabilizing the anionic species, presumably through suppressed delocalization of its negative charge.[55] While substitution of a positively charged lysine residue at position 69 reduces the pK_a of a second generation YFP, EYFP(Q69K), by approximately 1 order of magnitude (pK_a = 6.1), this variant still exhibits significant sensitivity to halide ions.[57]

Two third generation YFP variants, Citrine (EYFP/V68L/Q69M)[58] and Venus (EYFP/F46L/F64L/M153T/V163A/S175G),[59] produced the first members of this spectral class that exhibited no apparent pH- or halide-sensitivity. While the environmental insensitivity observed for Venus is attributed to a β-bulge at the dimer interface,[60] the improvements seen in Citrine are caused by specific alterations within the core of the protein.[58] Indeed, structural analysis demonstrated that the

Q69M substitution present in Citrine plugs an anion binding pocket which prevents the binding of Cl^- ions in the vicinity of the chromophore.[58,61] Moreover, the tight packing of the neutral methionine residue next to the chromophore leads to a modest reduction in its pK_a relative to that of the EYFP (Q69K) variant (pK_a = 5.7 vs 6.1).[61] Together, these effects serve to stabilize the highly fluorescent anionic species, thereby improving the fluorescence intensity of Citrine inside cells. As a consequence, the range of subcellular regions to which Citrine can be targeted is significantly expanded.

2.1.2.5. Spectral Properties. In addition to its fluorescence intensity, the spectral properties of the FP tag can also be important to the success of a live cell imaging experiment. For instance, several critical cellular components, including DNA, absorb maximally in the UV region of the electromagnetic spectrum. Depending upon the intensity of the light source, photoinduced DNA damage can activate repair, or even apoptotic, pathways that fundamentally alter the cellular context in which an experiment is being performed.[62,63] Over the course of an imaging experiment, repeated exposure to even low levels of UV light can wreak havoc on the cellular system under investigation. Therefore, the use of UV-excitable FPs should be approached with caution. In fact, the cytotoxicity of UV light was one of the driving forces behind the development of EGFP from wild-type *A. victoria* GFP. Recall that, in wild-type GFP, the neutral A form of the chromophore (ex = 396 nm, em = 508 nm) predominates over the phenolate anion, B (ex = 475 nm, em = 503 nm). Consequently, the wild-type protein is most strongly fluorescent when excited with UV light. As we have seen above, shifting the chromophore population to a predominantly anionic state was accomplished in EGFP by a single point mutation, S65T, that stabilizes the B state, simplifying the excitation/emission spectra and making this variant better-suited for live cell imaging.[3]

In addition to UV-induced perturbations to the intracellular environment, illumination with short wavelength light also stimulates cellular autofluorescence. Autofluorescence is caused by the excitation of abundant biomolecules, such as the flavins, which are themselves fluorescent.[64] Excitation of these molecules can lead to high background fluorescence, especially when imaging weakly fluorescent FPs. Because most endogenous fluorophores are excited by short wavelength light (<500 nm), RFPs and FRFPs that absorb at longer wavelengths (>550 nm) are desirable for cellular imaging applications, particularly those conducted in situ. As a consequence, much effort has been devoted to developing monomeric RFP (mRFP) and FRFP (mFRFP) variants suitable for protein fusion. These efforts have culminated in the development of two major families of mRFP/mFRFPs: the mFruits[65] and a series of eqFP578 derivatives consisting of TagRFP,[22] TagRFP-T,[54] mKate,[23] mKate2,[66] and Neptune.[67] Together, these proteins provide researchers with several monomeric FPs that are excited at wavelengths >550 nm. Though no single variant is optimal for all applications, the photophysical properties of mCherry and TagRFP-T make them the best general-purpose mRFPs for biosensor development.[40] Likewise, the mFRFPs, mKate2 and Neptune, are well-suited for imaging in tissue sections or even some translucent animals, such as zebrafish (*D. rerio*) and nematodes (*C. elegans*).[66,67]

That being said, to track cellular processes in most mammalian tissues, where light-scattering and absorbance by biomolecules such as hemoglobin and lipids severely limit penetration by even far-red light, infrared fluorescent proteins (IFPs) that emit at wavelengths >700 nm are required. To this end, Shu et al. recently reported the development of the first monomeric IFP, termed IFP1.4, from a bacteriophytochrome produced by *Deinococcus radiodurans*.[68] Though related to FPs, phytochromes do not generate their chromophores autocatalytically. Instead, they incorporate chromophores produced by complementary biosynthetic pathways. In the case of IFP1.4, the apoprotein binds biliverdin IXα (BV), a product of heme catabolism that is nonfluorescent in the unbound state. Upon binding IFP1.4, it is believed that BV adopts a more rigid conformation because of tight packing interactions within the protein binding pocket.[68] This limits rotation of BV's D pyrrole ring which, if left unconstrained, would lead to nonradiative decay back to the ground state. As a result, IFP1.4 exhibits excitation and emission maxima at 684 and 708 nm, respectively.[68] Though it exhibits poor quantum efficiency (ϕ = 0.07) and photostability in its current form,[68] IFP1.4 lays an important foundation for the development of brighter and more photostable phytochrome variants that will be invaluable for monitoring cellular processes in a truly in vivo environment.

2.1.2.6. Size and Oligomerization State of FP Family Members. Finally, when utilizing FP fusion tags for cellular imaging, it is important to consider the size of the FP itself. For instance, *A. victoria* GFP is comprised of 238 amino acid residues bearing a monomeric molecular mass of approximately 27 kDa.[69,70] Studies have shown that, save for a few residues at the extreme N- and C-termini, the entire primary sequence is required to generate the β-barrel and α-helical structures necessary for fluorescence activity (reviewed in refs 3 and 4). Fortunately, both biochemical and biophysical data suggest that FP fusion tags generally have little effect on the activity of the target protein.[71] Nevertheless, in some cases FPs have been shown to perturb the function of their partner proteins, particularly those that are a part of a tightly packed protein complexes.[72−74]

Under these circumstances, the limitations imposed by the size of FPs are compounded by the tendency of the wild-type proteins to form oligomers in solution. Importantly, aside from significantly increasing the functional mass of the protein chimera, oligomerization of FP fusion tags can also lead to the formation of insoluble protein aggregates. As a consequence, researchers have sought to develop monomeric FP tags within each spectral class using protein engineering. In the case of *A. victoria* GFP and its derivatives, a single-point mutation (A206K) is sufficient to generate the monomeric species. Presumably, the high energetic cost of placing two positively charged lysine residues in close proximity at the dimer interface disrupts the weak affinity of the wild-type proteins for one another.[8,75]

Because jellyfish GFP derivatives do not require dimerization for proper fluorophore maturation or function, disruption of their dimer interface does not dramatically affect the fluorescence properties of the monomeric species. However, the situation is considerably more complex with regard to many of the orange- and red-emitting FPs isolated from reef corals. Unlike *A. victoria* GFP, most of the Anthozoan FPs are obligate tetramers. Consequently, early attempts to generate monomeric versions of these proteins proved to be quite challenging. In a truly Herculean effort, Campbell et al. utilized a combination of site-directed and random mutagenesis to generate a monomeric form of DsRed, termed mRFP1.[76] Their basic strategy involved disruption of each of the dimer interfaces (AB and AC) followed by eight rounds of directed evolution to rescue red fluorescence.[76] Relative to the parent species, mRFP1 contains a total of

33 amino acid substitutions and exhibits an emission spectrum that is red-shifted nearly 25 nm.[76] Importantly, as the first monomeric FP with an emission maximum >600 nm and the starting point for the mFruit series described above, mRFP1 represents a significant milestone in FP technology. Indeed, with the development of monomeric RFP/FRFP color variants such as the mFruit series and TagRFP family members[22,23,54,66,67] from Anthozoan progenitors, bright, monomeric FP variants are now available within each FP spectral class. As a result, more sophisticated imaging techniques, such as multicolor imaging and multiparameter RET analysis, are now feasible.

2.1.3. Fluorescent Proteins for Resonance Energy Transfer-Based Studies. The discovery and development of GFP family members exhibiting either red- or blue-shifted excitation/emission spectra allows FPs to be used for a number of RET-based applications. RET is a photophysical phenomenon characterized by the nonradiative transfer of energy between two chromophores, called the donor and acceptor, located in close proximity (<10 nm) to one another.[77] RET can be broadly divided into two related classes, termed fluorescence RET (FRET) and bioluminescence RET (BRET),[78] according to the origin of the donated light energy. Whereas FRET requires prior excitation of the donor fluorophore via an external light source, the energy utilized for BRET is generated as the byproduct of an enzymatic reaction, such as the oxidation of the luciferin, coelentrerazine, by luciferase. Importantly, because their efficiencies (E) vary as a function of the interchromophore distance (r) according to the equation

$$E = [1 + (r/R_0)^6]^{-1} \quad (1)$$

these processes represent highly sensitive methods for measuring both protein−protein interactions and conformational changes within individual proteins.[77]

According to the above relationship, E is half-maximal when $r = R_0$, a value termed the Förster distance (R_0). R_0 is dependent upon many photophysical parameters, including the ϕ of the donor, the ε of the acceptor, and the degree of spectral overlap between donor emission and acceptor excitation.[79] In addition to these parameters, the relative orientation of the chromophore dipoles in space can also dramatically impact the efficiency of energy transfer during RET.

The most widely used BRET pair consists of *Renilla* luciferase (RLuc) as the energy donor, YFP as the energy acceptor and coelenterazine h as the luciferase substrate. In addition to RLuc, luciferases derived from several firefly species (e.g., *Hotaria parvula*,[80] *Photinus pyralis*[81]), click beetles (*Pyrophorus plagiophthalamus*),[82] and the copepod, *Gaussia princeps*,[83] have also been shown to serve as BRET donors when coupled with appropriate FP color variants. Recently, several groups have fine-tuned the spectral properties of both the luciferase enzyme and its luciferin substrate through mutagenesis[84−86] and chemical derivatization,[82,87,88] respectively. Though BRET signals are generally dimmer than those generated by FRET, this approach offers several potential advantages over FRET for live cell applications.[89] For instance, because BRET does not require excitation of the donor fluorophore for energy transfer to occur, it does not elicit cellular autofluorescence. As a consequence, BRET images exhibit signal-to-noise ratios that are much higher than those obtained using FRET. Likewise, the chemiluminescent nature of the excitatory light used for BRET simultaneously eliminates two of the primary sources of error associated with FRET-based measurements: (1) spectral bleed-through caused by direct excitation of the acceptor fluorophore at the donor wavelength and (2) photobleaching of the donor molecules by excitatory light. Finally, since the donor and acceptor molecules used for BRET generate luminescent and fluorescent signals, respectively, the expression levels of each component can be measured independently of the other. Thus, though often underappreciated, BRET-based probes hold great potential for live cell applications, including some unique applications in live cell-based high throughput compound screening[78,90] and in vivo pharmacodynamics studies for drug candidates.

That being said, FRET has traditionally been the RET technique of choice when engineering genetically encodable fluorescent biosensors designed to probe the cellular environment or to visualize protein−protein interactions *in situ*. Though the recent development of several red- and blue-shifted color variants has increased the popularity of GFP/RFP,[22,65,76] members of the CFP and YFP spectral classes remain the most popular FP FRET pairs for live cell imaging applications. In theory, the advent of several sets of spectrally distinct FP FRET pairs should facilitate dual FRET measurements, allowing multiple cellular processes to be imaged simultaneously within a single cell. While these types of experiments are feasible if the probes are targeted to distinct subcellular regions, aside from a few specialized cases,[91−93] multiparameter FRET imaging within the same subcellular locale has been hampered by spectral bleed-through caused by the broad excitation and emission profiles characteristic of most FP variants (typically ∼100 nm).[94] Under these circumstances, it is critical that donor FPs exhibit non-overlapping excitation spectra. This caveat was the driving force behind the development of the violet-excitable YFP variant, mAmetrine.[95] Because of the combined effects of ESPT and $\pi-\pi$ stacking interactions, mAmetrine exhibits an extremely large Stokes shift (ex = 406 nm, em = 526 nm)[95] that allows it to act as a FRET donor for the dimeric RFP variant, tdTomato (ex = 554 nm, em = 581 nm).[96] Therefore, when imaged in combination with a FRET pair consisting of the teal-hued mTFP1 (ex = 462 nm, em = 492 nm) and mCitrine (ex = 516 nm, em = 529 nm), the mAmetrine/tdTomato FRET pair can be coimaged with the mTFP1/mCitrine pair.[95] However, despite using carefully chosen filter sets, there still exists some degree of cross-excitation between the donors; most noticeably, the filter set used to excite mAmetrine also results in 14% excitation of mTFP1. As a result, correction factors have been derived to obtain corrected mAmetrine and mCitrine intensities based on the fact that both FPs use the same emission filter set. In general, the ability to image multiple cellular processes within a single cell will allow researchers to examine the spatial and temporal relationships between interdependent signaling pathways.

2.1.4. Photoinducible Fluorescent Proteins. As their name suggests, photoinducible FPs (PI-FPs) undergo changes in their spectral properties in response to specific light irradiation. Like the FPs discussed above, the photophysical properties of PI-FP chromophores are directly impacted by the protein matrix. PI-FPs can be divided into three categories based upon their mechanism of activation.[68] Below, we briefly discuss the molecular basis for photoconversion within each category, highlighting their advantages and disadvantages for live cell imaging. For a more thorough discussion on this topic, the interested reader is referred to several recent reviews.[97−99]

2.1.4.1. PI-FPs Based on Oxidative Decarboxylation. The first class of PI-FPs is comprised of a photoactivable version of

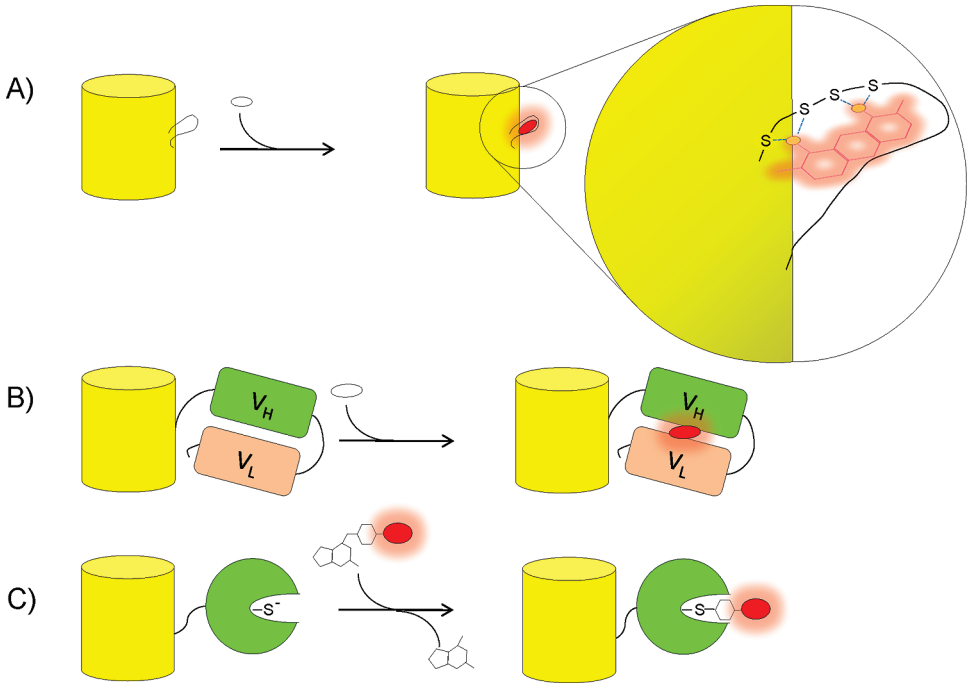

Figure 4. Genetically targetable chemical labeling methods. Cartoon depicting several genetically encodable fluorescent labeling methods that can be applied to biosensor development. The size of each tag is drawn roughly to scale relative to one another and to a FP family member (yellow cylinder). (A) The tetracysteine/biarsenical system. (B) The FAP/fluorogen system. (C) The SNAP-tag/BG system. Note that in the case of A and B, the ligand is virtually nonfluorescent prior to association with the tag.

A. victoria GFP (PA-GFP),[100] several photoactivatible mCherry constructs (PA-mCherry1−3)[101] and two photoswitchable CFP variants (PS-CFP and PS-CFP2) derived from *A. coerulescens* GFP (acGFP).[102] Members of this class were developed based upon the principle of photoisomerization first described for wild-type *A. victoria* GFP. Recall that, in the case of *A. victoria* GFP, the weakly fluorescent neutral form of the chromophore (A state) predominates over the highly fluorescent anionic species (B state) due, in large part, to destabilization of B in the ground state by electrostatic repulsion by a negatively charged glutamate residue, E222, located in close proximity to the chromophore. ESPT leads to neutralization of E222, which relieves this inhibition and shifts the equilibrium between A and B toward the B state. Interestingly, intense irradiation with UV light permanently relieves E222-mediated destabilization and converts the chromophore population to a predominantly anionic state. Both mass spectroscopy and crystallographic data suggest that this irreversible photoconversion of *A. victoria* GFP is caused by oxidative decarboxylation of E222 driven by high-energy UV light.[103] A similar decarboxylation reaction is thought to underlie the pronounced photoconversion of PA-GFP, PA-mCherry, and the PS-CFPs.[101,104]

Though wild-type *A. victoria* GFP is able to undergo photoconversion, it is not particularly useful as an optical highlighter for live cell imaging applications because the phenolate anion is significantly populated (∼15%) under steady-state conditions.[25] As a result, the contrast between the activated and nonactivated states is severely diminished. One way to improve the contrast upon photoconversion is to further destabilize the anionic form of the chromophore in the uninduced state. Since previous studies had shown that the point mutation, T203I, abolishes the absorbance spectrum characteristic of the phenolate species,[105,106] Patterson and Lippincott-Schwartz subjected T203 to random mutagenesis in a wild-type GFP background.[100] They found that substitution of a bulky histidine residue at this position (T203H) results in a GFP variant (PA-GFP) which exhibits no discernible absorbance at the longer wavelengths (475 nm) typical of the phenolate species. However, following intense irradiation with violet light (413 nm), PA-GFP undergoes rapid photoconversion to the anionic form of the fluorophore leading to a 100-fold increase in its emission at 517 nm when excited with a 488 nm laser line.[100] In the same way, photoactivation of PA-mCherry using 399 nm light results in the emergence of excitation and emission peaks at ∼570 and 596 nm, respectively. However, in this case, photoactivation is associated with a ∼4,000-fold increase in fluorescence intensity.[101] These properties render PA-GFP and PA-mCherry nearly invisible when exposed to excitatory light prior to photoactivation and easily discernible afterward. Because the photoconversion of these PA-FP variants is irreversible (presumably due to the decarboxylation of E222), subpopulations of PA-GFP and PA-mCherry can be selectively "turned on" in a defined region of the cell and their redistribution tracked over time.

Like PA-GFP and PA-mCherry, the photoconversion of the PS-CFPs likely involves photoinduced decarboxylation of E222.[102] However, in contrast to the other members of this class, PS-CFP variants fluoresce cyan (∼470 nm) prior to photoactivation and green (511 nm) thereafter. For instance, because of a 400-fold increase in green fluorescence and a 5-fold reduction in cyan fluorescence, the most recent PS-CFP, PS-CFP2, shows a 2,000-fold increase in its green-to-cyan fluorescence ratio.[99] Such a large ratiometric change improves the contrast of PS-CFP2 and helps to offset its reduced fluorescent intensity relative to PA-GFP and PA-mCherry. A ratiometric measure also offers advantages over intensity-based methods because it corrects for differences in cell thickness and the

intracellular concentration of the FP. However, since the PS-CFPs undergo photoconversion at wavelengths similar to those used to excite molecules in the uninduced state, they often suffer from artifacts stemming from continuous photoconversion.

2.1.4.2. Kaede-like Family of PI-FPs. The second class of PI-FPs was founded by Kaede, a FP isolated from the stony coral *Trachyphyllia geoffroyi*.[107] Kaede-like proteins are converted from a green- to a red-emitting species following irradiation with high intensity UV-violet light. The unique photophysical properties exhibited by members of this family are attributed to their chromophore-forming tripeptide, His62-Tyr63-Gly64. Indeed, analysis of the Kaede FP demonstrated that UV irradiation drives a β-elimination reaction between Nα and Cα of His62 leading to cleavage of the protein backbone.[108] This unconventional peptide cleavage reaction generates a double bond between Cα and Cβ of His62, thereby extending π-conjugation to the imidizole ring system. The resulting chromophore, 2-[(1*E*)-2-(5-imidazolyl)ethenyl]-4-(*p*-hydroxybenzylidene)-5-imidazolinone, exhibits excitation and emission spectra that are red-shifted relative to the uninduced GFP-like *p*-HBI species.

Due to their oligomeric state, the original Kaede family members—Kaede, KikGR and EosFP—are unsuitable for protein fusion and are thus of little use for tracking protein dynamics in cellular systems. The development of a monomeric version of EosFP, termed mEosFP, provided researchers with the first green-to-red PI-FP amenable to protein fusion.[109] Unfortunately, because its chromophore does not mature well at temperatures above 30 °C, mEosFP cannot be imaged in most mammalian cell types. In contrast, a recently described mEosFP derivative, termed mEos2, exhibits no ill effects at 37 °C.[110] Likewise, the monomeric Kaede-like proteins, Dendra and Dendra2, also mature efficiently at 37 °C, making these variants better-suited for studying protein dynamics in higher eukaryotes.[111] Like the PS-CFPs, each of these variants benefit from the contrast afforded by spectrally distinct excitation/emission maxima in the uninduced and induced states. For example, though relatively low values of ε in both the green and red states limit its fluorescence intensity, photoactivated Dendra2 is easily discernible inside the cell because of a 4,000-fold fluorescence contrast upon photoconversion.[112] However, this variant also suffers from rapid photobleaching in the red state, limiting its ability to track activated proteins over extended periods of time.[32]

2.1.4.3. Reversible PI-FPs. All of the PI-FPs described thus far undergo irreversible covalent modifications upon photoinduction. In contrast, the third class of PI-FPs can be reversibly (and repeatedly) switched between a fluorescent on-state and a nonfluorescent off-state by irradiation with different wavelength light. Members of this class include the tetrameric Kindling FP (KFP)[113] and the monomeric PI-FPs PA-mRFP1,[114] mTFP0.7,[115] rsCherry,[116] rsCherryRev,[116] mApple,[54] and Dronpa.[117] In addition, several Dronpa derivatives have recently been developed, including Dronpa-2 and -3,[118] rsFastLime,[119] bsDronpa,[120] and PaDron,[120] whose unique photophysical characteristics offer a diverse toolset of reversible PI-FPs for live cell imaging experiments.

Structural studies suggest that the photochromic behavior characteristic of this family of PI-FPs may be driven by cis−trans isomerization of their fluorophores.[115,121−124] Perhaps more importantly, isomerization is accompanied by a cascade of structural rearrangements within the protein core that alters the local environment encountered by the chromophore.[115,122,124,125] These changes directly impact the fluorescent properties of the protein by influencing both the geometry and the ionization state of its chromophore. This principle is illustrated by examining the on- and off-states of Dronpa, the prototypical member of this class of PI-FPs.

Dronpa is a monomeric PI-FP evolved from a species of *Pectiniidae* coral.[117] In the resting state, Dronpa is highly fluorescent (ε = 95,000 $M^{-1}cm^{-1}$; ϕ = 0.85), exhibiting excitation and emission maxima at 503 and 518 nm, respectively. However, upon irradiation with intense blue light (488 nm), its chromophore is converted to a nonfluorescent dark state that absorbs maximally at 390 nm. Exposure to low levels of UV light (405 nm) converts Dronpa back to the fluorescent on-state, thereby resetting the system. Interestingly, both the fluorescent and the nonfluorescent forms of the protein can be maintained for several days in the absence of inducing light, suggesting that each conformation is thermally stable.

As mentioned above, the reversibility of Dronpa has been attributed to subtle structural changes within the protein core induced by light irradiation. In support of this notion, structural analysis demonstrated that, in the fluorescent on-state, the chromophore adopts a cis-conformation.[123−125] In this conformation, the conjugated ring systems of the chromophore are oriented in a nearly coplanar configuration through interactions with neighboring amino acid residues, leading to strong fluorescence.[124,125] In contrast, the chromophore is thought to undergo isomerization to the trans state following irradiation with intense blue light (488 nm).[124] Computational analysis suggests that cis−trans isomerization likely occurs via a bottom hula twist mechanism along the methine bridge connecting the imidizolinone and *p*-hydroxyphenyl ring systems.[122,124] Unlike the cis-planar conformation observed in the on-state, the trans (off) state chromophore is characterized by a nonplanar geometry which is believed to increase its flexibility relative to the cis-configuration.[125] Not surprisingly, changes in the orientation of the chromophore are accompanied by several structural rearrangements within the protein core that underlie this conversion.[124,125] For instance, both stacking interactions (between His193 and the phenol ring of the chromophore) and hydrogen bonding interactions (between Ser142 and chromophore hydroxyl oxygen) which help hold the chromophore in a rigid conformation in the cis configuration are lost upon photoconversion.[124,125] The disruption of hydrogen bonding interactions with Ser142 may also facilitate protonation of the chromophore by destabilizing the phenolate oxyanion.[124,125] Together, these factors result in an almost complete loss of fluorescence in the dark state. However, it should be noted that, because the blue light used to excite Dronpa in the fluorescent on-state also induces photoconversion to the dark state, this PI-FP and many of its derivatives are susceptible to artifacts stemming from light-induced signal deterioration.

Interestingly, a handful of recent studies have reported that many FPs exhibit some degree of reversible photoswitching behavior.[54,126,127] These include some of the most commonly used FPs, such as Cerulean, EGFP, Citrine, mKO and mCherry, as well as several newly engineered constructs, such as mApple and mOrange2.[54,127] Though the extent to which a given FP undergoes transient dark state conversion appears to vary substantially among different FP family members, in each case photoconversion is believed to be caused by cis−trans isomerization of the chromophore following light-induced alterations

within the protein core.[54] However, unlike Dronpa and many of the PI-FPs mentioned above, once converted to the dark state, most FP variants appear to relax back to the fluorescent on-state in a matter of seconds or minutes, suggesting that the dark state is unstable. Nevertheless, this phenomenon may have important implications when utilizing FPs for certain imaging applications, such as fluorescence recovery after photobleaching (FRAP) experiments, which require changes in fluorescence intensity to be measured over relatively short periods of time.[127] Though it is currently unknown whether reversible photobleaching is an intrinsic property common to all FP variants, clearly it will be important to investigate this phenomenon further in the future.

2.2. Chemical Labeling Methodologies

Despite their utility to a wide variety of live cell imaging applications, some cellular processes have proven resistant to examination using FP chimeras. This is due, in large part, to inherent limitations imposed upon GFP family members by their size and/or spectroscopic properties. For instance, bulky FP fusion tags have been shown to perturb the activity of a (surprisingly) small number of cellular proteins. This phenomenon appears to be most pronounced when FPs are fused to membrane proteins like GPCRs or proteins involved in the formation of tightly packed protein complexes like microtubules.[128,129] In such systems, it is often possible to restore biological activity by replacing the large FP tag with a short peptide sequence designed to bind small molecule probes.[74,130]

In addition to being potentially smaller in size, the versatility afforded by small molecule chemical probes also enables researchers to track cellular processes in biological contexts that may not be accessible using FPs. For instance, chemical engineering efforts have produced genetically targetable fluorophores that span the visible spectrum and beyond.[131] These include dyes that cover most of the near-IR region, a region critical for deep tissue imaging in many higher organisms.[131] Together, these considerations have led to the development of several methodologies designed to label cellular proteins with functionally diverse chemical/fluorescent probes using genetically encodable tags (Figure 4). Since each of these techniques requires the addition of an exogenous ligand prior to imaging, several factors must be considered when they are employed for live cell imaging applications: (1) the probe must readily traverse the cellular membrane (or, in the case of cell-surface labeling, be excluded by it); (2) neither the ligand nor its byproduct should elicit a cytotoxic response or otherwise perturb the cellullar environment; (3) the probe should interact specifically and stably with the protein of interest; (4) ideally, the probe should be detectable only when bound to the tagged protein.[132] Below we highlight those techniques that hold the greatest promise for biosensor development, focusing on their advantages and disadvantages for live cell imaging. For a more comprehensive discussion on this topic, the interested reader is referred to excellent reviews by Chen and Ting[132] and O'Hare et al.[133]

2.2.1. Tetracysteine/Biarsenical System. Aside from FP tags, the most widely used genetically encodable protein labeling technique for live cell imaging applications is the tetracysteine/biarsenical system. This system, which is based upon high affinity interactions between trivalent arsenic compounds and a short peptide sequence containing pairs of closely spaced thiols,[134,135] offers a valuable alternative when bulky FP tags interfere with the cellular function of their partner proteins (Figure 4a).[74,130] Though the canonical tetracysteine motif consists of the sequence CCXXCC (where C is Cys and X is any amino acid), optimization of the intervening sequence revealed that tags containing a Pro-Gly dipeptide bind biarsenical conjugates, such as [4′-5′-bis(1,3,2-dithioarsolan-2-yl)]-fluorescein (FlAsH) and -resorufin (ReAsH), most effectively.[134,135] In this configuration, the peptide adopts a hairpin structure which places the cysteine residues in an orientation that promotes interactions with the arsenic atoms contained in the probes.[136] As a result, the tetracysteine motif forms a bidentate organoarsenic chelator characterized by rapid association (k_a = $\sim 10^5$ M^{-1} s^{-1}) and slow dissociation (k_d = $\sim 10^{-7}$ s^{-1}) of its ligands ($K_{D,app}$ = $\sim 10^{-12}$ M).[134,135] Such a high affinity ensures that complex formation proceeds even in the presence of low concentrations (10 μM) of a 1,2-ethanedithiol (EDT) antidote designed to reduce the cellular toxicity of the biarsenical probes.[134] While ligand binding can be disrupted by millimolar concentrations of EDT, signal deterioration is typically not an issue using this technique because the tetracysteine/ligand complex is essentially irreversible in the absence of excess dithiols.[134]

Though, in theory, tetracysteine tags possess sufficient versatility to utilize functionally diverse chemical probes, this technique has traditionally been used for fluorescence-based applications. To this end, a variety of cell-permeable biarsenical probes have been developed that exhibit various fluorescent properties.[134,135,137,138] These include the fluorescein and resorufin derivatives FlAsH and ReAsH mentioned above, as well as the Ca^{2+}-sensitive dye, calcium-green FlAsH (CaGF).[138] Each of these probes is virtually nonfluorescent in the unbound state, a phenomenon that is likely caused by the excited state quenching by processes such as vibrational deactivation or photoinduced electron transfer.[134] Association with the tetracysteine motif increases the rigidity of these chromophores, leading to an approximately 10^4-fold increase in their fluorescence intensity. This serendipitous property helps to decrease background fluorescence because unbound ligand molecules are virtually invisible compared to those associated with the tag. Nevertheless, the absolute contrast using the tetracysteine/biarsenical system is still an order of magnitude lower than that observed for FP tags. This decreased contrast can be attributed to nonspecific interactions with endogenous dithiols, despite coadministration of the EDT antidote.[139]

In addition to their utility as fluorescence probes, the tetracysteine/biarsenical system also offers researchers other benefits for studying protein dynamics because of its unique photophysical properties. For instance, like the chromophores utilized by GFP family members, FlAsH and ReAsH are known to generate ROS in the excited state.[135] However, whereas the FP core acts to shield the surrounding environment from the resulting $^1O_2$ molecules, the tetracysteine motif utilized by the biarsencial system offers no such protection. As a consequence, when subjected to intense illumination, short-lived ROS generated by FlAsH or ReAsH can be used to photoconvert diaminobenzidine (DAB) to an electron-rich osmiophilic polymer that is amenable to detection by electron microscopy (EM). Although cells must be fixed prior to analysis, the resolution afforded by this approach far surpasses that of standard light microscopy (and even immunogold EM).[137] Importantly, EM data can be correlated with results obtained using light microscopy in living cells, adding a critical ultrastructural component to live cell images. Though both the FlAsH and ReAsH ligands have been shown to photoconvert DAB, ReAsH and its derivatives appear to do so most efficiently.[135] As a consequence, correlated EM

Table 2. Fluorescent Biosensors for Studying Signaling Dynamics in Living Cells

biosensor names	reporter of	ref	comments
promoter/protein dynamics			
EGFP-MODC	promotor activity	164	PEST sequence of MODC reduces biological half-life of EGFP, allowing transient changes in promoter activation to be visualized.
DsRed-Timer	promotor activity	166	transitions from green-to-red in ~18 h; ratiometric readout
fast-, medium-, and slow-FT	promotor activity/ protein turnover	167	fast-FT exhibits rapid chromophore formation and then transitions from blue-to-red species in ~7 h; medium-FT and slow-FT exhibit moderate and slow chromophore formation and transition from blue-to-red in 4 and 18 h, respectively.
fluorescent highlighters	protein turnover/ localization	see text	permits light-induced pulse-chase analysis
tetracysteine/ biarsenical	protein turnover/ localization	137	permits fluorescent pulse-chase analysis
PI/lipid probes			
FP-Tubby; FP-PH$^{PLC\delta1}$	PI(4,5)P_2 dynamics	200	localization-based
CYPHER	PI(4,5)P_2 dynamics/ PLC activity	367	FRET-based; intrinsic molecular switch based on PH domain of PLCδ1
Pippi-PI(4,5)P2	PI(4,5)P_2 dynamics	494	FRET-based; instrinsic molecular switch based on PH domain of PLCδ1
PH$^{PLC\delta1}$-CFP, PH$^{PLC\delta1}$-YFP	PI(4,5)P_2 dynamics	308	bimolecular FRET (bystander FRET)
FP-PH^{GRP1}; FP-PH$^{Cytohesin-1}$; FP-PH^{Btk}; FP-PH^{ARNO}	PI(3,4,5)P_3 dynamics	200	localization-based
Fllip	PI(3,4,5)P_3 dynamics	306	FRET-based; intrinsic molecular switch based on PH^{Grp1}; hinge domain allows substitution of any effector domain
FP-PDK1; FP-CRAC; FP-PH^{Atk}	3′PI dynamics	200	localization-based
InPAkt	3′PI dynamics	307	FRET-based; molecular switch consists of PH^{Akt} and a pseudoligand
CAY	PI(3,4,5)P_3/PI(3,4)P_2 / PI(4,5)P_2 dynamics	495	FRET-based; intrinsic molecular switch based on ActA
FP-Svp1p; FP-ENTH^{Ent3p}; FP-PH^{TAPP1}	PI(3,4)P_2 dynamics	200	localization-based
Pippi-PI(3,4)P_2	PI(3,4)P_2 dynamics	349	FRET-based; intrinsic molecular switch based on PH^{TAPP1}
FP-FYVE^{EEA1}	PI(3)P dynamics	200	localization-based
FP-PH^{FAPP1}; FP-PH^{OSBP}; FP-PH^{OSH2}	PI(4)P dynamics	200	localization-based
FIRE-1,-2,-3	absolute $[IP_3]_i$	309, 310	FRET-based; molecular switches based on ligand binding domain of IP3R-1,-2 or −3; FIRE-3 is also known as LIBRA
IRIS-1	absolute $[IP_3]_i$	311	FRET-based; molecular switch based on ligand binding domain of IP3R1
DAGR	DAG dynamics	367	FRET-based; molecular switch based on CIA- and CIB-domains of PKCβII
DIGDA	DAG dynamics	494	FRET-based; molecular switch based on CI-domain of PKCβII
GFP-Lact-C2	PS dynamics	203	localization-based
Pii-DK	PA dynamics	496	FRET-based; molecular switch based on C-terminal region of human DOCK2
halide ion probes			
YFP(H148Q)	halide ion fluctuations	204	intensity-based
YFP(H148Q, I152L)	halide ion fluctuations	205	intensity-based; 30-fold selectivity for I^- over Cl^-
Clomeleon	halide ion fluctuations	207	FRET-based

Table 2. Continued

biosensor names	reporter of	ref	comments
Cl-Sensor	halide ion fluctuations	208	FRET-based; may be selective for I^- due to I152L
pH probes			
EGFP, EYFP	intracellular pH	219, 220	intensity-based; pK'_a = 6.15 and 7.1, respectively
SuperEcliptic-GFP pHluorin	intracellular pH	217	intensity-based; pK'_a = 7.1
ratiometric pHluorin	intracellular pH	217	ratiometric single FP; pK'_a = 6.9
deGFP family	intracellular pH	216	ratiometric single FP; pK'_a = 6.8−8.0 depending on deGFP species
E^1GFP and E^2GFP	intracellular pH	214, 215	ratiometric single FP; pK'_a = 6.5 and 7.5
GFpH	intracellular pH	497	FRET-based; pK'_a = 6.2
YFpH	intracellular pH	497	FRET-based; pK'_a = 6.5
mtAlpHi	intracellular pH	221	intensity-based; pK'_a = 8.5
redox sensors			
rxYFP^N_C family	redox status	229	intensity-based
roGFP family	redox status	225	ratiometric single FP
roGFP1-Rx family	redox status	227	ratiometric single FP; rate of S−S bond formation is increased by incorporation of positively charged residues around Cys residues
roGFP1-iX family	redox status	226	ratiometric single FP; roGFP1 derivatives contain various a.a. substitutions next to C147; better-suited for relatively oxidizing environments
calcium ion sensors			
Camgaroo-2	changes in $[Ca^{2+}]_i$	58	intensity-based; CaM serves as molecular switch
GCaMP2	changes in $[Ca^{2+}]_i$	234	intensity-based; CaM-M13 molecular switch
GCaMP3	changes in $[Ca^{2+}]_i$	250	intensity-based; mutations in EGFP reporter unit and EF hand of CaM increase dynamic range
flash-pericam	changes in $[Ca^{2+}]_i$	237	intensity-based; CaM-M13 molecular switch
inverse-pericam	changes in $[Ca^{2+}]_i$	237	intensity-based; decrease in intensity following Ca^{2+} binding
ratiometric-pericam	absolute $[Ca^{2+}]_i$	237	ratiometric single FP
Cameleon 3	absolute $[Ca^{2+}]_i$	232	FRET-based; CaM-M13 molecular switch
split cameleon	absolute $[Ca^{2+}]_i$	232	FRET-based (bimolecular); CaM-ECFP, M13-EYFP
D3cpv	absolute $[Ca^{2+}]_i$	244	FRET-based; bump-and-hole strategy reduces interactions with endogenous CaM
yellow cameleon 6.1 (YC6.1)	absolute $[Ca^{2+}]_i$	498	FRET-based; modified molecular switch consists of CaM(1−79)-CKKp-CaM(80−148)
TN-XXL	absolute $[Ca^{2+}]_i$	246	FRET-based; molecular switch consists of tandem repeat of the C-terminal region of csTnC
cAMP sensors			
PKA^{RII}-ECFP/ PKA^{cat}-EYFP	absolute $[cAMP]_i$	284	FRET-based (bimolecular)
ICUE3	absolute $[cAMP]_i$	499	FRET-based; cpVenus increases dynamic range compared to ICUE2
CFP-Epac (δDEP-CD)-YFP	absolute $[cAMP]_i$	287	FRET-based
Epac2-camps	absolute $[cAMP]_i$	282	FRET-based; EC_{50}(cAMP): 820 nM
PKA-camps	absolute $[cAMP]_i$	282	FRET-based; molecular switch is based on PKA-RIIβ subunit
HCN2-camps	absolute $[cAMP]_i$	500	FRET-based
cGMP sensors			
FlincG α	changes in $[cGMP]_i$	259	intensity-based; K'_D(cGMP) = 35 nM; cGMP/cAMP selectivity = 1,140-fold
FlincG β	changes in $[cGMP]_i$	259	intensity-based; K'_D(cGMP) = 1.1 μM; cGMP/cAMP selectivity = 30-fold
FlincG γ	absolute $[cGMP]_i$	259	ratiometric single FP; K'_D(cGMP) = 170 nM; cGMP/cAMP selectivity = 280-fold
Cygnet-2.1	absolute $[cGMP]_i$	261	FRET-based; selectivity cGMP/cAMP = > 500-fold; catalytically dead PKG; pH- and halide-insensitive
CGY (aka cgy-Del1)	absolute $[cGMP]_i$	394	FRET-based; selectivity cGMP/cAMP = 7.6

Table 2. Continued

biosensor names	reporter of	ref	comments
cGS-GKI	absolute $[cGMP]_i$	299	FRET-based; molecular switch based on PKG regulatory domain (a.a. 230−349)
cGi family members	absolute $[cGMP]_i$	301	FRET-based; molecular switches consist of various portions of PKGI regulatory domain
cGS-DE5 family members	absolute $[cGMP]_i$	299	FRET-based; molecular switches consist of various regions of PDE5
NO sensors			
FRET-MT	absolute [NO]	303	FRET-based
Piccell	NO release	392	coupled cell-based FRET reporter system
ROS sensors			
HyPer	absolute H_2O_2	263	ratiometric single FP; molecular switch consists of OxyR regulatory domain
mt-cpYFP	changes in superoxide	262	intensity-based
ATP sensors			
Ateam-1.03	absolute $[ATP]_i$	313	FRET-based; K_D(ATP) = 3.3 mM
Ateam-3.10	absolute $[ATP]_i$	313	FRET-based; K_D(ATP) = 7.4 μM
ATP/ADP ratio sensor			
Perceval	ratio of ATP to ADP	266	ratiometric single FP
glutamate sensors			
FLIPE-Y family members	extracellular [glutamate]	319	FRET-based; $Y = K_{d,app}$ (glutamate)
FLIP^{81}E-1 μ	extracellular [glutamate]	318	FRET-based; ECFP(1−232) inserted at residue 81; K_d (glutamate) = 1 μM
SuperGluSnFR	extracellular [glutamate]	321	FRET-based; S73T mutation reduces the affinity of YbeJ/Glt1 for glutamate, improving its ability to detect physiologically relevant [glutamate]
sugar sensors			
FLIPglu-Y series	absolute $[glucose]_i$	318, 501	FRET-based; $Y = K_{d,app}$ (glucose), range = 170 nM to 600 μM
FLIP^{N}glu-Y series	absolute $[glucose]_i$	318	FRET-based; X = site of ECFP insertion, Y = glucose affinity; 19 derivatives in total (see ref 318 for details)
FLIPmal-Y series	absolute $[maltose]_i$	502	FRET-based; $Y = K_{d,app}$ (maltose), range = 2−225 μM
FLIPrib-Y series	absolute $[ribose]_i$	503	FRET-based; $Y = K_{d,app}$ (ribose), 250 nM−12 mM
zinc ion sensors			
eCALWY series	absolute $[Zn^{2+}]_i$	323	FRET-based; $K_{d,app}$ (Zn^{2+}) range = 2 pM−3 nM
Cys_2His_2- and His_4-Zn^{2+} sensors	absolute $[Zn^{2+}]_i$	325	FRET-based; $K_{d,app}$ (Zn^{2+}) range = 2 μM−200 μM
sensors of membrane potential			
FlaSh family members	membrane potential	270, 271	intensity-based; based on nonconducting Shaker K+ channel (W434F)
FlaSh-IR	membrane potential	271	intensity-based; based on "impulse-response" Shaker K+ channel (D6-46)
FlaSh-L366A	membrane potential	271	based on "low-threshold" Shaker K+ channel
FlaSh-CFP/ FlaSh-YFP	membrane potential	271	FRET-based (bimolecular); based on nonconducting Shaker K+ channel (W434F)
Flare	membrane potential	270	intensity-based; based on Kv1.4 K+ channel
VSFP1	membrane potential	272	FRET-based; based on Kv2.1 K^+ channel
VSFP1-cpEGFP	membrane potential	273	intensity-based; based on Kv2.1 K^+ channel
VSFP2.1, VSFP2.3	membrane potential	275, 504	FRET-based; a R217Q mutation shifts the voltage dependency of these sensors into the physiological range (∼−70 mV)
VSFP2.42	membrane potential	277	FRET-based (yellow/red)
Mermaid	membrane potential	276	FRET-based; FP reporter units are less sensitive to changes in pH than AvGFP derivatives used in VSFP2.1
VSFP3.1	membrane potential	275	intensity-based; activation time constant of 1.3 ms at 70 mV
SPARCS	membrane potential	274	intensity-based; based on Mu-1 Na^+ channel; activation time constant of 2.0 ms at 70 mV

Table 2. Continued

biosensor names	reporter of	ref	comments
small G-protein activation sensors			
RBD-CFP/CD8-YFP	Ras activation	343	FRET-based (bimolecular/bystander)
Raichu-Ras	Ras activation	346	FRET-based
Raichu-Rap	Rap activation	346	FRET-based
Raichu-Rac1	Rac1 activation	347	FRET-based
Raichu-Cdc42	Cdc42 activation	347	FRET-based
Raichu-CRIB	Rac1 or Cdc42 activation	347	FRET-based
Raichu-RhoA	RhoA activation	348	FRET-based
RhoA sensor	RhoA activation	350	FRET-based; unique design allows reversible interactions between RhoA in reporter and RhoGDI at the plasma membrane
Raichu-RBD	RhoGDI activity/ endogenous RhoA activation	348	FRET-based
Raichu-Ral	RalA activation	349	FRET-based
kinase activation sensors			
Akind	Akt/PKB activation	349	FRET-based; intrinsic molecular switch consists of AktΔ*HM*
GFP-PKB-RFP	Akt/PKB activation	356	FRET-based; intrinsic molecular switch
ReAktion	Akt/PKB activation	173	FRET-based; intrinsic molecular switch
GMB	MK2 activation	355	FRET-based; intrinsic molecular switch
Miu2	ERK2 activation/ MEK binding	354	FRET-based; measures binding of the upstream kinase, MEK, which leads to ERK2 activation
GFP-PDK1-RFP	PDK1 activation	356	FRET-based; intrinsic molecular switch
kinase activity sensors			
DKAR	PKD activity	505	FRET-based; engineered molecular switch
CKAR	PKC activity	367	FRET-based; engineered molecular switch
KCP1	PKC activity	368	FRET-based; intrinsic molecular switch
AKAR4	PKA activity	506	FRET-based; engineered molecular switch
CRY-AKAR	PKA activity	361	FRET-based ; CRY-AKAR utilizes a tunable FRET circuit composed of Cerulean → cpVenus → mCherry
BKAR	Akt/PKB activity	370	FRET-based; engineered molecular switch
Aktus	Akt/PKB activity	371	FRET-based; engineered molecular switch
Aktar	Akt/PKB activity	372	FRET-based; engineered molecular switch
Erkus	ERK activity	376	FRET-based; ERK docking domain from RSK3 attached at the C-terminus of Erkus contributes to specificity
EKAR	ERK activity	377	FRET-based; An ERK docking site (FQFP) C-terminal to the substrate domain contributes to specificity of EKAR
Phocus-2pp	InsR kinase activity	371	FRET-based; engineered molecular switch
Sinphos family members	InsR kinase activity	507	intensity-based; green-, cyan-, and yellow-sinphos utilize cpEGFP, cpECFP and cpCitrine, respectively
Srcus	Src activity	371	FRET-based; engineered molecular switch
Src reporter	Src activity	374	FRET-based; improved specificity for Src compared to first generation Src indicator
Picchu	general RTK activity	508	FRET-based; intrinsic molecular switch based on CrkII
Picchu-Z/EGFR-Z	EGFR activity	380	FRET-based; interaction between ZIPB1 on Picchu-Z and ZIPA2 on EGFR-Z forms an Picchu-Z/EGFR-Z signaling complex
EGFR Reporter	EGFR activity	373	FRET-based; engineered molecular switch
ECaus	EGFR activity	391	FRET-based; engineered molecular switch
PTB-EYFP, EGFR-ECFP	EGFR autophosphorylation	381	FRET-based (bimolecular)
FLAME	EGFR autophosphorylation	381	FRET-based; engineered molecular switch
Crk-based Reporter	Abl and EGFR activity	373	FRET-based; responsive to both EGFR and Abl in vitro
ATOMIC	ATM activity	369	FRET-based; engineered molecular switch
Aurora B kinase sensor	Aurora B kinase	375	FRET-based; engineered molecular switch
cyclinB1-CDK1 sensor	cyclinB1-CDK1 activity	379	FRET-based; engineered molecular switch
H3 phosphorlyation reporter	histone H3 phosphorylation	509	FRET-based; this sensor recognizes phosphorylation of S28 on Histone H3

Table 2. Continued

biosensor names	reporter of	ref	comments
phosphatase activity sensor			
CaNAR1	calcineurin activity	383	FRET-based; intrinsic molecular switch based on NFAT1 regulatory domain
OGT activity sensor			
O-GlcNAc Sensor	O-glycosylation	384	FRET-based; engineered molecular switch
protease sensors			
caspase-3 activity sensor	Caspase-3 activity	359	FRET-based; DEVD molecular switch
CFP-*c3*-YFP-*c6*-mRFP	caspase-3/caspase-6 activity	360	FRET-based; DEVD linker is specifically cleaved by Caspase-3 while VEID linker is specifically cleaved by Caspase-6
MTI-MMP biosensor	MT1-MMP activity	510	FRET-based
histone acetylation/methylation sensors			
K9 Reporter	histone H3 (K9) methylation	386	FRET-based; engineered molecular switch
K27 Reporter	histone H3 (K27) methylation	386	FRET-based; engineered molecular switch
Histac	histone H4 acetylation	387	FRET-based; engineered molecular switch
cell cycle reporter			
Fucci	cell cycle progression	393	intenstiy-based; changes in fluorescence are due to ubiquitin-dependent degradation of Cdt1 (during S/G2/M) and Geminin (G1)
sensor of neurotrophic factor			
Becell	extracellular [BDNF]	391	coupled cell-based FRET reporter system
strain sensors			
TSMod	mechanical strain	511	FRET-based; "elastic domain" derived from the spider silk protein flagelliform functions as a molecular spring to sense strain
stFRET	mechanical strain	512	FRET-based; sensor domain is composed of a rigid 5 nm α-helical linker
PriSSM	mechanical strain	513	intensity-based; utilizes proximity imaging (PRIM) to detect strain-induced dissociation of two GFP molecules, GFP and cpGFP174, joined by a flexible linker

analysis allows the location of old versus new copies of a protein to be distinguished by pulse-chase analysis. In this way, researchers have been able to generate high-resolution images of protein trafficking events inside cells.[137]

2.2.2. Fluorogen Activating Proteins. Another genetically encodable fluorescent labeling technology that holds great promise for biosensor development utilizes fluorogen-activating proteins (FAPs) (Figure 4b). FAPs are derived from single-chain antibodies (scFvs) that range in size from 11 and 30 kDa.[140] Like the tetracysteine/biarsenical system, FAPs dramatically increase the fluorescence intensity of exogenous fluorogenic dyes (termed "fluorogens") by constraining the chromophore in a rigid conformation that prevents the dissipation of excited state energy as rotational energy.[140] In general, FAPs have been evolved to bind a particular fluorogen species. For example, whereas a FAP specific for a sulfonated derivative of thiazole orange (TO1) binds its ligand with nanomolar affinity (K_d = 3 nM), it failed to associate with a malachite green derivative (MG-2p) that interacts strongly with another FAP.[140] The reciprocal experiment showed similar selectivity of the second FAP for its MG-2p ligand, suggesting that these FAP/fluorogen pairs are amenable to coimaging studies.

On the other hand, the binding pockets of some FAPs are somewhat less discriminating. For instance, though the FAP "K7" was evolved to associate with the bulky cyanine dye, dimethylindole red (DIR), its large binding pocket can also accommodate a number of smaller fluorogens containing a variety of chemical modifications.[131] This promiscuity was exploited by Özhalici-Ünal et al. who synthesized a series of TO1 derivatives that, when complexed with K7, exhibited emission maxima that spanned most of the visible and near-IR regions of the electromagnetic spectrum.[131] Likewise, a particular FAP, termed L5-MG, was recently shown to bind various MG-based fluorogens.[140] Interestingly, each L5-MG/fluorogen pair exhibited different affinities, fluorescence intensities, and/or excitation/emission spectra. Thus, because of their broad substrate specificity and the unique spectral properties of their varied fluorogens, both the L5-MG and K7-TO1 FAP systems are well-suited for pulse-chase analysis.

It is important to recognize that, in principle, both the FAP and its fluorogen can be tuned, by molecular evolution and chemical engineering, respectively, to yield a wide variety of FAP/fluorogen pairs with unique spectral and biophysical properties desirable for live cell imaging. Such versatility is one of the primary

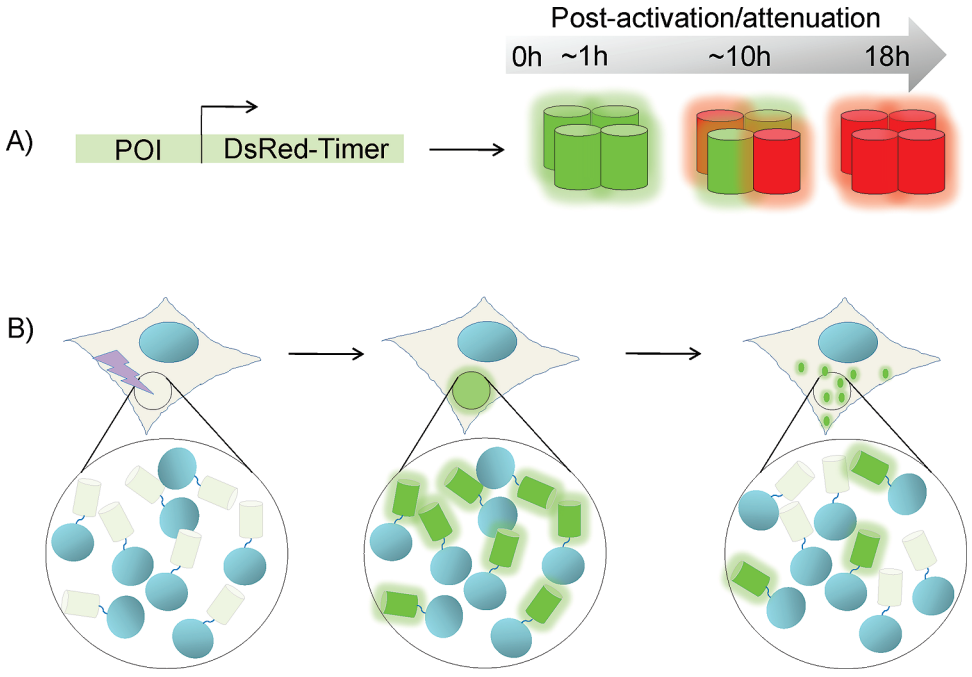

Figure 5. Genetically encodable fluorescent tools for studying protein expression/dynamics. (A) When placed under the control of a promoter-of-interest (POI), the maturation of DsRed-Timer from green to red, which occurs over a known period of time, provides information about the timing of promoter activation and attenuation. (B) Fluorescent highlighters composed of a protein-of-interest (blue ovals) and a PI-FP family member (cylinders) allow the movement of subpopulations of tagged proteins to be tracked over time. Here, irradiation with UV−violet light (lightning bolt) within a defined cellular region converts PA-GFP from a nonfluorescent state to a highly fluorescent form, allowing the movement of activated protein-PA-GFP chimeras to be tracked over time.

advantages of this system. However, until recently, the number of subcellular locales to which FAP-tagged proteins could be targeted was limited to nonreducing environments, such as those found on the cell surface or within secretory pathways.[131,140] This was because all known FAPs (which are only a subset of the complete complement of scFvs) contained internal disulfide bonds that could only form in an oxidizing environment. However, building on the finding that some scFvs can be engineered to function properly in the reducing environment of the cytoplasm,[141−143] Fitzpatrick et al. recently developed a FAP, termed H6.2-MG, that can be paired with the MG-2p fluorogen to image intracellular processes, as well.[518]

2.2.3. SNAP- and HALO-Tags. O^6-alkylguanine-DNA-alkyltransferase (hAGT) and a mutated form of bacterial halogene dehalogenase typify the final group of intracellular labeling techniques (Figure 4c). These enzymes irreversibly transfer their substrates to reactive residues located in the active site.[144,145] In the case of hAGT, nucleophilic attack by an activated cysteine residue covalently links the benzene moiety of O^6-benzylguanine (BG) to the enzyme.[145] Because of the open architecture of its active site, hAGT's rate of catalysis is unaffected by conjugation of a wide variety of functional groups to the benzene ring of BG at the para position.[145−147] The same versatility is observed for halogene dehalogenase, which normally mediates dehalogenation of haloalkane chains in *R. rhodochrous*.[144,145] In this case, substitution of Phe for His272 prevents hydrolysis of a covalent ester intermediate formed between the alkane chain of the substrate and Asp106.[145,148] This traps the enzyme in a conjugated state by prohibiting dissociation of the ligand.

Both hAGT and halogene dehalogenase have been optimized to form specific enzyme−substrate complexes quickly and efficiently in cells.[145,148,149] Therefore, when used as fusion tags, these enzymes are well-suited to covalently label a protein-of-interest within the cellular environment. This is the basis of the commercially available SNAP-tag and HaloTag systems which utilize hAGT and halogene dehalogenase fusion tags, respectively.[145,147−150] Since attachment of the probe is catalyzed by the fusion tag itself, these methods are highly specific and exhibit excellent signal stability. Importantly, the enzymatic activity of neither hAGT nor halogene dehalogenase is regulated by auxiliary factors, allowing these methods to be used to label proteins in nearly any cellular locale, including regions that are contiguous with both the cytoplasm and the extracellular environment.[148,151] However, like FPs, the size of hAGT and halogene dehalognase (182 and 293 amino acids, respectively) may be problematic in some contexts. As a consequence, certain cellular processes may not be amenable to imaging using these systems.

Nevertheless, as alluded to earlier, what these systems "lack" in size, they make up for in versatility. In fact, as a testament to the flexibility of the hAGT system, over twenty BG derivatives have been described to date.[152,153] These include BG derivatives conjugated to a diverse set of functional groups, ranging from fluorescent dyes to bifunctional protein cross-linking agents to biotin affinity handles.[147,154] The latter permits SNAP-tagged proteins to be conjugated to highly fluorescent quantum dot (QD) nanocrystals.[155] Though they do not readily traverse the plasma membrane, QDs are characterized by several impressive photophysical properties which make them ideal for single molecule imaging on the surface of living cells. For instance, QDs exhibit excellent photostability, ϕ values near unity, and ε's up to 100 times greater than those of small molecule fluorescent dyes and FPs.[139] Moreover, the high electron-density of their CdSe cores allow correlated electron microscopic (EM) detection of QD-conjugated molecules following cell fixation.[156]

Importantly, the versatility of their ZnS shells permits QD probes to be ligated to a number of protein-targeting molecules, conferring them with a high degree of specificity. For example, streptavidin-conjugated QDs have recently been targeted to biotinylated proteins on the cell surface using bacterial biotin ligase,[157] suggesting that biotin-BG derivatives attached to hAGT could be a powerful tool for QD-mediated imaging of cell surface processes.

Though most of the genetically targetable chemical labeling strategies discussed above have only been developed within the past decade, they have already begun to make important contributions to our understanding of cellular physiology.[74,130,137,138,158] In particular, the unique biophysical and spectroscopic properties of these labeling systems hold great promise for the future development of genetically encodable biosensors. For instance, because the ligands used by these systems are amenable to derivatization through chemical engineering, many existing small molecule fluorescent dyes may be converted to genetically targetable probes through conjugation to a "targeting" ligand specific for a genetically encoded tag. This strategy has already been successfully applied to the study of local Ca^{2+} dynamics using both the tetracysteine/biarsenical[138] and SNAP-tag/BG systems.[159] Moreover, these labeling systems may also be used to create biosensors based on novel design principles. To this end, the Johnsson laboratory recently described a SNAP-tag-based reporter system that is able to monitor protein/ligand interactions in the absence of a conformational change in the protein.[160] Instead of utilizing conformational changes in an attached protein module like all previously described FRET-based biosensors (see section 3.2.3.3), this reporter system, which is composed of a FP flanked on either end by a SNAP-tag and a metabolite binding protein, relies upon displacement of a tethered ligand to alter the FRET efficiency between the FP and a fluorophore built into the tether. Displacement of the ligand may be accomplished through competition with endogenous ligands or by inhibitor molecules, making this system well-suited for studying dynamic changes in the concentration of cellular metabolites and for drug screening and development. Importantly, because it does not require a conformational change in the protein to alter the FRET efficiency between the fluorophores, this system is predicted to be generalizable to measure a wide variety of metabolites.[160] However, since the tethered ligands utilized by this system are cell impermeable, for the time-being, these types of biosensors are restricted to studying fluctuations that occur at the cell surface.[160]

3. FLUORESCENT BIOSENSORS FOR STUDYING DYNAMIC SIGNALING PROCESSES

Together, the genetically targetable fluorophores described above equip researchers with a powerful set of molecular tools that can be used to build fluorescent biosensors to probe cellular components within their native environment (Table 2). These biosensors have been used to monitor a multitude of cellular processes, offering valuable insights into the dynamic nature of the signaling, metabolic and other regulatory networks that govern cell function. Below, we highlight the design and application of a series of fluorescent biosensors, ranging from relatively simple sensors designed to measure changes in the expression, localization, or turnover of cellular proteins in the cellular milieu (collectively, termed "intracellular protein dynamics") to more complex reporter systems designed to probe biochemical processes, such as second messenger turnover and enzyme activities, within their native cellular environment.[161]

3.1. Monitoring Protein Dynamics in Living Cells

Throughout its lifetime, a cell must continuously monitor both its internal and external environments and react accordingly. At the molecular level, the cellular response to environmental stimuli can be manifested in several different ways. One strategy employed by cells to modulate their behavior is to regulate the relative concentrations of the proteins responsible for a particular activity. This can be accomplished by varying either the global or the local protein concentration (or both) of a given gene product. While the global concentration of a protein species is dependent upon both its expression level and its rate of degradation, the local concentration is dictated by additional factors, such as molecular scaffolds and targeting sequences, which direct the protein to a given subcellular locale. Because of its importance to many aspects of cell signaling, the study of intracellular protein dynamics (which describes the ways in which cellular protein populations change in time and cellular space) has become an active area of research within the signaling community. Until recently, intracellular protein dynamics were generally studied using methods, such as isotopic pulse-chase analysis and immunofluorescence, which only provide a snapshot of the highly dynamic signaling networks underlying cellular behavior. However, with the advent of the fluorescent tools highlighted below, real-time analysis of protein dynamics inside individual cells has become a reality. Together, these studies have helped add a critical spatiotemporal element to our understanding of intracellular protein networks.

3.1.1. Monitoring Protein Expression. Many signaling pathways ultimately lead to changes in gene expression. Therefore, to better understand how gene expression is controlled in response to various cellular stimuli, it is important to characterize the timing of promoter activation. FP-based transcriptional reporters have proven to be valuable tools for studying transcriptional activity. In fact, one of earliest uses of GFP as a biological probe involved the in vivo visualization of promoter activation in *C. elegans*.[5] During these studies, GFP cDNA was placed under the control of the *mec-7* promoter and GFP gene expression was measured during different stages of nematode development.[5] Over the years, similar studies have been conducted in a variety of cellular contexts, offering valuable information about the activation and regulation of cellular promoters. However, it is important to note that, while the stability of GFP inside the cell ($t_{1/2}$ = ~1 day)[162,163] allows the activation of weak promoters to be measured using this approach, this property of the fluorophore can be a double-edged sword of sorts. Indeed, the persistence of GFP molecules long after transcription has stopped may also mask transient changes in gene expression. One way to overcome this limitation is to fuse a degradation sequence, such as the PEST domain from mouse ornithine decarboxylase (MODC), to the FP indicator.[164] Using this strategy, the fluorescent half-life of an EGFP-MODC chimera was reduced nearly 12-fold, to approximately two hours. The increased temporal resolution afforded by this probe allowed the observation of transient changes in NF-κB-mediated gene expression that could not be observed using longer-lived EGFP reporters.[164] Moreover, with the development of rapidly maturing GFP variants, such as superfolder GFP,[37] Venus,[59] or DsRed-Express2,[165] the temporal resolution of this approach may be further improved by substituting one of these variants for the EGFP indicator.

Fluorescent timers (FTs), whose spectral properties change over a set period of time, also provide an attractive means of visualizing promoter activation inside cells (Figure 5a). Because they utilize a ratiometric readout to monitor promoter dynamics, these reporter systems are less susceptible to artifacts stemming from differences in cell thickness and morphology that often plague intensity-based methods. The first FT was developed based upon a DsRed variant termed DsRed-E5 (DsRed/V105A/S197T).[166] This variant, also known as DsRed-Timer (Clonetech, Inc.), transitions from green to red fluorescence in a known amount of time (~18 h) because of the slow conversion of its fluorophore from a green *p*-HBI-like intermediate to the mature red species. By measuring the ratio of red to green fluorescence (R/G), researchers can deduce the timing of promoter activation/termination (e.g., a low R/G implies recent activation of the promoter, while high R/G suggests transcription has been attenuated).

More recently, Subach and colleagues described a series of monomeric FTs derived from mCherry.[167] These probes, which consist of fast-, medium-, and slow-versions, mature from a blue- to a red-emitting species over distinct time periods ranging from ~2.5 to 18 h.[167] Unlike DsRed-Timer, whose tetrameric oligomerization state limits its utility as a fusion tag, the mCherry derivatives are not expected to dramatically alter the intracellular behavior of their protein partners. Therefore, in addition to promoter activation, these probes represent potentially powerful tools for monitoring the timing (and spatial organization) of other dynamic cellular processes, such as protein trafficking and degradation. Indeed, as we will see below, similar approaches based upon different genetically targetable fluorophores have recently made important contributions to our understanding of the spatiotemporal aspects of protein dynamics.

3.1.2. Measuring Protein Turnover. Traditionally, pulse-chase experiments using ^{35}S-labeled methionine have been used to track the turnover of a particular protein species within a population of cells. However, because the cells must be lysed prior to analysis, this approach offers little information about the spatial aspects of protein turnover. Moreover, it cannot be conducted in real-time at the single cell level. In contrast, the flexibility of several recently developed fluorescent tags allows "fluorescence pulse-chase" experiments to be performed inside single living cells. Such studies not only allow newly synthesized proteins to be distinguished from older ones, but they also offer insights into the spatial regulation of protein turnover. Several of these methods are discussed below.

When fused to a cellular protein-of-interest, the biological half-life of a FP mirrors that of its fusion partner.[164,168] As a consequence, FP-chimeras have been used to measure the stability of many proteins in a variety of cellular contexts. This approach is particularly useful if the rate of synthesis/degradation of a given protein species changes with time. For instance, experiments using FP-tagged proteins have shed light on the turnover of regulatory elements involved in meiosis and cell cycle progression.[169,170] However, since newly synthesized fusion proteins also contribute to the measured fluorescence intensity, standard "static-color" FPs are ill-suited for measuring the rate of protein degradation under steady state conditions. Fluorescent highlighters, as well as the recently developed mCherry-based FTs, offer an elegant solution to this problem. Because these techniques allow older copies of a tagged protein species to be distinguished from newer ones based upon the spectral properties of their fluorescent tag, specific subpopulations of proteins can be tracked within the cell over time. For instance, mCherry-based FTs hold great potential for studying the spatiotemporal aspects of protein turnover, particularly for proteins that exhibit biological half-lives ranging from a few hours to approximately one day.[167] Since these probes rely on the spontaneous transition of their chromophores from a blue- to a red-emitting species, aside from expression of the protein-FT chimeras themselves, no further manipulation of the cellular system under study is required when using this approach. It should be noted, however, that while this property ensures that the entire population of tagged proteins matures at the same rate, it also prevents the fate of select subpopulations of tagged proteins from being tracked apart from the larger population.

On the other hand, fluorescent highlighters, whose PI-FPs can be acutely activated within a defined subcellular region or at a specific time point, offer researchers the flexibility to monitor the turnover of a specific subpopulation of proteins over time (Figure 5b). To this end, the green-to-red photoconvertible PI-FP, Dendra2, was recently used to perform light-induced pulse-chase photolabeling experiments at the single cell level.[171] During these studies, Dendra2 was fused to the NFκB inhibitor, IκBα, and expressed in HEK293 cells. Upon photoactivation, pre-existing Dendra2-IκBα molecules were converted from a green- to a red-emitting species whose rate of decay could be tracked in response to phorbol 12-myristate 13-acetate (PMA), a known agonist of the IκBα degradation pathway. Importantly, since newly synthesized chimeras fluoresced green, de novo synthesis of the fusion protein had no effect on the measured rate of decay of the photoconverted molecules.

Similarly, the tetracysteine/biarsenical system is well-suited to track protein turnover inside living cells with high spatiotemporal resolution. During a tetracysteine/biarsenical pulse-chase experiment, cells expressing a tetracysteine-tagged version of the protein under study are incubated with one type of biarsenical dye, say FlAsH. Since the engineered tetracysteine motif exhibits high affinity for its biarsenical ligand, existing copies of the tagged proteins will be labeled within minutes.[135] Importantly, once the uncongugated dye molecules have been washed away, the remaining fluorescent complexes are stable for several days. This property allows newly synthesized proteins to be distinguished from older ones following the addition of a second biarsenical dye, such as ReAsH. According to this scheme, researchers can monitor the turnover (and relative position) of old vs new protein species based upon the distribution of red- and green-labeled proteins. Using this approach, Gaietta and colleagues demonstrated that newly synthesized connexin43 molecules are incorporated at the periphery of existing gap junctions, while older copies of the protein are removed from the center of the channel.[137] Similar results were also obtained using fluorescence recovery after photobleaching (FRAP) and fluorescence recovery in photobleaching (FLIP) to track the movement of GFP-tagged connexin43 molecules.[172] It is important to note that the exquisite spatial resolution afforded by these approaches would not be possible using traditional radiolabeling techniques. Indeed, the ability to highlight a specific population of proteins and to track their fate over a defined period of time underscores the utility of these labeling methods for studying protein turnover. Though still in their infancy, these approaches offer researchers a series of powerful, noninvasive methods for studying protein stability within the endogenous cellular environment.

3.1.3. Tracking Protein Localization. As illustrated by the above discussion, the ability to visualize protein

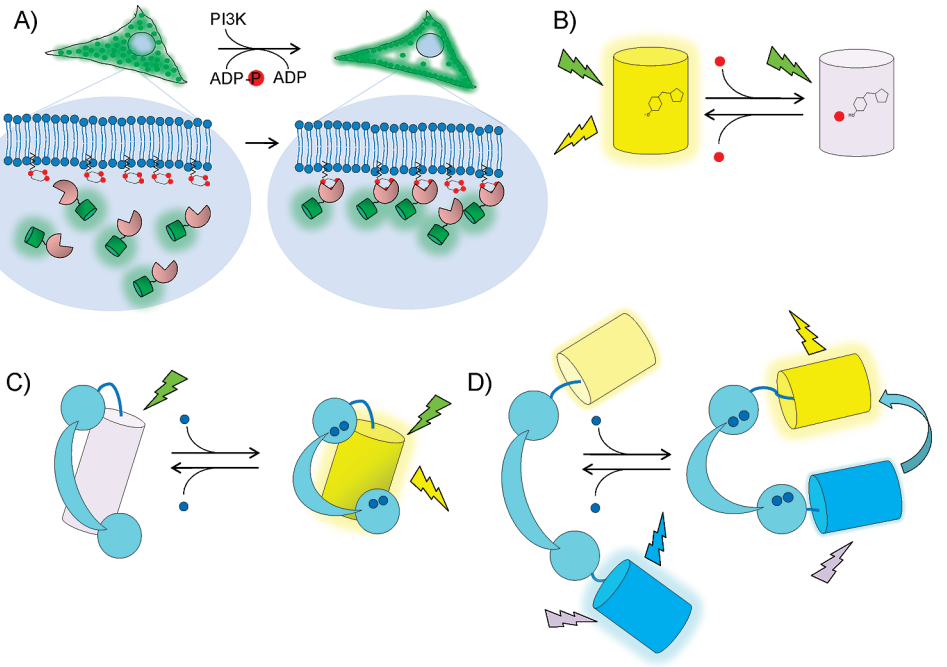

Figure 6. Fluorescent biosensors to probe biochemical changes within the cellular environment. (A) Localization-based probes for studying lipid dynamics. This example depicts the relocalization of a PtdIns(3,4,5)P_3 probe based on the PH domain of Akt (pink pacman) tagged with GFP (green cylinder) from the cytosol to the plasma membrane following generation of PtdIns(3,4,5)P_3 by PI3K. (B) A pH/halide sensor based on EYFP. Decreases in intracellular pH and/or increases in halide ion concentration (red ball) stabilize the neutral chromophore species, leading to a reduction in fluorescence. (C) Basic design of a single FP-based biosensor. In the example shown, in the "off" state, the sensor unit induces strain on the architecture of an attached FP reporter unit that reduces the fluorescence intensity of the FP. Upon ligand binding (blue circles), the sensor unit undergoes a conformational change that relieves the strain, leading to increased fluorescence in the "on" state (e.g., Camgaroo-2[58] and HyPer[263]). Alternatively, conformational changes in the sensor unit can alter the excitation or emission profile of the FP reporter unit, permitting ratiometric measurements (e.g., ratiometric pericam[237]). (D) Basic design of a FRET-based biosensor. Conformational changes in the sensor unit caused by ligand binding or post-translational modification alter the distance and/or orientation of the attached FP FRET pair, resulting in changes in the efficiency of energy transfer between them (blue arrow).

expression/degradation profiles in real-time and at single-cell resolution has the potential to provide valuable insights into the mechanisms governing critical cellular activities. Equally important to the proper execution of intracellular signaling cascades is the spatial organization of the cellular machinery. For instance, over the past decade, it has become clear that compartmentalization of signaling molecules (via scaffold proteins, for example) can profoundly influence both the specificity and the timing of many signal transduction pathways. As outlined below, fluorescent tags have helped to reshape our notions about the spatial organization and dynamic reorganization of the cellular environment.

Over the years, genetically encodable fluorescent tags have been used extensively to study the localization and redistribution of fluorescently tagged proteins in response to various cellular stimuli. In many cases, these analyses are aided by the translocation of tagged molecules from one subcellular compartment to another. For instance, GFP chimeras have been used extensively to study the translocation of protein kinases such as Akt[173−176] and protein kinase C (PKC)[177−181] from the cytoplasm to the plasma membrane following specific stimulation. Likewise, FP-based reporters have shed light on the dynamic regulation of the nucleocytoplasmic shuttling behavior of several transcription factors, such as NFκB[182−184] and nuclear factor of activated T-cells (NFAT) family members,[185−188] that play a central role during the immune response. Though these types of studies are relatively straightforward, they can provide important information about the timing and coordination of protein translocation patterns.

Recently, the development of super-resolution microscopy techniques, such as photoactivated localization microscopy (PALM), fluorescence PALM (FPALM), stimulated emission destruction (STED), and stochastic optical reconstruction microscopy (STORM), has revolutionized our understanding of protein localization patterns and cellular architecture. With the exception of STED, these imaging methods rely upon the photoconversion of photoinducible fluorescent molecules which act as point scatterers to break the diffraction limit of ~200 nm for light microscopy. Using these approaches, researchers have achieved 20 nm resolution in biological systems.[189] While STORM utilizes photochromic dyes such as rhodamine, diarylethenes and photoswitchable cyanines that must be conjugated to the protein-of-interest in vitro (or perhaps targeted to the protein in cellulo using one of the chemical labeling methodologies described in section 2.2), the PI-FPs employed by PALM and FPALM (e.g., Eos2, Dronpa, and PS-CFP2) can be genetically fused directly to a target protein. Though most super-resolution microscopy studies to date have been conducted in fixed cells, several groups have recently extended this approach to live cells.[190−193] These studies, which tracked dynamic cellular processes at 40−75 nm resolution, have the potential to offer unprecedented insights into the assembly and redistribution of cellular machinery. For an in-depth discussion of the past, present and future of live cell super-resolution microscopy, the interested reader is referred to excellent reviews by Fernandez-Suarez and Ting[189] and Huang et al.[194]

PI-FPs are also powerful tools for monitoring protein movement inside the cell using conventional fluorescence microscopy. Indeed, since PI-FPs exhibit an easily detectable change in their spectral properties following irradiation with light of a specific wavelength and intensity, fluorescent highlighters can be used in combination with time-lapse imaging to track the movement of cellular proteins in response to a variety of cellular ques. Importantly, the contrast afforded by PI-FPs offers distinct advantages over traditional photobleaching techniques, such as FRAP, for studying a variety of cellular processes—particularly when the density of the protein-of-interest is high. This notion is illustrated by a recent study designed to measure microtubule dynamics during mitosis. Because of difficulties detecting photobleached marks in regions of high microtubule density, rather than using FRAP, Tulu et al. elected to follow the distribution of α-tubulin molecules conjugated to PA-GFP during mitosis.[195] These studies demonstrated that, in addition to the predominantly inward movements typically observed using standard fluorescence microscopy, some microtubules migrated away from the poles. This unexpected finding suggests that microtubule transport may be regulated by the activities of antagonistic motors. Importantly, the authors noted that this behavior likely went undetected during previous imaging studies because such infrequent motions are difficult to detect when all the microtubules are uniformly fluorescent. Indeed, only when the contrast of the images was enhanced by using fluorescent highlighters to monitor a relatively small number of α-tubulin molecules could such motions be observed.

The high contrast afforded by PI-FPs also allows quantitative analyses to be performed in the context of live cells. Indeed, by probing the movement of a small pool of photoactivated chimeras, the kinetic properties of a protein-of-interest can be measured directly within the endogenous cellular environment.[102,196] To this end, PS-CFP was fused to human dopamine transporter (hDAT) and used to study hDAT trafficking in the filapodia of living cells.[102] After irradiation with a 404 nm laser line, both the direction and rate of movement of photoactivated PS-CFP-hDAT molecules could be measured amidst a pool of unactivated molecules. These studies demonstrated that hDAT moves rapidly toward the cytoplasm, reaching speeds of nearly 25 nm/second.[102] Such behavior suggests that hDAT is actively transported within filapodia via a retrograde transport system. More recently, Fuchs and co-workers introduced mIrisFP, a green-to-red photoconvertable PI-FP that also exhibits reversible photoswitching behavior in both the green and the red states.[197] These characteristics render mIrisFP uniquely amenable to pulse-chase analysis at the "super" resolution afforded by PALM. For instance, using a paxillin-mIrisFP fusion protein, the authors were able to track both the assembly and disassembly of individual focal adhesion molecules during cell migration. Interestingly, these studies suggest that both the assembly and disassembly of individual focal adhesions occur over a similar time interval of ~300 s.[197]

Importantly, the unique properties associated with PI-FPs make fluorescent highlighters suitable for studies that are intractable using conventional imaging techniques. For example, because of its ability to be repeatedly turned on and off, the reversible PI-FP, Dronpa, can be used to monitor dynamic cellular processes that occur on a rapid time scale.[117,196] In an innovative study, Ando and co-workers fused Dronpa to Erk1 to explore its nucleocytoplasmic shuttling behavior. These studies demonstrated that, after EGF stimulation, the nuclear import of Erk1 was greatly enhanced. Surprisingly, the nuclear export of Erk1 was also increased at a similar time point, suggesting a more dynamic model of nucleocytoplasmic shuttling than the widely accepted notion that a decrease in nuclear export accounts for the accumulation of Erk1 in the nucleus.[117]

3.2. Monitoring Biochemical Changes within the Cellular Environment

To this point, we have focused on the utility of fluorescent biosensors for monitoring the turnover/redistribution of proteins within the cellular environment. However, this approach can also be extended to probe the regulation of other important signaling molecules inside the cell. Under these circumstances, changes in the distribution or spectral properties of fluorescently tagged proteins can be used to track biochemical changes in the subcellular environment. For instance, if a protein (or protein domain) that specifically recognizes a small molecule-of-interest is conjugated to a fluorescent tag, changes in the subcellular localization of the chimera can often be correlated with fluctuations in the local concentration or distribution of the small molecule under study. In other cases, through protein engineering efforts, the fluorophore itself can be modified in such a way that its spectral properties are altered in response to specific cellular factors. In the following section, we will examine the properties of these types of probes and explore some of the ways in which they have been used to track changes in the biochemistry of live cells.

3.2.1. Monitoring Signaling Molecules Using Translocation Probes. Members of the first type of biochemical biosensors utilize changes in the subcellular distribution of fluorescently tagged protein domains to gain insights into the relative concentrations of a specific signaling molecule (Figure 6a). Such translocation-based sensors have been particularly useful for studying the turnover of membrane lipids involved in the regulation of cell signaling pathways. For instance, our understanding of the spatiotemporal aspects of phosphoinositide (PI) dynamics has greatly benefited from a series of PI probes designed to measure the distribution of various PI species at the plasma membranes of individual cells. These probes, which generally consist of a FP fused to the effector domain[198] of one of several PI-binding proteins, rely upon migration of the probe to the plasma membrane following the generation of the PI species under study (reviewed in refs 199 and 200). In theory, the ability of the effector domain to selectively bind a particular PI species confers a high degree of specificity to these types of sensors. However, it is important to note that, since the binding specificities of the effector domains are generally determined in vitro, when placed in the context of live cells, factors other than PIs can also impact their subcellular distribution (for an insightful discussion on this topic, see ref 200). Nonetheless, provided that the proper controls are instituted, the data obtained from these types of experiments can be quite informative. A classic example of how this approach has been used to dissect critical spatiotemporal aspects of PI dynamics was described by Servant et al., who developed a PI probe to study PtdIns(3,4,5)P_3 generation in neutrophils after exposure to chemoattractants.[201]

Neutrophils are motile cells that respond to chemoattractants, even in shallow chemoattractant gradients. To address the role of PtdIns(3,4,5)P_3 in morphologic polarity, the PH domain of Akt was fused to GFP (PH^{Akt}-GFP) and used to monitor PtdIns(3,4,5)P_3 production.[201] While the authors observed that a uniform concentration of the chemoattractant, *N*-formyl-Met-Leu-Phe (fMLP),

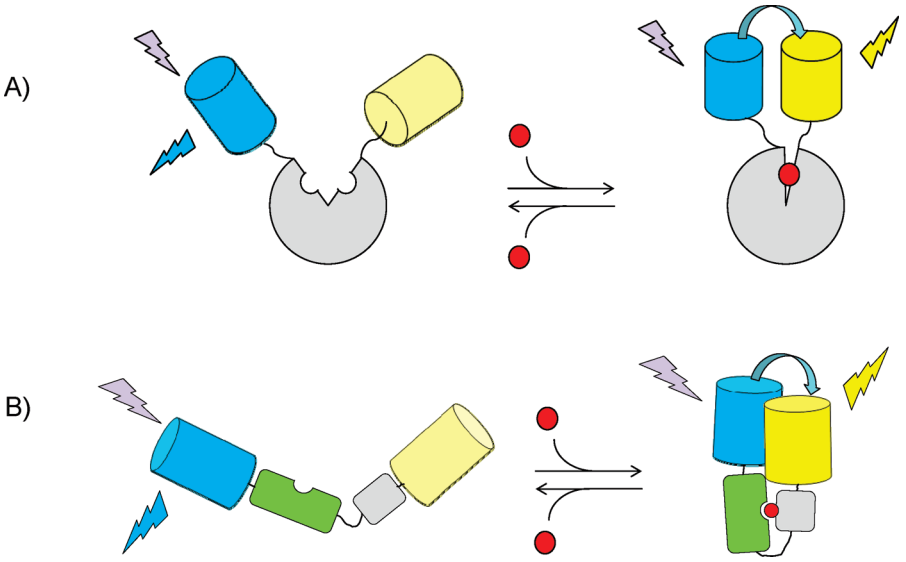

Figure 7. Origins of a molecular switch. A molecular switch can be generated by either (A) a conformational change intrinsic to a protein or protein domain or (B) by an engineered conformational change driven by interactions between a receiver module (gray block) and a switching module (green block). In each case, the conformational change is converted to a change in FRET efficiency (blue arrow) by altering the distance and/or orientation of the attached FP reporter units (cylinders). Alternatively, a single FP may serve as the reporter unit, as in Figure 6c.

led to translocation of PH^{Akt}-GFP to the plasma membrane throughout the cells, a gradient of fMLP caused translocation of the reporter exclusively to parts of the cell that received the strongest stimulation. Interestingly, these studies also demonstrated that the internal cellular gradient of PtdIns(3,4,5)P_3 was at least six times steeper than the extracellular chemoattractant gradient, underscoring the amplification of the signal by a "cellular compass system" composed of factors such as the phosphatidylinositol 3-kinase, PI3K, and other signaling molecules.[201]

More recently, a similar approach was used to track changes in the distribution of the membrane phospholipid, phosphatidylserine (PS), during phagosome maturation.[202] Like PIs, PS is a negatively charged phospholipid found on the cytoplasmic face of developing phagosomes. Though both types of lipids are believed to play a role in the conversion of phagosomes into degradative organelles by mediating interactions between phagocytic vesicles and various signaling proteins, little is known about how the distribution of each species changes throughout the maturation process. This is due, in large part, to the fact that, until recently, no suitable probe existed to visualize real-time changes in PS inside live cells. To create such a PS probe, various FP color variants were fused to the discoidin-type C2 domain of lactadherin, a milk glycoprotein that binds PS in a Ca^{2+}-independent manner.[203] Together with several PI probes, these PS reporters have helped uncover important clues about the roles that each lipid species may play during phagosome maturation. For instance, researchers showed that while other polyanionic phospholipids, such as PtdIns(4,5)P_2 and PtdIns(3,4,5)P_3, disappear either before or almost immediately after phagosome formation, PS appears to persist at high levels throughout the maturation process.[202] Interestingly, when cells were infected with viral pathogens that subvert maturation away from the endolysosomal pathway, PS was no longer detectable in the phagocytic vesicles.[202] Together, these data support the notion that, while both PS and PI species may help coordinate the early stages of vesicle formation, PS plays a central regulatory role throughout the entire maturation process, particularly during the later stages of phagosome development.

3.2.2. Probes That Rely upon the Direct Sensitization of Fluorescent Proteins. In addition to the "monochromic", localization-based indicators described above, FP-based reporters that change their spectral properties in response to cellular parameters have also been used extensively to study the regulation of many cellular processes. While in some cases these types of sensors exploit photophysical properties intrinsic to the FP tags themselves, in others, the spectral properties of the chromophore are altered by distorting the β-barrel architecture of the FP using integrated protein sequences that are sensitive to the signaling molecule under study. Below we highlight several biosensors within each class, focusing on their specific design features as well as their utility for studying biological phenomena.

3.2.2.1. Halide Sensors. Unlike wild-type *A. victoria* GFP, whose spectral properties remain relatively unchanged over a wide range of physiological conditions, the mutations introduced into many engineered FP variants often render them sensitive to fluctuations in the cellular environment. For example, because of changes in their internal hydrogen bonding networks, the chromophores of EGFP and several EYFP family members fluoresce very weakly in the protonated state. As a consequence, cellular components that promote protonation of *p*-HBI, such as hydronium or halide ions, can lead to markedly reduced fluorescence intensities. This intrinsic property has been exploited to measure several important cellular parameters, including pH and chloride ion concentrations (Figure 6b).

Several GFP variants have been successfully used to study changes in the concentration of halide ions within the cellular environment. The most straightforward of these probes are composed of a single fluorophore whose fluorescence intensity decreases as the halide ion concentration increases. For instance, as mentioned earlier, many YFP variants are highly sensitive to halide ions because of ground-state binding of the halide in the vicinity of the chromophore. In particular, the YFP variant, YFP(H148Q), exhibits a dramatic reduction in its fluorescence intensity at elevated halide concentrations. This property has been exploited to monitor fluctuations in chloride ion (Cl^-)

concentration in cells overexpressing the Cl^- transporter, cystic fibrosis transmembrane regulator (CFTR).[204] These studies demonstrated that YFP(H148Q) faithfully reports Cl^- flux through the CFTR in response to elevations in intracellular cyclic 3′,5′-adenosine monophosphate ($[cAMP]_i$), providing an attractive alternative to chemical halide dyes. Interestingly, YFP-based halide sensors can be tuned to selectively detect a particular ion. For instance, by substituting Leu for Ile at position 152, the YFP (H148Q)-based Cl^- sensor was made more sensitive to I^- ions.[205] In fact, due to its increased affinity for I^-, YFP(H148Q, I152L) exhibits an approximately 30-fold selectivity for I^- over Cl^-. This feature has made YFP(H148Q, I152L) a useful sensor for monitoring I^- uptake via a sodium-iodide symporter.[206]

Of course, the primary disadvantage of intensity-based probes for live cell imaging is that they are susceptible to variations stemming from differences in probe concentration or cell thickness. To overcome these limitations, a series of ratiometric FRET-based indicators have been developed to measure intracellular Cl^- concentrations ($[Cl^-]_i$).[207,208] The first of these, termed Clomeleon, was generated by linking the YFP variant, Topaz, to a halide-insensitive CFP donor.[207] This reporter, which is characterized by $K_{app,Cl}$ of 160 mM and only marginal pH-sensitivity at $[Cl^-]_i < 50$ mM typical of most cell types, has been used to measure $[Cl^-]_i$ in a variety of cellular contexts.[207,209−212] More recently, Markova and colleagues created a modified version of Clomeleon, termed Cl-sensor, by replacing Topaz with an EYFP variant, EYFP/H148Q/I152L/V163S, that exhibits high sensitivity to Cl^- ions within the physiological range (K_{app} = ∼30 mM).[208]

In some respects, Clomeleon and Cl-sensor work much like the intensity-based sensors described above, that is, increases in Cl^- concentration quench the YFP moiety, reducing its fluorescence intensity. However, in these FRET-based probes, since CFP fluorescence is unaffected by Cl^- ions, Cl^--dependent quenching of the acceptor (YFP) leads to recovery of the donor (CFP) fluorescence. Since the stoichiometry of the donor and acceptor is fixed in these probes, changes in the Cl^- concentration can be detected as a change in the donor (CFP) to acceptor (YFP) emission ratio, which is, by definition, a unitless measure. As a consequence, these probes are largely immune to differences in cell shape and sensor concentration. Importantly, whereas intensity-based probes are generally only able to measure *changes* in $[Cl^-]_i$, a ratiometric measure allows FRET-based Cl^- probes to be calibrated in such a way that the absolute $[Cl^-]_i$ can be measured over a wide range of probe concentrations.[207,209] Together, these properties make Clomeleon and Cl-sensor well-suited for measuring $[Cl^-]_i$ in neurons and other cells with complex geometries. To this end, Clomeleon was placed under the control of the neuron-specific promoter, thy1, and used to measure synaptic inhibition in brain slices isolated from a variety of neuronal regions, including the hippocampus, deep cerebrallar nucluei and the amygdala.[209] These studies, which permitted changes in postsynaptic $[Cl^-]_i$ associated with the activity of inhibitory synapses to be quantitatively measured for the first time, demonstrated that $[Cl^-]_i$ nearly doubles, from 5 to ∼9 mM, in hippocampal pyramidal cells following repetitive activation of inhibitory synapses.[209] It is believed that such fluctuations could underlie some forms of ionic plasticity exhibited by neuronal networks.

3.2.2.2. pH Sensors. Like the FP-based Cl^- sensors described above, genetically encodable pH sensors represent valuable tools for studying cellular processes. These types of sensors have been used to visualize changes in intracellular pH gradients as well as for measuring the pH of several subcellular compartments (reviewed in ref 213). Location-specific genetically encodable pH probes, which include both ratiometric[214−217] and intensity-based indicators,[217−220] are typically generated by appending subcellular localization sequences to GFP mutants that exhibit pH-dependent changes in their absorbance and emission spectra. Using this approach, researchers have been able to measure pH fluctuations in a number of subcellular regions, including the cytoplasm, the medial/trans-Golgi,[220] the mitochondrial matrix,[220,221] the mitochondrial intermembrane space[222] and the endoplasmic reticulum.[223] Importantly, the choice of the specific FP used in these types of sensors is dependent upon the properties of the organelle under study. For instance, while EGFP (pK_a = 6.15) is well-suited for the detection of pH fluctuations within acidic organelles, EYFP (pK_a = 7.1) is preferable in more basic environments like the mitochondrial matrix where equilibrium pH values are closer to 8.0.[220]

Many important cellular processes are associated with changes in pH. As a consequence, FP-based pH sensors can also provide valuable information about the timing and regulation of these events. For instance, to monitor vesicle exocytosis and recycling, Miesenbock and co-workers used structure-directed combinatorial mutagenesis to generate several pH-sensitive mutants of EGFP, collectively termed pHluorins.[224] By fusing the pHluorins to vesicle membrane proteins, the authors were able to correlate pH changes with synaptic vesicle regeneration and exocytosis at individual synaptic boutons. In this way, the "synapto-pHluorins" provide a powerful tool for studying the dynamics of vesicle formation and regeneration. In another study, the ratiometric EYFP-based pH indicator, E^2GFP, was used to measure cellular pH at different stages of the cell cycle in CHO cells.[214] These studies demonstrated that while the cellular environment appears to be relatively alkaline during mitosis, it becomes more acidic as the daughter cells transition into G_1 phase.[214] Such fluctuations in pH are thought to impact the activity of a variety of signaling molecules involved in cell cycle progression.

3.2.3. Engineered Indicators That Do Not Directly Perturb Fluorescent Protein Fluorescence. In addition to environmental parameters such as pH and halide ion concentration, FP-based biosensors can be engineered to directly sense other small molecules critical to cellular function. However, rather than relying solely on point mutations to alter FP fluorescence, this type of sensitization often involves extensive engineering efforts. In general, engineered fluorescent biosensors contain two basic components: (1) a "sensor unit", which senses a specific cellular analyte and (2) a "reporter unit", which generates a fluorescent readout (Figure 6c, d). In the case of FP-based sensors, the reporter unit usually consists of a pair of FPs that undergo FRET or a single FP whose photophysical properties are altered in response to a conformational change in the sensor unit. Meanwhile, the sensor unit can assume many forms provided that it promotes a conformational change in response to the small molecule under study.

Sometimes a sensor unit can be constructed by introducing residues on the surface of a FP variant that renders it sensitive to a particular cellular parameter. This is the basis for a class of redox-sensitive FP indicators, termed roGFPs, which use disulfide bond formation between pairs of strategically placed cysteine residues on the surface of GFP to alter the β-barrel architecture of the protein[225−227] (reviewed in ref 228). In the case of roGFP2, structural analysis suggests that the formation of a disulfide bond between the engineered cysteine residues promotes

reorganization of two β-strands in close proximity to the chromophore, causing subtle rearrangements in the residues surrounding the chromophore.[225] These conformational changes ultimately shift the equilibrium between the neutral (A) and phenolic (B) states of the chromophore, resulting in reciprocal changes in the excitation maxima at 400 and 480 nm in response to changes in the redox potential.[225] As genetically encodable and genetically targetable redox sensors, roGFP family members, as well as the related rxYFPs,[229] have proven to be valuable tools for measuring the redox potential of many subcellular compartments, including the cytosol,[225] mitochondria,[225] the ER,[230] and endosomes.[231]

Though roGFPs and rxYFPs employ a relatively simple sensor unit to sense changes in the cellular environment, in general, more complex sensor units are required to convert changes in other cellular parameters into a fluorescence output. Under these circumstances, a "molecular switch" can be derived from a conformational change intrinsic to an endogenous protein or it can be generated via an engineered switch (Figure 7). Engineered molecular switches, which are constructed based on a modular design, consist of a "receiver" module that specifically recognizes the small-molecule-of-interest linked to a "switching" module that converts the binding event into a conformational change (Figure 7b). By combining the molecular switch with an appropriate reporter unit—either by flanking the switch region with complementary RET pairs or by grafting it into the FP itself—small molecule-dependent changes in the sensor unit can be translated into a fluorescence readout from the reporter unit. Using this basic design, researchers have constructed a diverse set of FP-based biosensors capable of probing a large number of small molecule analytes involved in cellular signaling.

Below, we examine several FP-based biosensors designed to detect a particular analyte within the cellular milieu. For clarity, we have divided these sensors into two classes, single fluorophore sensors and RET-based reporter systems, according to the number of fluorescent moieties contained in their reporter unit. However, as we will see, certain design features, particularly those found in the sensor unit, are often shared by reporters within different classes. This is because many of the engineering strategies used by one class of reporters to generate the conformational switch have been borrowed or adapted for use in sensors within the other class. To illustrate this point, and to highlight some of the general design principles important for the construction of fluorescent biosensors, we will first explore the evolution of a series of genetically encodable reporters designed to measure changes in the ubiquitous second messenger, Ca^{2+}. During this discussion, we will highlight reporters that utilize both single-fluorophore and dual-fluorophore designs, paying special attention to the similarities and differences between them. We will then turn our attention to the development of sensors designed to detect changes in other small molecules inside the cell, focusing first on single-fluorophore reporters and then on RET-based biosensors.

3.2.3.1. Evolution of genetically encodable Ca^{2+}sensors. The first genetically encodable Ca^{2+} indicator (GECI), termed cameleon-1, was generated by sandwiching a fusion protein composed of the C-terminus of calmodulin (CaM) and the CaM-binding peptide, M13, between the FP FRET pair, BFP and GFP(S65T).[232] Previous studies using NMR spectroscopy had shown that, when exposed to Ca^{2+}, the CaM-M13 fusion protein is converted from an extended, dumbbell-like conformation to a highly compact structure[233] This conformational change is utilized by cameleon-1, as well as several related single-fluorophore Ca^{2+} sensors (see below).[234−237] In the case of cameleon-1, Ca^{2+}-induced conformational changes in the CaM−M13 fusion are converted into an increase in FRET efficiency between its flanking FPs by changing the relative distance and orientation of their fluorophores. As a consequence, changes in FRET can be correlated to fluctuations in intracellular Ca^{2+} ($[Ca^{2+}]_i$) by measuring the ratio of donor to acceptor fluorescence when the donor is excited (i.e., the emission ratio). Moreover, because several point mutations are known to impact the affinity of CaM for Ca^{2+}, the sensitivity of cameleon-1 and its derivatives can be tuned to measure Ca^{2+} over a wide range of concentrations, ranging from 10^{-7} to 10^{-4} M.[232]

As a prototype biosensor, cameleon-1 demonstrated the feasibility of using a genetically encodable reporter to measure fluctuations of small molecules that do not directly affect FP fluorescence. Nonetheless, several features of the reporter limited its utility for live cell imaging. For instance, though cameleon-1 was acutely sensitive to changes in Ca^{2+} concentrations in vitro, the poor photophysical properties of its BFP donor resulted in weak fluorescence and a low signal-to-noise ratio when the probe was expressed in mammalian cells.[232] Therefore, in order to increase the brightness of the sensor and to reduce the effects caused by autofluorescence, the BFP/GFP FRET pair was replaced with ECFP and EYFP, respectively, yielding a "yellow cameleon" (YC) more suitable for live cell imaging applications.[232] Unlike its predecessor, YC faithfully detected fluctuations in $[Ca^{2+}]_i$ induced by a variety of stimuli. Importantly, because the CaM−M13 interaction is readily reversible, YC was also found to be sensitive to the ebb and flow of Ca^{2+} ions inside the cell. As a testament to the targetability of this construct, YC and its derivatives have been used to measure transient changes in $[Ca^{2+}]_i$ in a variety of subcellular locales, including secretory vesicles,[238] caveolae[239] and the endoplasmic/sarcoplasmic reticulum.[240−242]

Despite its utility as a genetically targetable biosensor, Ca^{2+} imaging using YC proved more difficult within certain cellular environments. For instance, when YC was targeted to the plasma membrane of hippocampal neurons, its dynamic range was markedly decreased.[243,244] This decline was attributed to high concentrations of CaM at the mouths of calcium channels, leading to nonproductive interactions between endogenous CaM and the peptide portion of the probe. Not only does endogenous CaM appear to reduce the sensitivity of early YC probes, but perhaps more importantly, overexpression of the reporter likely interferes with the proper function of endogenous CaM molecules. Therefore, to generate GECIs that are more suitable for measuring Ca^{2+} transients in regions of the cell where CaM is abundant, the Griesbeck and Tsien groups have both reduced the sensitivity of the sensor region to wild-type CaM.[243,244] However, they have done so in fundamentally different ways. Below, we examine each of their strategies and briefly highlight how the resulting biosensors have been used to measure Ca^{2+} transients under physiological conditions.

In the first approach, Heim and Griesbeck replaced the CaM−M13 molecular switch with a truncated form of the Ca^{2+}-binding protein, troponin C (TnC), to create the FRET-based indicator, TN-L15.[243] Since the sensor region of TN-L15 is derived from an endogenous protein that does not associate with CaM, the reporter does not experience any ill-effects stemming from endogenous CaM.[245−247] Moreover, the response of TN-L15 to changes in $[Ca^{2+}]_i$ is both large (the acceptor to donor

emission ratio increases 140% in the presence of saturating Ca^{2+}) and fast (the rate of Ca^{2+}-binding is diffusion-limited while the rate of dissociation is described by τ = 860 ms),[243] making it an attractive tool for studying rapid Ca^{2+} fluctuations in cell types such as cardiomyocytes and neurons. Indeed, improved versions of TN-L15 have recently been used to measure Ca^{2+} dynamics both in cellulo, in cardiomyocytes[247] and hippocampal neurons,[246] and in vivo, using transgenic mouse and fruit fly lines.[245,246,248] Importantly, the ability of TnC-based reporters to accurately measure Ca^{2+} dynamics in living animals is believed to be due, in large part, to the reduced sensitivity of their sensor region to endogenous CaM.[243,244]

Rather than changing the molecular switch all together, CaM−M13-based GECIs have also been made less sensitive to the effects of endogenous CaM by modifying the properties of M13 and CaM themselves. This was the approach taken by Palmer et al., who employed a "bump-and-hole" strategy to diminish interactions between wild-type CaM and the M13 peptide in the sensor while maintaining the sensitivity of the reporter. To this end, the authors first conducted an in silico alanine scan across M13 to identify points of interaction between CaM and the peptide. Several small, nonpolar amino acids found to be important for M13−CaM binding were then mutated to residues with bulky or charged side-chains to create steric "bumps" that lowered the affinity of wild-type CaM for the peptide. Finally, to reconstitute the molecular switch, corresponding "holes" were engineered into the CaM binding pocket, permitting specific interactions with the modified M13 peptide.[244] This approach led to the generation of D3cpv, a YC variant that was able to sense changes in $[Ca^{2+}]_i$ while exhibiting no adverse effects in the presence of high concentrations of wild-type CaM.[244] Indeed, D3cpv accurately reported changes in $[Ca^{2+}]_i$ when targeted to several subcellular regions, including the plasma membrane of hippocampal neurons.

Like TnC-based reporters, the decreased sensitivity of D3cpv to wild-type CaM also makes it a potentially valuable tool for measuring Ca^{2+} transients in vivo. In fact, when targeted to upper-layer cortical neurons via an adenoviral delivery system, D3cpv faithfully reported Ca^{2+} transients produced by single action potentials firing at rates of 1 Hz in living mice.[249] This is similar to the sensitivity reported for the most recent TN-L15 variant, TN-XXL, which was recently used to measure changes in $[Ca^{2+}]_i$ induced by action potentials as short as 10 Hz in motor neuron boutons of transgenic flies.[246] The ability to detect such subtle changes in $[Ca^{2+}]_i$ in intact animals has important implications for understanding the ways in which Ca^{2+} signals are coordinated under truly physiological conditions. Indeed, when combined with the ability of genetically encodable reporters to be targeted to specific cell types and/or subcellular compartments, these reporter systems promise to uncover important details about Ca^{2+} signaling largely inaccessible using other methods.

As its name suggests, D3cpv utilizes a cpVenus variant that dramatically improves dynamic range of the reporter. This strategy, which was first demonstrated in the case of YC3.60,[39] has been used to improve the sensitivity of many FRET-based reporter systems, including TN-L15 family members.[245,246] In the context of RET-based reporters, it is believed that circular permuation of a FP causes subtle changes in the relative orientation of the donor and acceptor chromophores, leading to an increase in FRET efficiency between the two.

Circular permutation of the FP reporter unit has also proven to be an effective strategy when designing single fluorophore reporter systems. However, the molecular basis for this effect appears to be quite different in the case of single FP reporters. For instance, two related sensors, the cpEGFP-based GCaMPs[234−236,250] and their cpEYFP-based cousins, the pericams,[237] are among the most popular single fluorophore GECIs. Like the cameleons, GCaMPs and pericams derive their Ca^{2+}-specificity from the CaM−M13 interaction. However, rather than sandwiching CaM-M13 between complementary FP FRET pairs, in these reporters the switch is grafted into a single cpFP variant—either cpEGFP (GCaMPs) or cpEYFP (pericams). In the presence of Ca^{2+}, the CaM−M13 interaction induces conformational changes in the reporter that result in a change in the fluorescence intensity of the chromophore. Two recent crystallographic studies, which each captured GCaMP2[234] in both the apo- and Ca^{2+}-bound states, provide a plausible mechanism for this behavior.[251,252] These studies demonstrated that, compared to its EGFP progenitor, the circular permutant utilized by GCaMP2 contains a small hole at the site of permutation.[251,252] The structural changes caused by this hole have two major effects: (1) the chromophore is exposed to bulk solvent, promoting protonization of the phenolate oxygen of the chromophore[252] and (2) the hydrogen bonding network that normally stabilizes the fluorescent phenolate species is disrupted.[251] Together, these effects likely contribute to the poor fluorescence intensity exhibited by GCaMP2 in the apo-state. Interestingly, in the presence of Ca^{2+}, CaM binds to M13 and induces conformational changes in the reporter that seal the channel, simultaneously blocking solvent exposure, re-establishing the hydrogen bonding network and stabilizing the fluorescent phenolate ion.[251,252] These studies, which provide important clues about the molecular mechanisms underlying the fluorescence intensity changes exhibited by GCaMP family members, will be critical for the rational design of improved reporter systems. To this end, the Looger laboratory recently used a combination of structure-guided mutagenesis and semirational library screening to create GCaMP3. GCaMP3 contains two point mutations in the cpEGFP reporter unit that improve the brightness of the fluorophore and a single N → D substitution in the CaM domain that increases its affinity for Ca^{2+} 1.3-fold.[250] As a consequence, GCaMP3 exhibits a larger dynamic range and signal-to-noise ratio than its GCaMP2 progenitor. These properties, coupled with its high degree of photostability, make GCaMP3 an attractive tool for long-term imaging studies aimed at understanding intracellular Ca^{2+} dynamics associated with learning and development in the brains of live animals.[250]

Like their RET-based counterparts, single fluorophore GECIs have been used to measure Ca^{2+} fluxes in a variety of cell types and even whole animals, offering valuable insights into the timing and regulation of Ca^{2+} transients during many cellular processes, including neuronal signaling and cardiac function. For example, expression of GCaMP2 in mitral and tufted neurons of the glomerulus was instrumental in dissecting the complex spatial activity patterns underlying murine olfactory codes critical to discriminating various odors from one another.[253] These studies, which used GCaMP2 to measure Ca^{2+} transients in defined populations of postsynaptic neurons, demonstrated that the identity of a given odorant is encoded by a distinct set of glomerulus cells.[253] While these studies utilized an untargeted version of GCaMP2, targeted versions of these sensors have also provided important information about Ca^{2+} dynamics within

various subcellular compartments. For instance, lipid raft-targeted GCaMP derivatives have been used to assess the degree of crosstalk between specialized microdomains located within the plasma membrane and subjacent "junctional" sarcoplasmic/endoplasmic reticula of mouse brain astrocytes and arterial smooth muscle cells.[254] Meanwhile, a ratiometric version of pericam, which exhibits a Ca^{2+}-dependent increase in its emission intensity when excited at 494 nm and a concomitant decrease when excited at 415 nm, has been used to characterize Ca^{2+} dynamics in mitochondria and the ER.[255−257] In these cases, the ability to track changes in $[Ca^{2+}]_i$ within discrete subcellular regions was particularly important because specific spatiotemporal patterns of Ca^{2+} are believed to encode distinct signals inside the cell.

The ability to measure changes in $[Ca^{2+}]_i$ in a defined subcellular region was also the impetuous for the development of a new type of GECI which is based not on FPs but on the tetracysteine/biarsenical system.[138] Indeed, perhaps one of the most tantalizing and as yet relatively untapped aspects of the tetracysteine/biarsenical system is its potential for targeting a diverse set of fluorescent indicators to specific subcellular locations. To this end, Tour et al. recently synthesized the Ca^{2+}-sensitive dye, CaGF, to monitor rapid changes in $[Ca^{2+}]$ dynamics generated by discrete microdomains located at the cell surface.[138] CaGF is a triple hybrid molecule composed of fluorescein conjugated to biarsenical substituents and the BAPTA-like chelator, APTRA. In the unbound state, CaGF is virtually nonfluorescent because of photoinduced electron quenching of the fluorescein moiety by APTRA. Binding of Ca^{2+} relieves this inhibition, causing a 10-fold increase in the fluorescence intensity of fluorescein. Because its biarsenical side chains target the indicator to tetracysteine motifs genetically fused to a protein-of-interest, CaGF is able to sense highly localized Ca^{2+} concentrations surrounding the tagged protein. Using this method, researchers were able to detect Ca^{2+} microdomains near the channel mouths of α_{1C} L-type calcium channels as well as "hot spots" of Ca^{2+} influx, each of which exhibited a heterogeneous pattern of responses.[138]

Together, RET-based and single fluorophore GECIs have enabled researchers to track Ca^{2+} dynamics in discrete cell types and within distinct subcellular regions. These studies have provided intriguing clues about the timing and regulation of Ca^{2+} signals and may soon help decipher the rich information embedded in Ca^{2+} oscillations and waves. In addition to these valuable biological contributions, the design and development of GECIs has laid the foundation for the construction of similar genetically encodable reporters designed to measure other cellular analytes involved in intracellular signal transduction. Below, we will examine several single fluorophore biosensors before turning our attention to RET-based systems.

3.2.3.2. Engineered Single-Fluorophore Biosensors.

3.2.3.2.1. Engineered Single-Fluorophore Sensors for Measuring cGMP Dynamics. Like Ca^{2+}, the second messenger, cyclic 3′,5′-guanosine monophosphate (cGMP), is a central regulator of a variety of cellular processes.[258] It has been hypothesized that compartmentalization of cGMP into discrete subcellular pools could be an effective means of controlling spatially restricted cellular processes. Therefore, in order to examine cGMP patterning in vascular smooth muscle (VSM) cells, a series of fluorescent indicators of cGMP (FlincGs) based on the regulatory domain of protein kinase G I (PKGI) was developed by the Dostmann laboratory.[259] These sensors, which consist of a cpEGFP variant fused to two cGMP binding sites derived from various regions of the PKG regulatory domain, were modeled after the Cygnet family of FRET-based cGMP biosensors (see section 3.2.3.3.1.2 below).[260,261] To probe changes in cGMP concentration over a wide range of conditions, FlincG family members have been engineered to bind cGMP with K_D's ranging from 35 nM (α-FlincG) to 1.1 μM (β-FlincG).[259] Nucleotide binding induces conformational changes in the PKG regulatory domain that lead to a corresponding increase in the fluorescence intensity of the reporter.[259] Importantly, each of the FlincG probes also exhibits a high degree of selectivity for cGMP relative to the chemically similar second messenger, cyclic 3′,5′-adenosine monophosphate (cAMP).[259] This specificity for cGMP, coupled with their rapid and reversible binding kinetics and relatively good pH stability, makes FlincGs well-suited for measuring cGMP inside cells. For instance, a FlincG probe with intermediate cGMP affinity, δ-FlincG (K_D = 170 nM), was used to examine the spatiotemporal patterning of cGMP in response to two different stimulants: (1) nitric oxide (NO), which activates soluble guanylyl-cyclases (GCs) in the cytoplasm, and (2) atrial natriuretic peptide (ANP), which activates transmembrane GCs. While NO treatment induced a global, but transient, elevation in cGMP concentrations, ANP caused sustained, spatially segregated increases in cGMP that localized exclusively to the plasma membrane.[259] Interestingly, the spatial segregation observed in response to ANP stimulation was abolished when cells were pretreated with the phosphodiesterase-5 (PDE5) inhibitor, sildenafil, suggesting that PDE5-mediated degradation is critical to maintaining local pools of cGMP following ANP-induction.[259]

3.2.3.2.2. Engineered Single Fluorophore Reporters for Measuring Reactive Oxygen Species. A growing body of evidence suggests that reactive oxygen species (ROS) play an important role in many physiological and pathological processes. Therefore, the ability to sense specific ROS species in living cells is highly desirable. However, until recently, the paucity of genetically targetable, species-specific ROS sensors has severely limited the study of ROS dynamics within the native cellular environment.[262] Fortunately, two genetically encodable ROS indicators that specifically sense either hydrogen peroxide (H_2O_2)[263] or superoxide ($O_2^{\bullet-}$)[262] have recently been described. These FP-based sensors have already uncovered tantalizing nuances of ROS dynamics in a variety of cell types.

Like the pericam series of Ca^{2+} indicators, the H_2O_2 sensor, HyPer, was generated by inserting cpEYFP into the regulatory domain of the H_2O_2 sensing bacterial protein, OxyR.[263] HyPer is similar to ratiometric pericam in that it exhibits reciprocal changes in the emission intensity at 520 nm when excited by 405 and 488 nm light.[263] Using this sensor, Belousov et al. observed fast and reversible changes in the fluorescence intensity of cpEYFP in HeLa cells after exposure to 50 μM H_2O_2. Moreover, HyPer could detect endogenous production of H_2O_2, as demonstrated by its response either to TRAIL in HeLa cells or to neuronal growth factor (NGF) in PC-12 cells. In the latter set of experiments, two types of responses to NGF were observed in different PC-12 cell populations. The first set of cells showed an immediate but transient production of H_2O_2. Meanwhile, the second set of cells were characterized by a biphasic response in which a small initial increase in H_2O_2 was followed by a larger, more sustained increase that eventually returned to basal levels.[263] Interestingly, the shape and duration of the second H_2O_2 peak was reminiscent of that observed in the first set of cells. Though the cellular mechanisms underlying this biphasic response are unclear, the detection of distinct responses from

two subpopulations of cells may have important implications for understanding cellular behaviors following oxidative stress. It is important to note that these two subpopulations of cells would not be discernible using conventional imaging methods.

To create a genetically encodable sensor that specifically measures intracellular $O_2^{\bullet-}$ species, Wang et al. took advantage of a serendipitous property of the cpEYFP variant used in the pericam indicators: specifically, they noticed that the fluorescence intensity of this cpEYFP variant increases over 4-fold in the presence of $O_2^{\bullet-}$.[262] When localized to the mitochondrial matrix of cultured adult cardiomyocytes via a targeting sequence from cytochrome C oxidase subunit IV (mt-cpYFP), this reporter was able to detect transient "flashes" of $O_2^{\bullet-}$ within discrete mitochondrion.[262] These flashes, which apparently arise from functional coupling between transient mitochondrial permeability transition pore openings and components of the electron transport chain, were very short, with the average flash peaking after only 3.5 s and dissipating with a half-time of just under 9 s.[262] Interestingly, $O_2^{\bullet-}$ flash frequency appears to vary substantially across different cell types. For instance, the $O_2^{\bullet-}$ flash frequency (defined as the number of events per 1000 μm^2 cell area per 100 s) varies ~15-fold between adult cardiomyocytes (frequency = 3.8 ± 0.5) and PC12 pheochomocytoma cells (frequency = 63 ± 6), suggesting that $O_2^{\bullet-}$ flashes are generated differently in different cell types.[262] The authors hypothesize that such differences could have functional consequences, perhaps by creating microdomains of high ROS concentration which could lead to the localized activation of high-threshold ROS signaling pathways that remain inactive in other areas of the cell where global ROS remains low.[262] Importantly, these studies also provided the first evidence that the destructive ROS bursts that occur during reoxygenation of cardiomyocytes following hypoxic stress are correlated with a flurry of mitochondrial $O_2^{\bullet-}$ flashes. Since the observed $O_2^{\bullet-}$ flurries are attenuated by pharmacological interventions that are known to reduce the damage associated with ischemia/reperfusion, such as preconditioning with adenosine, the authors propose that $O_2^{\bullet-}$ flashes may be used as a quantitative biomarker for disorders characterized by increased oxidative stress.[262]

3.2.3.2.3. Engineered Single-Fluorophore Sensors for Measuring ATP/ADP Ratio. In addition to serving as the primary energy source in cells, ATP also acts as a potent signaling molecule by coordinating the activities of many enzymes involved in the regulation of cellular energy status.[264,265] Inside the cell, ATP's regulatory effects are often dependent upon its concentration relative to that of the other major adenylate phosphates, ADP and AMP. To better understand how the ATP/ADP ratio changes under various physiological conditions, Berg and co-workers developed Perceval, an ATP/ADP indicator based upon the bacterial ATP-binding protein, GlnK1, and a circularly permutated version of Venus.[266] Perceval was created by first inserting cpVenus into the T-loop of GlnK1 and then optimizing the properties of the probe for live cell imaging via semirandom mutagenesis.[266] The design principle utilized by Perceval is analogous to that employed by the CaM-based probe, Camgaroo:[267] in the presence Mg-ATP, the T-loop is converted from an extended structure to a highly compact form[268] that is believed to relieve strain on the integrated cpVenus module. In Perceval, T-loop closure leads to reciprocal changes in cpVenus emission intensity when excited with 405 and 490 nm light.[266] Therefore, like ratiometric-pericam and HyPer, Perceval offers the advantage of a ratiometric readout. Importantly, Mg-ADP also elicits a change in the emission ratio of the probe; however, because of incomplete loop closure, this change is only about half that observed upon Mg-ATP binding.[266] As a consequence, Perceval can be calibrated to measure the relative ratio of ATP to ADP inside cells based upon competition between the two molecules for T-loop binding. As a proof of principle, the authors demonstrated that Perceval could detect global metabolic changes caused by the inhibition of glycolysis or the modulation of external glucose levels.[266] In the future, Perceval and its derivatives will be important tools for measuring variations in cellular metabolism, at both the cellular and the subcellular level, and for understanding the consequences that these fluctuations have on growth and signaling in normal and diseased states.

3.2.3.2.4. Engineered Single-Fluorophore Sensors for Measuring Membrane Potential. As illustrated in the examples described above, structural rearrangement of GFP family members can yield very sensitive fluorescent sensors capable of detecting dynamic changes in various cellular parameters with high spatial and temporal resolution. In the same way, direct sensitization of FPs can be used to monitor ion flux in cells. Because they can be targeted to specific cell types and allow changes in membrane potential to be measured in multiple cells simultaneously, these types of biosensors are extremely attractive tools for examining the propagation of electrical signals in excitable cells, such as kidney cells and neurons. In general, FP-based voltage sensors modulate fluorescence intensity of the FP reporter module by placing it between regions of an ion channel or voltage-sensitive protein that undergoes a conformational change in response to changes in the membrane potential (reviewed in ref 269). For example, the first FP-based voltage sensor was created by inserting a truncated form of *A. victoria* GFP into a nonconducting mutant of the potassium channel, Shaker. The resulting sensor, termed fluorescent Shaker or FlaSh (not to be confused with the biarsenical dye, FlAsH), exhibited a decrease in fluorescence intensity in response to changes in membrane potential.[270] Because the fluorescence emission of GFP was coupled to voltage-dependent structural rearrangements of the Shaker channel, FlaSh and its derivatives[271] can be used to monitor changes in membrane potential. However, with the exception of FlaSh-ElipticGFP, which exhibits a τ_{on} of ~5 ms,[269,271] the slow activation/deactivation kinetics of most FlaSh variants limits their ability to detect rapid changes in the membrane potential characteristic of many action potential trains.[269−271] Likewise, a single-FP version of the FRET-based voltage-sensitive fluorescent protein 1 (VSFP1),[272] which exploits voltage-dependent conformational changes caused by rotation of the fourth transmembrane segment of the voltage-gated potassium channel, Kv2.1, to alter the fluorescence intensity of an attached cpEGFP molecule, is plagued by a slow response.[273]

In contrast, two single FP-based voltage sensors exhibit response kinetics in the low millisecond time frame. The first of these, termed sodium channel protein-based activity construct (SPARC), is based upon the activation of the voltaged-gated sodium channel, Mu-1.[274] SPARC was created by fusing wild-type GFP within the first intracellular loop of the Mu-1 channel.[274] Because the gating of sodium channels is generally more rapid than that of potassium channels, SPARC faithfully reports depolarizing pulses as short as 2 ms.[274] As a consequence, though SPARC has a smaller overall response than FlaSh and VSFP1, its fast kinetics enable it to more accurately report changes in membrane potential that occur on a rapid time scale. More recently, Lundby and colleagues described VSFP3.1, a Cerulean-based voltage sensor that utilizes conformational

changes in the voltage-sensitive domain of the voltage sensor-containing phosphatase from *Ciona intestinalis* (*Ci*-VSP) to affect the fluorescence intensity of Cerulean.[275] The molecular mechanisms underlying the fluorescence changes observed in VSFP3.1 are believed to be similar to those utilized by the Kv2.1-based VSFP1; however, due to fast coupling between *Ci*-VSP gating and CFP fluorescence, VSFP3.1 is characterized by large response amplitudes and an activation time constant of just 1.3 ± 0.1 ms.[275] These properties make VSFP3.1 well-suited to measure the fast neuronal electrical signals often observed during signal propogation. Interestingly, the same molecular components used to create several single-FP voltage sensors, namely the voltage sensor domains from VSFP1 and VSFP3.1, have also been used to construct FRET-based voltage sensors.[273,275−277] As we will see below, RET-based biosensors represent another important class of fluorescent biosensors for probing the cellular environment.

3.2.3.3. RET-Based Biosensors. In addition to the single-fluorophore probes described above, RET-based biosensors have proven to be valuable tools for studying signaling dynamics within the cellular environment. These include both uni- and bimolecular reporter systems, each of which utilizes a molecular switch to convert activity-dependent changes in the reporter into a measurable RET response. In each case the molecular switch is designed to alter the distance or relative orientation of a RET pair in response to specific cellular cues. For instance, whereas most unimolecular biosensors rely upon a conformational change to reposition their fluorophores in space, bimolecular probes typically bring their RET pairs into close proximity via protein−protein interactions. It is important to note that these differences carry with them important consequences that must be considered when conducting live cell imaging experiments using RET-based biosensors.

One of the primary advantages of a bimolecular design is that the reporter typically exhibits a larger dynamic range than its unimolecular counterpart. Presumably, this phenomenon can be attributed to lower basal FRET caused by a large degree of separation between the donor and acceptor fluorophores in the unbound state.[232,273,275] However, despite this potential advantage, bimolecular RET-based reporter systems also present researchers with certain challenges not typically encountered when using unimolecular sensors. Chief among these is the requirement to strictly regulate the stoichiometric ratio between donor and acceptor molecules. This task is nontrivial considering the variability that often exists in parameters such as DNA transfection efficiency, transcriptional regulation and protein translation, to name a few. It can also affect the way that RET changes are measured when utilizing these biosensors. Indeed, when the stoichiometry of donor and acceptor fluorophores is fixed, as it is in the case of unimolecular probes, the donor-to-acceptor emission ratio is generally the easiest and most convenient means of measuring changes in RET.[278] On the other hand, if the stoichiometries between the donor and acceptor are variable, as is often the case when using bimolecular reporter systems, more sophisticated measures of RET efficiency, such as donor fluorescence recovery after acceptor photobleaching and fluorescence lifetime imaging (FLIM), must be used.[278] Moreover, because of the effects of diffusion, the large spatial separation between sensor halves in the "off" state has the potential to render bimolecular sensors less sensitive to the temporal regulation of cellular activities, particularly those that occur on a rapid time scale. Finally, when targeting a bimolecular reporter to a specific subcellular location, care must be taken to ensure that both sensor halves can access the same subcellular compartment. Nonetheless, as we will see below, both uni- and bimolecular RET-based reporter systems have been used effectively to probe the inner-workings of the cell, offering important information about the organization and regulation of signal transduction pathways.

3.2.3.3.1. RET-Based Sensors to Measure Small Molecule Second Messengers and Cellular Analytes. Aside from Ca^{2+}, RET-based biosensors have been used to monitor the turnover of other important second messengers and cellular analytes involved in signal transduction. Like the RET-based GECIs described above, these include genetically targetable probes capable of measuring the concentration of the small molecule-of-interest in real-time and at single-cell resolution. Below, we highlight some of these reporter systems, focusing on the properties that enable them to specifically monitor the production and degradation of these signaling molecules within the cellular environment.

3.2.3.3.1.1. RET-Based Sensors for Studying cAMP Turnover. As alluded to earlier, the ubiquitous second messenger cAMP plays a pivotal role in regulating a variety of cellular processes. Inside the cell, it is believed that discrete pools of cAMP are constantly being shaped and reshaped by the opposing actions of adenylate cyclases (AC) and phosphodiesterases (PDEs) to create highly dynamic and compartmentalized signaling activity. Though the notion of cyclic nucleotide compartmentalization was first proposed nearly thirty years ago to explain the distinct physiological outcomes associated with the activation of transmembrane ACs by different G-protein coupled receptors (GPCRs),[279] it was not until recently, with the advent of genetically targetable biosensors, that the existence of distinct pools of cAMP could be visualized at the single cell level.[280,281] So far, several RET-based biosensors have been developed to better understand how the concentrations of this second messenger fluctuate over time and throughout the cell. These include bimolecular cAMP indicators based on the PKA holoenzyme[282−284] as well as unimolecular reporter systems derived from various portions of the guanine nucleotide exchange factor, exchange protein activated by cAMP (Epac).[282,285−287] Together, these sensors have greatly enhanced our understanding of compartmentalized cAMP signaling in a number of cellular contexts.

The first genetically encodable reporter used to study cyclic nucleotide dynamics in live cells was developed based upon the cAMP-dependent protein kinase, PKA.[283] PKA exists as a heterotetramer comprised of two regulatory subunits (either RI or RII) and two catalytic subunits. The binding of cAMP induces a conformational change in the regulatory subunit that causes dissociation of the catalytic subunits from the complex. Therefore, to create a bimolecular reporter of cAMP dynamics, researchers fused the catalytic subunit and the regulatory RII β-subunit of PKA to GFP and EBFP, respectively.[283] In the presence of elevated cAMP levels, dissociation of the catalytic subunit from the regulatory complex resulted in a decrease in FRET. More recently, an improved version of this cAMP sensor was created by replacing GFP and EBFP with the more efficient FRET pair, CFP and YFP.[284] Using this second generation sensor, Zaccola and Pozzan demonstrated that increases in intracellular cAMP concentrations were not homogeneous in cardiac myocytes, suggesting the presence of distinct cAMP signaling domains.[280,281]

While PKA-based biosensors have proven useful for studying the compartmentalization of cAMP pools, their mode of action

also presents several obstacles to tracking dynamic changes in $[cAMP]_i$. For instance, because two cAMP molecules must bind each regulatory subunit before the catalytic subunit is released, PKA-based probes are hampered by slow response kinetics at low cAMP concentrations.[288] This effect may be compounded by mixed tetramers caused by nonproductive interactions between fluorescently tagged and endogenous components of the PKA holoenzyme, the formation of which is also expected to decrease the dynamic range of the reporter. Finally, it is worth noting that the presence of an intact kinase domain in PKA-based probes has the potential to perturb cellular cAMP dynamics by impacting feedback mechanisms involved in cAMP regulation.[289] As a consequence, several intramolecular cAMP reporters have been developed based upon another cAMP effector, Epac1 and −2.[282,286,287] These reporters, termed indicator of cAMP using Epac (ICUE),[286,292,459] CFP-Epac (δDEP-CD)-YFP,[287] Epac1-camps,[282] and Epac2-camps,[201,282] all exhibit decreasing FRET following cAMP binding. Presumably, the binding of cAMP induces an intrinsic conformational change in Epac isoforms that liberates the catalytic domain from intrasubunit allosteric inhibition, thereby altering the distance and relative orientation of their flanking CFP/YFP FRET pairs.[290,291] Importantly, since the Epac-based reporters contain only one cAMP binding site and are therefore not susceptible to artifacts stemming from cooperative cAMP binding, they are able to rapidly and accurately report changes in $[cAMP]_i$.[282,287] Furthermore, mutations have been introduced to abolish the guanine exchange factor (GEF) activity of Epac, thereby reducing the effects that overexpression of the biosensor may have on cellular signaling pathways.

Compared to the PKA-based cAMP indicators, the unimolecular design of Epac reporters also offers several other advantages. For instance, these unimolecular reporters do not require the expression levels of CFP- and YFP-fusion proteins to be matched to one another. Moreover, subcellular targeting of the Epac-based reporter molecules is much easier due to their unimolecular design.[286,287] The latter feature has permitted the visualization of discrete pools of cAMP within various subcellular regions, including the nucleus, cytoplasm, mitochondria, plasma membrane[286] and even submicroscopic nanodomains, such as lipid rafts and intracellular signaling complexes.[289,292] Together, these types of studies have begun to uncover important details about the role of subcellular compartmentalization in shaping cAMP dynamics during GPCR activation. For instance, the type I (RI) and type II (RII) isoforms of PKA are known to be targeted to specific signaling complexes through their association with A-kinase anchoring proteins (AKAPs). Since AKAPs also bind other signaling molecules involved in the formation of cAMP gradients, it has been suggested that RI and RII are activated by distinct pools of cAMP generated by unique combinations of cAMP-metabolizing enzymes localized to a given signaling complex. To test this hypothesis, researchers targeted the Epac1-camps reporter to two AKAPs, ezrin and AKAP79, which specifically bind the RI or RII isoforms of PKA, respectively.[289] In this way, changes in cAMP levels could be measured within RI- and RII-associated regions following treatment with various GPCR agonists.[289] These studies demonstrated that, in neonatal cardiomyocytes, the β-adrenergic receptor agonist, isoproterenol, induces more pronounced elevations in cAMP within RII-associated regions than in those associated with RI.[289] In contrast, several GPCR agonists, including prostaglandin-E_1 (PGE_1), generated cAMP pools that were restricted primarily to the RI-associated regions.[289] These differences appear to be mediated, at least in part, by the PDE isoforms, PDE2 and 4, which were found to degrade cAMP within the RI- and RII-associated signaling complexes, respectively.[289] Importantly, the observed differences in cAMP within each region could have functional consequences during PKA signaling. For example, while isoproterenol treatment led to increases in the phosphorylation status of several downstream substrates of PKA, stimulation with PGE_1 failed to induce a similar increase in the phosphorylation levels of the same substrates, even at concentrations ten times higher than those used to induce changes in RI-specific cAMP pools.[289] Together with similar studies designed to probe cAMP dynamics within other nanodomains, these findings highlight one of the ways in which spatially restricted signaling complexes can confer specificity to a relatively promiscuous kinase, such as PKA.

Interestingly, the spatiotemporal resolution afforded by genetically encodable fluorescent biosensors has also helped researchers uncover compartmentalized cAMP pools generated by the same agonist/receptor pair. For instance, using intact thyroid follicles isolated from transgenic mice expressing the Epac1-camps reporter, the Lohse group recently demonstrated that the thyroid signaling hormone (TSH) receptor remains active following internalization.[293] Intriguingly, the cAMP pools generated by internalized TSH receptors appear to regulate signaling pathways distinct from those triggered at the plasma membrane. This finding, which suggests that GPCR/agonist complexes may form intracellular signaling platforms with unique cellular outcomes following internalization, challenges long-held notions about the consequences of receptor internalization during cell signaling.[293,294]

Finally, by replacing the CFP donor in Epac-based sensors with *R.* Luc, several groups have created cAMP reporters that utilize BRET as the fluorescent readout.[285,295] Though until recently their emission intensity has prevented BRET-based sensors from being used to measure biochemical changes at the subcellular level,[296] BRET-based cAMP reporters have proven to be powerful tools for examining drug effects in cell populations in a medium- to high-throughput manner and for screening fluorescent compounds whose excitation/emission profiles preclude the use of FRET-based probes.[295] For instance, using a BRET-based cAMP biosensor derived from the second generation ICUE reporter, ICUE2, the Caron laboratory recently examined the impact of nine clinically effective antipsychotics on D2 class dopamine receptor (D2R) activity.[295] Though all clinically effective antipsychotics are believed to act via the D2R GPCR pathway, which reduces cAMP production by coupling to inhibitory $G_{i/o}$ proteins in the cell, it is unclear what impact these drugs have on G-protein-independent pathways, such as those involving β-arrestin. Therefore, to better understand the mode of action of each drug, the authors first used their BRET-based ICUE2 reporter to examine the intrinsic and the antagonistic activities of each compound on the $G_{i/o}$ pathway.[295] These data demonstrated that while nearly all of the drugs acted as inverse agonists with similar efficacies, they exhibited a much wider range of potencies when their antagonistic activities toward quinpirole-induced cAMP inhibition were measured (though all were antagonists).[295] Interestingly, using a parallel BRET assay designed to measure β-arrestin/D2R interactions, the authors discovered that even though each antipsychotic also potently inhibited quinpirole-induced recruitment of β-arrestin to the D2R, the majority of compounds did so with a markedly lower

K_B than that observed for the $G_{i/o}$ pathway. The apparent differences in antagonistic potency between the two pathways provide a plausible mechanism by which cells can discriminate one signaling pathway from the other.[295]

3.2.3.3.1.2. RET-Based Sensors for Studying cGMP Dynamics. In addition to cAMP reporters, RET-based cGMP reporters have also contributed to our understanding of the ways in which fluctuations in cyclic nucleotide concentrations regulate signaling pathways inside cells.[297,298] These types of sensors can be broadly divided into two classes based upon the origins of their sensor unit. The first group of reporters exploits cGMP-induced conformational changes in the regulatory region of PKGI to change the distance or orientation of attached FP fluorophores. For instance, the sensor unit of the Cygnet series, which are some of the earliest and most popular members of this class, consists of an N-terminally truncated version of PKGI containing two tandem cGMP binding sites and the kinase domain of PKGI.[260,261] A T516A mutation renders the kinase domain catalytically dead in second generation Cygnets, reducing the adverse effects caused by overexpression of the reporter. Importantly, the Cygnets are highly selective for cGMP over cAMP.[260,261] For example, the most recent Cygnet family member, Cygnet 2.1, exhibits a >600-fold selectivity for cGMP over cAMP.[299] This reporter has been used to study cGMP dynamics in a variety of cellular contexts, including the kinetics of NO-induced cGMP transients in vascular smooth muscle cells.[300] More recently, a similar PKGI-based probe lacking the kinase domain, termed "cyclic GMP indicator with an EC_{50} of 500 nM" (cGi-500), was used in conjunction with a modified Epac2-camps reporter to unravel the interplay between cGMP and cAMP during meiotic arrest in mouse oocytes.[298] These studies demonstrated that luteinizing hormone promotes the closure of gap junctions between the oocyte and neighboring mural granulosa cells, limiting the diffusion of cGMP into the oocyte. The resulting drop in $[cGMP]_i$ within the oocyte (from ~1 μM to ~40 nM) appears to relieve cGMP-mediated inhibition of PDE3A, causing a decrease in cAMP levels that ultimately leads to resumption of meiosis.[298]

The second family of FRET-based cGMP reporters was developed using the cGMP binding domain of PDE5.[299,301] The molecular switch utilized by this family of sensors relies upon conformational changes in either one or both of the GAF[302] domains of PDE5. For instance, the most prominent member of this class, cGES-DE5, contains a single GAF domain, GAF A, sandwiched between ECFP and EYFP.[299] Like the Cygnets, cGES-DE5 preferentially binds cGMP, exhibiting a >400-fold selectivity for cGMP over cAMP.[299] Because of its large dynamic range, faster binding kinetics and rapid reversibility, cGES-DE5 may be used to monitor subtle and rapid changes in cGMP levels.[299] For instance, when cells transfected with either Cygnet2.1 or cGES-DE5 were exposed to intermittent doses of the NO-donor, sodium nitroprusside (SNP), those cells expressing cGES-DE5 showed transient changes in soluble GC-mediated cGMP levels that could not be resolved in Cygnet2.1-expressing cells.[299]

3.2.3.3.1.3. RET-Based Sensors to Study Nitric Oxide Signaling. As a highly reactive, membrane permeable small molecule second messenger, the free radical, NO, plays an important role in regulating autocrine and paracrine signaling pathways, alike. One of the primary means by which NO elicits a cellular response is through the activation of soluble GCs, leading to increases in local cGMP production. Thus, in theory, cGMP sensors such as Cygnet 2.1 could be applied to the study of NO signaling inside cells. Recently, Sato and colleagues took this concept a step further by tethering a PKGI-based cGMP reporter, CGY, directly to the α- and β-subunits of soluble GC.[297] Using this chimeric NO-sensor, which is able to detect NO concentrations as low as 0.1 nM, the authors uncovered unexpectedly high basal levels of NO (~1 nM) in endothelial cells, but not in nonendothelial CHO-K1 cells. This observation, which suggests that NO may play a critical role in maintaining vascular tone, may have important implications to a variety of cardiovascular diseases, including hypertension and atherosclerosis.[297]

While the above approach benefits from enzymatic amplification of the primary NO signal by sGC, it is also susceptible to artifacts stemming from NO-independent changes in cGMP levels. In contrast, sensors that rely upon the S-nitrosylation of thiol-containing proteins, such as metallothionein (MT), are designed to measure NO species directly. To this end, the FRET-based NO biosensor, FRET-MT, was created by sandwiching the human MT isoform, MTIIa, between ECFP and EYFP at the N- and C-termini, respectively.[303] This construct undergoes a decrease in the yellow over cyan emission ratio in the presence of NO.[303] Such behavior has been attributed to intrinsic conformational changes in MT caused by the formation of nitrosothiols and the concomitant release of bound metal ions.[303] When expressed in sheep pulmonary artery endothelial cells (SPAECs), FRET-MT rapidly and reversibly detected NO derived both from exogenous sources, such as the NO-donor S-nitrosylglutathione, and from endogenous sources, such as endothelial NO synthase (eNOS), suggesting that it is able to measure changes in $[NO]_i$ under a variety of conditions.[303] However, to date, FRET-MT has been used primarily to study S-nitrosylation of MTIIa itself, rather than NO dynamics inside cells.[303−305]

3.2.3.3.1.4. RET-Based Sensors to Study Phosphoinositide Dynamics. As discussed in section 2.2.1, many sensors of phosphoinositide dynamics rely upon the translocation of an effector domain-FP chimera to the plasma membrane upon generation of phosphoinositides. While this approach has proven to be quite fruitful, alternative strategies that utilize ratiometric, RET-based PI sensors offer potential advantages, such as subcellular targeting, that are not readily available from translocation-based probes.[306−308] For instance, to create a FRET-based probe that could specifically detect the turnover of PtdIns-(3,4,5)P_3 species at the plasma membrane, Sato and co-workers used rigid α-helical linkers composed of EAAAR repeats to position the PH domain of Grp1 between complementary CFP and YFP color variants.[306] Importantly, one of the linker segments contained a diglycine motif that disrupted its α-helical character, essentially functioning as a molecular hinge. When the reporter was targeted to the plasma membrane, this hinge region allowed the otherwise rigid molecule to undergo large-scale conformational changes in the presence of PtdIns(3,4,5)P_3. These changes, in turn, reoriented the FP FRET pair, causing a change in FRET.[306] Using this reporter, the authors were able to track PtdIns(3,4,5)P_3 dynamics in a variety of subcellular locales, including in the intercellular face of the ER and the plasma membrane. Interestingly, these studies revealed that, though de novo synthesis of PtdIns(3,4,5)P_3 occurs at the plasma membrane almost immediately after PDGF stimulation, two- to three-times higher levels of PtdIns(3,4,5)P_3 are produced at the ER following a short lag phase (~500 s).[306] This behavior was shown to be caused by clathrin-dependent endocytosis, which serves to relocalize activated PDGF receptors to ER endosomes via receptor internalization.[306] It is important to note that,

though the reporter described above is specific for PtdIns(3,4,5)P_3 because of its PH domain, in theory, this general design could be used to construct FRET-based sensors for any PI species-of-interest, provided that an appropriate effector domain is available.

More recently, our lab constructed a PI reporter, termed InPAkt, that allows changes in PtdIns(3,4,5)P_3 and PtdIns(3,4)P_2 (collectively termed 3′PI) concentrations at the plasma membrane to be measured in real time.[307] InPAkt consists of the PH-domain of Akt and a negatively charged pseudoligand sandwiched between FP FRET pairs. In this design, the negatively charged pseudoligand binds to the PH-domain in the absence of phosphoinositides and is released in the presence of competing PtdIns(3,4,5)P_3 and PtdIns(3,4)P_2 molecules. Dissociation of the pseudoligand from the PH-domain induces a conformational change in the reporter that leads to a change in FRET, which can be plotted as the donor to acceptor emission ratio. Using both targeted and untargeted versions of InPAkt, we were able to show that, in NIH3T3 cells, different growth factors stimulate the production of varying amounts of 3′PI at varying rates. For instance, while PDGF treatment induced a rapid increase in 3′PI at the plasma membrane, the response to insulin-like growth factor 1 (IGF-1) was much slower and less pronounced.[307] Because NIH3T3 cells express a similar number of PDGF and IGF-1 receptors, these data suggest that differential coupling may occur between PI3K and the activated forms of the receptors.

Finally, in addition to membrane-associated PI species, genetically encodable fluorescent biosensors have also been developed to measure the products of PI metabolism, such as inositol triphosphate (IP_3), which function as second messengers in the cytosol.[309−312] Though subtle differences exist between the design features used in their construction, all of the IP_3 biosensors developed to date utilize a molecular switch derived from the IP_3 binding region of one of three IP_3 receptor isoforms (IP_3R1−3). For instance, the most recent IP_3 biosensor, termed IP_3R-based IP_3 sensor 1 (IRIS-1), is composed of a truncated version of the IP_3 binding motif from mouse IP_3R1 sandwiched between ECFP and Venus.[311] This sensor is characterized by a relatively large dynamic range (∼25%) and rapid response kinetics, making it an attractive tool for examining the relationship between cytoplasmic IP_3 dynamics and oscillatory Ca^{2+} waves.[311] To this end, the Mikoshiba laboratory recently conducted a series of coimaging experiments in which IRIS-1 and the Ca^{2+}-specific dye, Indo-1, were used to measure changes in $[IP_3]_i$ and $[Ca^{2+}]_i$ in HeLa cells expressing the metabotropic glutamate receptor (mGluR5a).[311] During these studies, the authors observed both Ca^{2+} waves and fluctuations in IP_3 levels following glutamate stimulation.[311] However, in contrast to the widely held notion that IP_3 and Ca^{2+} function as a pair of reciprocally coupled messengers that spike in synchrony with one another, no $[IP_3]_i$ spikes were detected during periods of Ca^{2+} oscillations.[311] Rather, $[IP_3]_i$ increased steadily throughout the course of receptor stimulation.[311] Moreover, though fast acquisition of both signals showed that $[IP_3]_i$ began to rise prior to increases in $[Ca^{2+}]_i$, suggesting that IP_3 may promote the initial release of Ca^{2+} through its association with ER-associated IP_3Rs, a concomitant increase in the rate of IP_3 production was not observed, as would be expected if Ca^{2+} increases phospholipase C (PLC) activity.[311] Together, these results imply that a positive feedback loop involving IP_3, Ca^{2+}, PLC and IP_3R may not be the primary mechanism by which Ca^{2+} spikes are generated inside the cell, at least in mGluR5a-expressing HeLa cells.[311]

3.2.3.3.1.5. RET-Based Sensor to Measure ATP. As mentioned in section 3.2.3.2.3, ATP is an important signaling molecule involved in both intracellular and extracellular signaling processes, including insulin secretion, neurotransmission, cell motility and organ development.[313] Recently, the Noji laboratory created a series of FRET-based biosensors, termed ATP indicators based on epsilon subunits for analytical measurements (Ateams), that are able to measure $[ATP]_i$ over a wide range of concentrations.[313] For instance, Ateam-1.03, which is composed of the epsilon subunit of the *Bacillus subtilis* F_1F_o-ATP synthase sandwiched between MseCFP and cpVenus at the N- and C-termini, respectively, exhibits a $K_{D,ATP}$ of 3.3 mM, making it well-suited to measure ATP in the millimolar range.[313] Meanwhile, substitution of the epsilon subunit from *Bacillus* sp. PS3 for the molecular switch results in a related reporter, Ateam-3.10, whose high affinity for ATP ($K_{D,ATP}$ = 7.4 μM) allows it to monitor $[ATP]_i$ in the micromolar range.[313] Importantly, previous studies had shown that the epsilon subunits from both species bind ATP in a highly specific manner without leading to its hydrolysis.[314,315] Moreover, because ATP binding converts the epsilon subunit from an extended conformation to a highly compact form,[315,316] the Ateams are characterized by more than a 2-fold increase in their FRET efficiency at saturating levels of ATP.[313] Using both targeted and untargeted versions of these reporters, the authors measured $[ATP]_i$ in several subcellular compartments, including the cytoplasm, nucleus and mitochondria.[313] Surprisingly, these studies revealed that, in both HeLa and NIH3T3 cells, $[ATP]_i$ is significantly lower in mitochondria than in either the cytoplasm or the nucleus.[313] Such differences, which may be attributed to the action of the mitochondrial adenine nucleotide translocator, are likely to have important implications both for ATP-dependent signaling networks and for cellular physiology, at large.[313]

3.2.3.3.1.6. RET-Based Probes to Measure Other Cellular Analytes. Several FRET-based biosensors have also been developed for measuring fluctuations in the intra-, and in some cases, the extracellular concentration of critical small molecule analytes, such as maltose,[317] glucose,[317,318] ribose,[317] and the neurotransmitter, glutamate.[318−321] Though structurally diverse, these reporter systems all utilize a similar molecular switch to report changes in the analyte under study. In each case, ligand-induced conformational changes in a bacterial periplasmic binding protein (PBP) family member specific for the analyte-of-interest lead to a change in the relative distance and orientation of an attached FP FRET pair.[317−321] Using these biosensors, researchers have been able to observe the import, redistribution, and turnover of select metabolites at the single cell level in real time.

Along with a few other systematic studies aimed at improving the dynamic range of FP-based FRET probes (e.g., ref 322), the molecular evolution of this family of reporters has offered valuable insights into many of the molecular parameters that impact probe performance.[318,321] For instance, Deuschle and colleagues recently demonstrated that the dynamic range of the glucose reporter, fluorescent indicator protein for glucose (FLIPglu), could be improved several-fold by inserting the ECFP donor at various sites within the mature glucose/galactose binding protein (MglB) sensor domain.[318] To this end, the authors used the crystal structure of MglB to select several solvent-exposed regions that lie between secondary structural elements of the protein. They then grafted an ECFP molecule into each position (recall that N- and C-termini of wild-type

A. victoria GFP and its color variants are in close proximity to one another in space) so that the distance and orientation between the ECFP donor and the YFP acceptor varied within each construct.[318] Of the 28 sensors tested, 22 exhibited a dynamic range greater than or equal to that of the original sensor. The best of these, a reporter in which the ECFP fluorophore was inserted at position 12 of MglB, was characterized by a nearly 5-fold increase in its dynamic range relative to the parent species ($\Delta R/R_0$ = 58% vs 12%, respectively).[318] Similar results were also obtained for the YbeJ/GltI-based glutamate reporter, FLIPE, even in the absence of a YbeJ/Glt1 structure.[318] In this case, the authors used automated structure prediction software to identify the sites of ECFP insertion. This approach led to the creation of an improved FLIPE reporter whose dynamic range was 4.5 times that of the original.[318]

In addition to these examples, several studies have also shown that the length of the peptide linkers connecting the sensor domain to each of the FP reporter elements can have a profound effect on the dynamic range of FRET-based biosensors.[318,321,322] These changes can be quite subtle. For example, within a library composed of 176 linker truncation mutants of the glutamate-sensing fluorescent reporter (GluSnFR), only one, GluSnFR$_{8N5C}$ (lacking 8 and 5 residues from the N- and C-terminal FP linkers, respectively), exhibited a dramatic improvement in its dynamic range.[321] This reporter, which was termed SuperGluSnFR, exhibited a 44% change in emission ratio at saturating glutamate concentrations, representing a 6.2-fold improvement over the original GluSnFR. SuperGluSnFR also contains a S73T mutation that reduces the affinity of its YbeJ/Glt1 sensor domain for glutamate, making it well-suited for the measurement of synaptic glutamate during several neuronal processes, including burst stimulation and glutamate recycling.[321]

It should be noted that, in addition to the dynamic range of a given reporter, the length of the linker can also impact other properties important for probing the intracellular environment. For instance, during the development of a series of Zn^{2+} biosensors termed eCALWY1−6, Vinkenborg et al. were able to fine-tune the Zn^{2+} binding affinities of several of the sensors by simply varying the length of the linker region connecting their tandem metal binding domains.[323] Using this approach, the authors created sensors with K_D's that spanned the picomolar to nanomolar range. Interestingly, to increase the dynamic range of this set of reporters, the authors introduced two mutations, S208F and V224L, in the Cerulean and Citrine FPs. These mutations, which are known to promote FP dimerization, appear to lock the reporter in a conformation conducive to FRET in the apo-state while allowing FP separation upon Zn^{2+} binding. As a result, eCALWY-1 exhibits a >15-fold increase in its dynamic range relative to its progenitor, CALWY.[323,324] This sensitivity, coupled with a versatile toolchest of reporters exhibiting a wide range of binding affinities, enabled the authors to more accurately measure $[Zn^{2+}]_i$ in various compartments of pancreatic β cells. Likewise, targeted versions of another set of FRET-based Zn^{2+} sensors have recently uncovered transient changes in cytosolic and mitochondrial $[Zn^{2+}]_i$ in rat hippocampal neurons following glutamate stimulation.[325] These studies suggest that mitochondria may function not only as storage depots for cellular Zn^{2+} but that these organelles may also be a source of Zn^{2+} signaling inside the cell. Importantly, the knowledge gained from the development of each of the reporters described above will be useful for the future design and optimization of many FRET-based biosensors.

3.2.3.3.2. RET-Based Reporters to Probe the Activation/Activity Of Cellular Macromolecules. In addition to small molecule second messengers and cellular analytes, a large number of RET-based biosensors have also been developed to visualize the action of specific macromolecular machines within the cellular environment. These types of biosensors can be broadly divided into two classes: activation sensors and activity reporters. The primary difference between these two families of biosensors is the number of signaling "events" captured by each sensor molecule. For instance, activation sensors generally measure activation-induced conformational changes in the macromolecule under study (or some derivative, thereof) and therefore exhibit a linear relationship between the number of activated species and the biosensor signal. In contrast, RET-based activity sensors, which are designed to measure the *activity* of signaling enzymes, are subject to enzymatic amplification. This is usually accomplished through the incorporation of a surrogate substrate region within the molecular switch. As a consequence, a large number of sensor molecules can be modified by a single activated signaling molecule (e.g., a protein kinase or a protease), leading to a nonlinear, logarithmic relationship between the number of activated signaling molecules and the biosensor signal. Below, we examine several sensors from each class, highlighting some of the ways in which they have been used to answer important biological questions pertaining to intracellular signaling pathways.

3.2.3.3.2.1. RET-Based Sensors to Measure the Activation of Macromolecules. RET-based activation sensors have been used to study the regulation of a wide variety of signaling molecules, including transmembrane receptors and several signaling enzymes. As alluded to above, with a few notable exceptions, all activation sensors utilize a molecular switch based upon intrinsic conformational changes in the receptor- or enzyme-of-interest to distinguish between the active and inactive states of the molecule. Aside from offering important insights into the timing and spatial distribution of activation, these types of reporters also have the potential to provide quantitative information about critical biochemical parameters, such as the kinetics of enzyme activation/deactivation, that help determine the speed with which cellular signals are transmitted inside the cell.

3.2.3.3.2.1.1. RET-Based Probes for Measuring G-Protein-Coupled Receptor Activation. The GPCR superfamily, which represents the largest family of proteins involved in signal transduction, is composed of structurally-similar receptor proteins characterized by seven α-helical membrane-spanning domains. As the primary upstream activators of many intracellular signaling pathways, GPCRs play a key role in converting extracellular stimuli, such as hormones and neurotransmitters, into an intracellular response. The dysregulation of GPCRs is also critical to the etiology of many diseases. In fact, roughly one half of the drugs on the market today target GPCRs.[326] Though detailed biochemical and physiological analyses have yielded much information about GPCR-mediated signaling and the resulting functional response, these techniques have provided relatively little information about the spatial and temporal aspects of GPCR activation and signaling. To better understand these important aspects of GPCR signaling, as well as to gain insights into the mechanistic basis of the signaling process itself, several RET-based sensors have been created to study receptor activation in the context of single, living cells (reviewed in ref 327).

Upon ligand binding, GPCR family members act as guanine nucleotide exchange factors that facilitate the exchange of GDP for GTP in the Gα subunit of associated trimeric G-protein

complexes. Nucleotide exchange promotes the dissociation of the Gα subunit from the Gβγ subunits of the complex which, in turn, leads to the activation of downstream effectors, such as PLC and transmembrane ACs involved in PI- and cAMP metabolism, respectively.[328] Several biochemical studies suggest that ligand binding causes the reorganization of the receptor's transmembrane helices resulting in changes in the relative positions of the second and third intracellular loops (reviewed in ref 329). To capture activation-induced conformational changes in GPCR family members, several groups have fused CFP and YFP color variants to the third intracellular loop and the C-termini of the receptor molecule to yield sensitive GPCR activation sensors.[330−332] These sensors, which all exhibit modest (but reproducible) decreases in emission ratio following agonist stimulation, have been used to study GPCR activation kinetics in the presence of full agonists,[330−332] as well as partial[331,333] and even inverse agonists.[334] These studies revealed that while most GPCR family members undergo very rapid activation in the presence of full agonists ($t_{1/2}$ = 30-50 ms), their rate of activation is much slower ($t_{1/2}$ = ∼1 s) when treated with partial and inverse agonists.[331,334] Interestingly, rather than generating an *increase* in FRET like that observed in the presence of full or partial agonists, inverse agonists appear to cause a *decrease* in FRET that may be attributed to distinct conformational states of the receptor.[334]

One of the primary concerns when using the sensor design outlined above is that insertion of either CFP or YFP into the primary sequence of the receptor will interfere with its normal function. For instance, although activation of adenosine A_{2A} receptors can be probed by fusing CFP and YFP to the third intracellular loop and C-terminus, respectively, previous studies have shown that the bulky FP fusions eliminated coupling between the receptor and downstream components such as transmembrane ACs.[74] To circumvent this issue, researchers inserted a tetracysteine motif in place of YFP and labeled the chimeras with FlAsH.[74] In response to adenosine, the amount of FRET generated by the CFP-FlAsH-labeled receptor was five-fold higher than that of the original CFP/YFP-based reporter. More importantly, the CFP-FlAsH labeled receptor preserved the activation of AC, providing a more accurate picture of adenosine A_{2A} receptor regulation.[51] Recently, Zürn and colleagues elaborated upon this approach to detect distinct, agonist-specific conformational changes in the α_{2a}-adrenergic receptor (α_{2a}-AR).[158] To this end, they generated three reporter constructs with a tetracysteine motif placed within different regions of the third intracellular loop.[158] Using these reporters, the authors observed differences in both the magnitude and the kinetics of receptor activation between different constructs depending on the type of agonist used (that is, full, strong-partial or weak-partial agonist).[158] These data, which correlate nicely with recent in vitro studies,[335] suggest that GPCRs may adopt several distinct conformations inside the cell, perhaps corresponding to partially and fully active states, in the presence of different types of agonists.[158]

In addition to conformational changes in the receptor itself, a variety of BRET- and FRET-based probes have also been developed to measure other steps in the GPCR signaling cascade. These include bimolecular reporters designed to visualize interactions between (1) receptors and G-protein complexes,[336−338] (2) activated receptors and β-arrestin, an adaptor protein involved in regulating, transducing and re-directing GPCR signals,[339] and (3) the Gα and Gβγ subunits of the heterotrimeric G-protein complex.[336,340] Together, these reporter systems have offered important insights into the timing[336,337,341] and selectivity[337] of GPCR-G-protein association/dissociation as well as receptor desensitization.[339] Importantly, when data obtained from these probes are combined with those generated using the GPCR activation reporters and cAMP sensors discussed above, these assays have the potential to provide quantitative kinetic analysis of several steps associated with GPCR signal transduction in living cells.[342]

3.2.3.3.2.1.2. Monitoring the Activation of Small G-Proteins. Small G-proteins of the Ras superfamily play critical roles in activating intracellular signaling cascades. Moreover, their dysregulation contributes to many diseases, including a large number of cancers. Therefore, in order to better understand how these enzymes are regulated, several live cell imaging approaches have been developed to monitor G-protein activation within the cellular environment. For instance, a bimolecular FRET-based reporter system has been used to visualize the endogenous activation of Ras along the secretory apparatus of COS-1 cells.[343] Though previous studies had shown that, aside from the plasma membrane, Ras is also present on the ER and Golgi membranes,[344,345] the question remained as to whether these pools of Ras were active, that is, were they capable of undergoing GTP-GDP exchange and propagating a signal? To address this question, the Ras binding domain (RBD) of c-Raf-1 was fused to CFP, while the transmembrane marker protein, CD8, was fused to YFP. Since the RBD is only recruited to membranes by the active form of Ras, increased FRET between CFP and YFP provides a readout for the presence of activated Ras. An interesting feature of this bimolecular reporter system is that, rather than relying upon direct protein−protein interactions to drive changes in FRET, it utilizes bystander FRET between YFP and the CFP moiety of membrane-associated RBD as the primary readout. Because bystander FRET was detected at both the plasma membrane and the Golgi following EGF stimulation, these studies provided some of the first evidence that, in addition to the plasma membrane, Ras can also be activated at the Golgi.

To monitor the activation of small G-proteins directly, a series of unimolecular FRET-based sensors have also been constructed. These probes each utilize an engineered molecular switch consisting of the small G-protein-of-interest and an effector domain that specifically recognizes the active (GTP-bound) state of the protein. For example, to measure Ras activation in response to various growth factors, the RBD of its downstream effector, Raf, was fused to Ras. The resulting reporter, which is named Ras and interacting protein chimeric unit (Raichu), reported activation of Ras after epidermal (EGF) or neuronal growth factor (NGF) stimulation.[346] Similar reporters have been constructed based upon different G-protein/RBD pairs.[346−349] Together, these reporters have offered important insights into the spatiotemporal regulation of G-protein activation. For instance, using a pair of Ras and Rap reporters termed Raichu-Ras and Raichu-Rap, researchers demonstrated that, while EGF promotes Ras activation at the cell periphery where membrane ruffling is prominent, Rap activity is restricted to the internal perinuclear region.[346] To visualize RhoA activation within distinct subcellular regions, the Hahn laboratory created a single-chain RhoA biosensor by fusing the RhoA-binding domain of rhotekin to CFP, followed C-terminally by a flexible linker region, YFP and full-length RhoA.[350] The unique design of this reporter allowed it to be targeted in a manner more similar to wild-type RhoA via interactions with the regulatory factor, Rho guanosine dissociation inhibitor (RhoGDI) located at the plasma

membrane. This feature allowed the authors to show that, contrary to previously held notions about the spatial organization of RhoA activity during cell migration, RhoA activity is actually concentrated at the leading edge of membrane protrusions in both randomly migrating and PDGF-stimulated mouse embryonic fibroblast (MEF) cells.[350] Interestingly, a high degree of RhoA activation was also observed at the distal side of serum-induced, but not PDGF-stimulated, peripheral ruffles, suggesting that distinct signaling mechanisms may control actin dynamics at different ruffling structures.[350] Building upon these findings, researchers recently examined the activation profiles of RhoA and two other G-proteins known to control cytoskeletal dynamics, Cdc42 and Rac1, during the migration of mouse embryonic fibroblasts.[351] This study, which also described a novel computational multiplexing methodology designed to compare the activation profiles of enzymes visualized in separate experiments, revealed a high degree of coordination between these proteins in both space and time.[351] For instance, whereas RhoA activation occurs at the cell edge coincident with edge advancement, Cdc42 and Rac1 are each activated approximately 2 μm from the cell edge with a lag time of almost 40 seconds. Together, these findings suggest that RhoA plays a primary role during the initial events of protrusion while Cdc42 and Rac1 are involved in reinforcing/stabilizing newly formed protrusions.[351]

Lipid rafts are also believed to play a role in the compartmentalization of some signaling molecules. By targeting Raichu-Ras probes to specific plasma membrane microdomains, researchers were able to uncover spatially- and temporally-distinct patterns of Ras activation within raft- and non-raft regions.[352] Specifically, these studies showed that while the activation of Raichu probes targeted to non-raft regions was accompanied by a 1−2 minute delay following EGF stimulation, raft-targeted versions were activated on a much faster time scale (~0.25 minutes). These differences were largely negated following pre-treatment with methyl-β-cyclodextran, which specifically disrupts lipid rafts. Together, these data are consistent with the notion that upstream activators of Ras activity, such as EGF receptors (EGFRs), may be clustered within cavaloe/raft microdomains where they preferentially activate raft-targeted Ras molecules, such as H-Ras.[352]

3.2.3.3.2.1.3. Monitoring the Activation of Protein Kinases. By catalyzing the trans-phosphorylation of specific amino acid residues on target proteins, protein kinases modulate the activity, localization or stability of their protein substrates inside the cell. It has been estimated that in humans roughly one-third of all cellular proteins are modified by kinase-mediated phosphorylation,[353] establishing protein kinases as one of the most important and most well-studied families of signaling enzymes. Indeed, their ubiquitous cellular distribution, coupled with their ability to rapidly and specifically modify a large number of target proteins (including other kinases and signaling enzymes), allows protein kinases to function as central nodes in many signaling cascades. Therefore, it is not surprising that, inside the cell, the activation of protein kinases must be regulated in a spatially and temporally restricted manner. Together, these regulatory mechanisms lead to highly coordinated kinase activation kinetics that directly impact downstream cellular processes. As a consequence, there has been much interest in characterizing when and where kinase activation occurs inside cells. This has resulted in the development of several RET-based sensors for studying kinase activation.

In most cases, kinase activation can be assessed by monitoring the conformational state of the kinase, itself. This approach has been successfully used to study the spatiotemporal aspects of kinase activation for several important kinases, including extracellular-regulated kinase 2 (ERK2),[354] MAP kinase-activated protein kinase 2 (MK2),[355] and Akt.[173,356] For example, to study the change in conformation associated with MK2 activation, Neininger et al. flanked full length MK2 with EGFP and EBFP at the N- and C-terminus, respectively.[355] Under resting conditions, the resulting reporter, termed GFP-MK-BFP (GMB), was distributed exclusively in the nucleus where it exhibited a high FRET emission ratio. In contrast, cellular stress induced phosphorylation-dependent conformational changes in GMB that led to a dramatic decrease in FRET followed by nuclear export.[355] Importantly, these changes could be correlated with MK2 activation, as indicated by a nearly 3-fold increase in the phosphorylation of the MK2-specific substrate, Hsp25, following activation. Taken together, these results imply that, while in the nucleus, MK2 exists in a closed conformation corresponding to the inactive state. Following stimulation, the kinase is converted to an open, active form which translocates to the cytoplasm where it exerts its effects. The ability to simultaneously measure activation kinetics and protein translocation using a single reporter provides researchers with complementary information that can be used to make quantitative comparisons between these two parameters. As we will see in the following example, this feature has facilitated the development of computational models that promise to expand our understanding of the regulation and control of intracellular signaling networks.

The Ras/ERK MAPK signaling cascade, whose principle components include several Ras, Raf, MEK, and ERK isoforms, is a central regulator of many cellular processes, including cell proliferation, differentiation, and survival (reviewed in ref 357). To better understand the temporal relationship between ERK2 activation and its nucleocytoplasmic shuttling behavior following EGF stimulation, the Matsuda laboratory generated a reporter of ERK2 activation, termed MAPK indicator unit ERK2 (Miu2), by fusing YFP and CFP variants to the N- and C-termini of *Xenopus* ERK2.[354] Inside the cell, both the activation and cytoplasmic distribution of ERK2 is dependent upon its upstream activator, MAPK/ERK kinase (MEK). Following growth factor stimulation, it is believed that MEK-mediated phosphorylation of ERK2 leads to ERK2 activation, dissociation of the complex and translocation of activated phospho-ERK2 molecules to the nucleus. Consistent with this model, when Miu2 was co-expressed with wild-type MEK in the absence of growth factor, the reporter localized primarily to the cytoplasm and exhibited an elevated FRET efficiency.[354] In contrast, EGF stimulation caused an immediate drop in the emission ratio followed by nuclear import of the reporter several minutes later, suggesting that ERK2 activation precedes nuclear import.[354] Interestingly, a series of point mutations at sites of MEK phosphorylation suggest that, as opposed to the GMB reporter described above, the conformational changes associated with ERK2 activation are dependent upon MEK binding rather than ERK2 phosphorylation, per se.[354] Importantly, the kinetic data generated using the Miu2 probe could be combined with that obtained from Ras/Raf activation reporters and several Dronpa-tagged localization probes to construct a computational model which captured the essential features of the Ras/ERK/MAPK signaling pathway. As we will see in the Conclusions and Future Perspectives section below, their ability to generate quantitative information about a diverse set of biochemical parameters within a live cell context makes genetically-encoded fluorescent biosensors well-suited for generating the data required for model building.

3.2.3.3.2.2. RET-Based Sensors to Measure Enzyme Activity. Aside from enzyme *activation*, RET-based biosensors have been developed to visualize the *activities* of specific enzymes within the native cellular environment. Because they have the capacity to measure the activity of a given enzyme in the presence of endogenous levels of its regulatory elements, these types of sensors are powerful tools for understanding the spatiotemporal regulation of signaling enzymes under physiological conditions. Moreover, like several of the fluorescent probes described above, the targetability of genetically encodable activity reporters allows specific pools of a given enzyme to be imaged in real-time within select subcellular regions. In addition, these biosensors allow sensitive detection of kinase activity because of the enzymatic amplification discussed above. Together, these types of reporters have offered unprecedented insights into the regulation of enzymatic processes within the cellular environment. Below, we highlight several kinds of enzyme activity sensors and discuss the ways in which they have been used to study biological phenomena.

3.2.3.3.2.2.1. Protease Activity Sensors. Many proteases involved in intracellular signaling processes catalyze the cleavage of their protein substrates at specific recognition sites. As important upstream activators of many critical cellular processes, including apoptosis, these enzymes must be precisely regulated in both space and time. RET-based reporters have been instrumental in characterizing the spatiotemporal control of protease activity inside cells. In fact, the earliest intramolecular FRET-based sensors were developed to measure protease activity. These sensors consisted of a protease sensitive linker sandwiched between the FP FRET partners, BFP and GFP.[36,358] In the absence of proteases, the close proximity of the FPs resulted in efficient energy transfer from BFP to GFP. In contrast, cleavage of the peptide linker caused the FPs to diffuse away from one another which, in turn, led to a precipitous drop in FRET. A similar design was used to study the activation of caspases during apoptosis in HeLa cells. These probes, which consist of a short linker region containing the caspase-specific cleavage site, DEVD, flanked by EBFP and EGFP, were specifically cleaved in response to the apoptotic agonists, tumor necrosis factor (TNF) and cycloheximde.[359] More recently, this approach has been extended to measure the activity of two caspases simultaneously inside MCF-7 cells.[360] Accordingly, the caspase-3 specific substrate, DEVD, was inserted between CFP and YFP variants while the caspase-6 specific substrate, VEID, was sandwiched between YFP and mRFP in the same construct. Using this dual-specificity reporter system, the authors demonstrated that, during the induction of apoptosis, caspase-3 activity consistently preceded caspase-6 activity by approximately thirty minutes. However, it should be noted that, when co-imaging FP FRET pairs, care must be taken to account for cross-talk between the two FRET circuits. Indeed, we have recently shown that despite a large degree of spectral separation, the bright CFP variant, Cerulean, is able to undergo energy transfer with mCherry.[361]

3.2.3.3.2.2.2. Protein Kinase Activity Sensors. As discussed above, protein kinases must be tightly regulated inside cells. To better understand the regulation of these enzymes within their endogenous environment, several kinase activity reporters have been developed. Many of the kinase activity reporters in use today utilize an engineered molecular switch based upon a modular design (reviewed in ref 362 and 363). Accordingly, a consensus phosphorylation site specific for the kinase-of-interest serves as the "receiving segment" while a phosphoamino acid binding domain (PAABD) functions as the "switching segment". These regions are concatenated together by a flexible linker and sandwiched between a FP FRET pair. Whereas the length of the linker and the choice of FRET pairs influence the dynamic range of the reporter, the "receiving and switching segments" contribute to its specificity and reversibility, respectively. This basic modular design has been applied to a number of protein kinases, including PKA,[361,364−366] protein kinase C (PKC),[367,368] ATM,[369] Akt,[370−372] Abl,[373] Src,[371,373,374] aurora kinase B,[375] ERK,[376,377] c-jun N-terminal kinase (JNK),[378] cyclin-dependent kinase 1 (CDK1),[379] and the epidermal growth factor receptor (EGFR).[373,380,381]

Because protein kinases are often dynamically regulated, it is important that biosensors designed to track their activities exhibit reversible responses to allow continuous tracking of upregulated and downregulated kinase activities. In the case of the modular kinase activity reporters discussed above, this can be achieved by incorporating a PAABD that displays an intermediate binding affinity for the phosphorylated substrate region. For instance, although the first generation A-kinase activity reporter, AKAR1, enabled kinetic analysis of subcellular PKA activity induced by the β-AR agonist, isoproterenol, this sensor was unable to report the attenuation of PKA activity because its response was irreversible in cellulo.[364] This is likely due to the fact that the 14-3-3τ PAABD utilized by AKAR1 binds the phosphorylated form of the substrate domain very tightly, preventing cellular phosphatases from gaining access to the substrate region as PKA activity declines. Therefore, in order to visualize both increases and decreases in PKA activity, a second generation PKA reporter, AKAR2, was constructed by replacing 14-3-3τ with the weaker-binding PAABD, forkhead-associated 1 (FHA1).[365] While AKAR2 is activated with kinetics similar to those observed for AKAR1, the former is also readily reversible following removal of agonist or treatment with the PKA inhibitor, H89. Interestingly, the reversibility of AKAR2 was further enhanced by replacing ECFP and Citrine with their monomeric counterparts.[382] Presumably, the incorporation of monomeric FP variants in AKAR2.2 reduces interactions between the FPs, allowing the reporter to adopt a more open conformation for dephosphorylation by phosphatases.[382]

Kinase activity reporters have also revealed new information about temporal regulation of kinases. For instance, it has long been known that, in response to certain stimuli, the concentration of second messengers such as Ca^{2+} oscillate in a periodic fashion. However, until recently, it has been difficult to gauge what affect these oscillations have upon the activities of downstream kinases. Therefore, to examine the relationship between second messenger oscillations and kinase activity, several groups have employed kinase activity sensors to track changes in kinase activity under cellular conditions in which second messengers oscillate in a periodic fashion. For example, to assess the impact of histamine-induced Ca^{2+} waves on PKC activity, Violin et al. used the PKC activity reporter (CKAR) in conjunction with the calcium indicator, Fura-Red, to simultaneously measure dynamic changes in PKC activity and $[Ca^{2+}]_i$ at the single cell level.[367] These studies demonstrated that, in HeLa cells, Ca^{+} oscillations are phase-locked with oscillations in PKC activity following histamine stimulation.[367] More recently, AKAR2.2 and the cAMP sensor, ICUE2, were used to uncover a link between depolarization-evoked Ca^{2+} oscillations and the cAMP/PKA signaling pathway in neonatal rat retinal explants.[382] Previous studies had shown that, in the early stages of retinal development, retinal ganglion cells (RGCs) spontaneously send a wave of

action potentials across the ganglion cell layer. These retinal waves play an important role in the development of vision. Because PKA has also been implicated as a major player during retinal development, its spatiotemporal dynamics were investigated in rat retinal explants. Using AKAR2.2, spontaneous oscillations in PKA activity were visualized.[382] Interestingly, oscillations in PKA activity correlated temporally with spontaneous depolarizations associated with retinal waves, supporting the notion that retinal waves play a role in the regulation of PKA activity dynamics.[382] This work establishes a connection between spontaneous neural activity with temporal oscillations in kinase activity during retinal development. Together, these data provide convincing evidence that Ca^{2+} oscillations and the information contained therein can be directly coupled to downstream effectors, such as PKC and PKA.

As alluded to earlier, the targetability of genetically-encoded reporter systems allows researchers to monitor specific pools of a given biomolecule within the cellular environment. This feature is particularly valuable in the case of kinase activity reporters because the subcellular localization of protein kinases often plays a critical role in achieving specific and effective regulation of kinase-mediated signaling events. For instance, during anaphase, a dividing cell must establish a cell-division plane midway between segregating chromosomes. It is believed this division plane is established by a self-organizing system composed of several factors associated with the "chromosome passenger complex", including the mitotic regulator, aurora B kinase. However, until recently, it was not clear how the signal was maintained from the spindle midzone to the cell cortex—a distance which spans several micrometers in the average cell. To assess the role of aurora B kinase in this process, researchers targeted a FRET-based aurora B kinase activity reporter to several chromosomal regions, including centromeres (by fusion to CENP-B) and chromatin (by fusion to histone H2B), and tracked changes in both sensor phosphorylation and chromosome location at different times throughout anaphase.[375] In this way, changes in the phosphorylation status of the reporter could be correlated with chromosome position. These studies demonstrated that while aurora B was most active near the midzone prior to chromosome segregation, its activity decreased markedly as the chromosomes moved toward the mitotic poles.[375] Together with the finding that active aurora B kinase is associated with microtubules located at the spindle midzone, these data support a model in which the cell-division plane is established and maintained by an aurora B phosphorylation gradient emanating from the midzone.[375]

3.2.3.3.2.2.3. Phosphatase Activity Sensors. In the above discussion, we highlighted several kinase activity reporters and outlined some of the ways in which they have been used to visualize reversible protein phosphorylation inside cells. Equally important to the dynamic regulation of protein phosphorylation is the activity of protein phosphatases. Protein phosphatases counteract the effects of kinase-mediated phosphorylation by catalyzing the hydrolysis of phosphate groups from amino acid side chains. However, whereas a relatively large number of molecular probes have been developed to track kinase activity inside cells, until recently, a general design for phosphatase activity biosensors had not been described. To address this issue, we engineered a phosphatase activity sensor designed to measure the activity of the Ca^{2+}/calmodulin-regulated serine/threonine protein phosphatase, calcineurin (CaN), within its endogenous environment.[383] This reporter, termed CaN activity reporter 1 (CaNAR1), utilizes an intrinsic molecular switch based upon dephosphorylation-induced conformational changes within the regulatory region of NFAT1 to change the distance/orientation of ECFP and a circularly-permuted version of Venus. As a consequence, CaNAR1 exhibits an increase in its yellow over cyan emission ratio following treatment with the Ca^{2+} ionophore, ionomycin. Importantly, because the regulatory region of NFAT1 is hyperphosphorylated by cellular kinases, such as p38 and the constitutively-active kinase, casein kinase 1 α (CK1α), in resting cells, CaNAR1 does not require activation of additional kinases to put it into a "dephosphorylation competent" state. This feature ensures that the cellular environment remains relatively unperturbed prior to Ca^{2+} stimulation. This and other design features utilized by CaNAR1 should be generally applicable to other protein phosphatases as specific molecular switches are identified or engineered. Thus, as a prototype phosphatase activity sensor, CaNAR1 lays a foundation for studying the targeting and compartmentation of protein phosphatases within the cellular environment.

3.2.3.3.2.2.4. Activity Sensors to Measure O-Glycosylation. Protein O-glycosylation is catalyzed by O-GlcNAc transferase (OGT). Among other functions, OGT-mediated glycosylation opposes the action of many serine/threonine protein kinases in a manner similar to phosphatases. However, rather than removing a phosphate group, OGT-mediated glycosylation prevents phosphorylation altogether by reciprocally modifying serine and threonine residues. Therefore, the dynamic interplay between protein phosphorylation and O-glycosylation plays a potentially important role in many signaling processes. To develop a FRET-based biosensor capable of monitoring OGT activity in mammalian cells, a molecular switch composed of the OGT substrate domain (the receiving domain) from casein kinase II and an O-GlcNAc binding domain (the switching domain) from the bacterial lectin, GafD, were sandwiched between ECFP and Venus.[384] This reporter, which can be reversibly GlcNAcylated by purified OGT and the deglycosylating enzyme, O-GlcNAcase, provides an attractive means of studying dynamic O-glycosylation processes inside living cells. For instance, when expressed in HeLa cells, the O-GlcNAc indicator exhibited a slow, but steady, increase in its yellow over cyan emission ratio following the addition of glucosamine. Variations of this sensor design, for instance using substrates that are phosphorylated and O-GlcNAcylated in a reciprocal manner, promise to offer valuable information about cross-talk between these important signaling pathways.

3.2.3.3.2.2.5. Activity Reporters to Measure Histone Acetylation and Methylation. The reversible alkylation/acylation of cellular proteins, usually by covalent attachment of either a methyl or an acetyl moiety to the ε-amino group of specific lysine residues, is believed to function in a manner analogous to protein phosphorylation. Indeed, by altering the shape, surface charge distribution (acetylation, for example, masks the positive charge on lysine) or hydrogen-bonding potential of modified proteins, these modifications can directly influence the biochemical properties of modified proteins, often affecting their interactions with surrounding biomolecules such as DNA and other proteins.

Over the past decade, it has become clear that, through modification of the N-terminal tails of histones involved in chromatin assembly, reversible protein alkylation/acylation plays a major role in the epigenetic regulation of DNA replication and transcription.[385] For instance, during transcription, histone

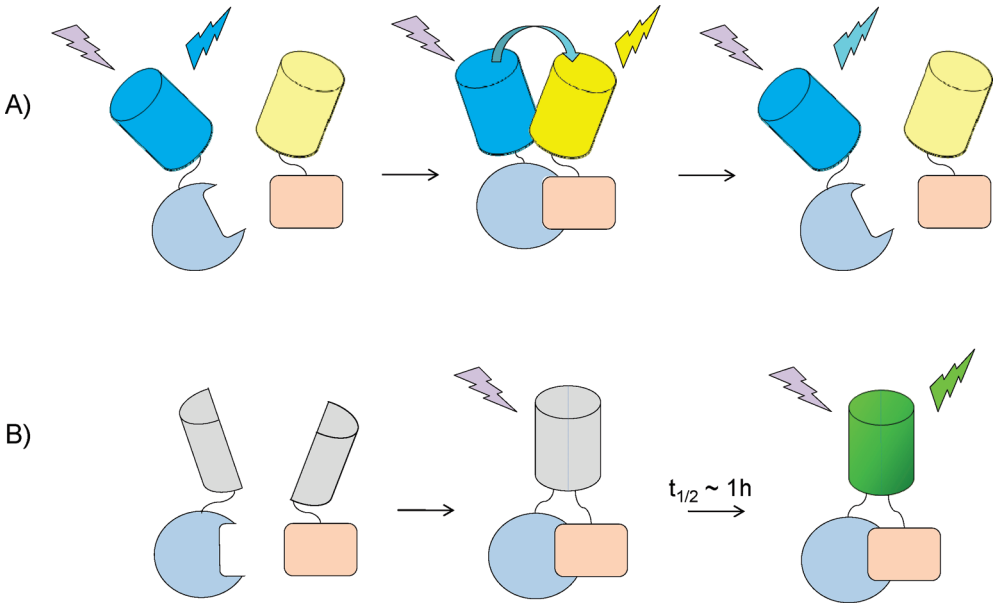

Figure 8. Fluorescent reporters to track protein−protein interactions. (A) FRET-based interaction sensors, which use the association of fluorescently tagged proteins to change the distance or orientation of a FRET pair, allow reversible interactions to be monitored in real-time. (B) Meanwhile, BiFC-based interaction sensors, which are essentially irreversible, use the association of proteins tagged with complementary halves of split FP molecules to promote fluorophore formation. Though the relatively slow maturation of the fluorophore prevents BiFC-based probes from measuring protein−protein interactions in real-time, the large dynamic range of these sensors allows interactions to be detected at protein concentrations that do not dramatically alter the cellular context in which the interactions occur.

alkylation/acylation is believed to affect both chromatin superstructure and the recruitment of transcriptional proteins, such as transcriptional co-activators, to intragenic regions. Moreover, modification of specific lysine residues appears to be highly dynamic, suggesting that histone alkylation/acylation is tightly controlled inside the cell. Therefore, to monitor the reversible methylation/acetylation of histones in cellulo, a series of FRET-based reporters have been developed based on a modular design.[386,387] These reporters all utilize an engineered molecular switch flanked by FP FRET pairs. For instance, the first reporters of histone methylation, termed K9 and K27 (according to the position of their methylated lysine residues in the histone H3 primary sequence), were constructed by fusing CFP and YFP variants to short N-terminal fragments of histone H3 and a chromodomain derived from histone-binding protein 1 (HP1) and the Polycomb (Pc) protein, respectively.[386] Since HP1 and Pc chromodomains have been shown to associate specifically with methylated lysine residues at the K9 and K27 position of histone H3, respectively,[388,389] they not only drive conformational changes in the switch region, but they also impart specificity to these types of reporters. Indeed, both the K9 and K27 methylation reporters have been shown to exhibit methyl transferase-dependent changes in their emission ratios both in vitro and in live cells, suggesting that they are able to detect the methylation of histone H3.[386]

More recently, Sasaki et al. used a similar approach to develop a reporter of histone acetylation termed Histac.[387] However, unlike the methylation reporters discussed above, the molecular switch utilized by Histac is composed of full-length histone H4 fused to a tandem bromodomain from the testis-specific chromatin remodeling protein, BRDT.[390] While the bromodomain specifically recognizes acetylated lysine residues, the use of full-length histone H4 ensures that the Histac reporter is targeted to chromatin. Chromatin localization appears to be important for histone acetyl transferase (HAT)-mediated acetylation since a C-terminally truncated reporter lacking the globular histone domain showed neither chromatin localization nor trichostatin A (TSA)-dependent acetylation.[387] In contrast, the full-length reporter exhibited robust activation in the presence of TSA, a potent inhibitor of histone deacetylase (HDAC) activity.[387] Importantly, the FRET response was readily reversible following TSA withdrawal, suggesting that Histac offers information about both acetylation and deacetylation reaction kinetics. Using this reporter, the authors observed striking differences in histone H4 acetylation levels during various stages of mitosis, with a marked decrease in acetylation beginning at prophase and reaching its nadir during anaphase.[387] Moreover, Histac was also able to detect localized differences in histone deacetylase activity (HDAC) during interphase, as evidenced by differences in the rates of deacetylation within two sub-nuclear regions of a transfected cell.[387]

3.2.4. Coupled Fluorescent Indicator Systems. Recently, the ability of genetically encoded fluorescent probes to sense biochemical changes in living systems has been further expanded through the development of coupled fluorescent indicator systems. These systems, which couple the signal output from two or more individual fluorescent biosensors or couple responses of endogenous and/or engineered signaling molecules with those of fluorescent biosensors, have been used to probe changes in the extracellular environment[391,392] or to report the status of cellular processes, such as cell cycle progression.[393] Because many coupled reporter systems benefit from several rounds of enzymatic amplification,[391,392] they have the potential to be highly sensitive reporters of signaling molecules involved in many important biological processes. This property was first exploited by the Umezawa lab to create a cell-based reporter of NO release called "Piccell".[392] Piccell was generated by transfecting PK15 cells with the FRET-based cGMP indicator,

CGY.[392,394] In response to elevations in $[cGMP]_i$ produced by NO-dependent activation of sGC molecules, CGY exhibits a rapid and reversible decrease in emission ratio.[394] Since it is estimated that a single NO molecule generates nearly 6,000 cGMP molecules/min, Piccell is extremely sensitive to NO release.[392] In fact, Piccell is able to detect NO concentrations in the midpicomolar range, several orders of magnitude lower than the most recent organic fluorescent indicator of NO, DAC-P.[395] This exquisite sensitivity, coupled with the reversibility of the CGY response (mediated by PDEs expressed by the PK15 "host" cell), allows Piccell to detect subtle fluctuations in NO concentrations that other approaches may miss. Indeed, when cocultured with hippocampal neurons, Piccell uncovered oscillatory release of picomolar concentrations of NO from neurons, even in the absence of stimulation.[392] Interestingly, using the Ca^{2+} indicator, YC3.60,[39] the NO oscillations detected by Piccell could be correlated to Ca^{2+} oscillations occurring in the neurons.[392] It should be noted that, though Piccell is extremely sensitive to NO concentrations, the dynamic range of its CGY reporter element is substantially lower than that of several recently developed cGMP reporters, especially those based on PDE5.[299,301] Therefore, the sensitivity of the Piccell system may be further enhanced by substituting one of these reporters for CGY.

More recently, the same group used a similar approach to visualize the secretion of endogenous levels of brain-derived neurotrophic factor (BDNF) from living neurons.[391] To this end, the FRET-based EGFR biosensor, ECaus, was expressed in MCF-7 cells along with a chimeric receptor tyrosine kinase (RTK) composed of the extracellular binding domain of TrkB and the intracellular kinase domain of EGFR (BBD-ECat).[391] The TrkB binding domain renders BBD-ECat sensitive to BDNF, while the EGFR kinase domain ensures robust phosphorylation of the fluorescent ECaus reporter. In this manner, MCF-7 cells expressing ECaus and BBD-ECat are themselves converted into highly sensitive reporters of BDNF secreted into the extracellular environment.[391] Using this cell-based reporter system, the authors visualized BDNF secretion from cultured hippocampal neurons in response to glutamate stimulation. These studies suggest that, under their experimental conditions, approximately 200 pM of BDNF is secreted upon glutamate stimulation.[391] However, it is not clear whether this value corresponds to the amount of growth factor excreted by one neighboring neuron or a group of surrounding neurons. Importantly, because the TrkB binding domain can be replaced with any RTK binding domain, in theory this system is amenable to the detection of several different growth factors secreted by cells. Therefore, the modular design of this reporter system should facilitate the development of similar cell-based fluorescent indicators which could provide valuable insights into the dynamics of other important regulatory factors involved in cell−cell communication.

Finally, the Miyawaki laboratory applied knowledge about cell-cycle dependent protein turnover to develop an exciting new biosensor system designed to track cell cycle progression in real time in vivo.[393] Their approach, dubbed fluorescent ubiquitin-based cell cycle indicator (Fucci), exploits the cell cycle-dependent proteolysis of the ubiquitination oscillators, Cdt1 and Geminin, to specifically mark the G_1/S transition in living cells. By fusing the red- and green-emitting fluorescent proteins Kusabira Orange 2 (mKO2) and Azami Green (mAG) to portions of Cdt1 and Geminin, respectively, the authors achieved striking contrast between various stages of the division cycle, effectively painting the nuclei of cells in G_1 phase red and those in $S/G_2/M$ green. This approach allowed cell-cycle dynamics to be monitored during several biologically relevant events, including the migration and differentiation of neural progenitor cells in brain slices and the movement of tumor cells across blood vessels in live mice. Because it allows various stages of the cell cycle to be correlated with cellular behaviors without the need to synchronize or otherwise perturb normal cell cycle progression, the Fucci technology promises to benefit many areas of cell biology. Moreover, with the development of future probes designed to mark other cell cycle transitions, such as G_2 to M, the ability of genetically encoded biosensors like Fucci to track different phases of the cell cycle will be further enhanced.

3.3. Measuring Protein−Protein Interactions

In one way or another, protein−protein interactions impact nearly every aspect of cell physiology, and cellular signaling is no exception. Inside the cell, the activity profiles of signaling enzymes are continuously modulated through specific interactions with regulatory factors, such as activators, inhibitors, adaptor molecules or scaffolding proteins, that rely upon direct protein−protein interactions. In fact, recently constructed interaction maps suggest that a given signaling protein may have tens, hundreds, or even thousands of transient interaction partners inside the cell, each of which could modulate its function in some manner.[396−398] Furthermore, an emerging concept in the field of intracellular signaling dynamics centers around the essential role of multiprotein signaling complexes, dubbed "signalosomes", in coordinating the behavior of signaling networks inside the cell.[399−401] Therefore, to better understand how signaling networks are constructed and controlled, it is important to define when and where in cellular space protein interactions occur.

Ideally, methods designed to probe protein−protein interactions would be able to detect binding events directly inside living cells, within the native subcellular environment of the interacting proteins. To this end, several fluorescent imaging techniques have been developed to probe protein−protein interactions under physiological conditions. These include both FRET- and BRET-based detection systems analogous to several of the bimolecular reporters described above as well as approaches, such as bimolecular fluorescence complementation (BiFC), which utilizes the phenomenon of protein fragment complementation to generate fluorescence from split FP molecules (Figure 8).[402−405] Recently, several insightful reviews have been published that discuss the advantages (and disadvantages) of using these approaches to study protein−protein interactions in living cells.[402−406] Therefore, here we will briefly describe each technique and discuss only a few of the innovative ways in which they have been applied to study protein−protein interactions that occur during signal transduction.

3.3.1. Detecting Protein−Protein Interactions Using Resonance Energy Transfer. Recall that RET efficiency (E) can be described by the equation $E = [1 + (r/R_0)^6]^{-1}$. This relationship implies that the effective range of energy transfer occurs at chromophore distances less than 10 nm. For most FP-based RET pairs, the Förster distance, R_0, is between 4 and 6 nm. Serendipitously, this distance corresponds nicely to the dimensions of most protein species[407] and many multimeric protein complexes.[405] Moreover, because it does not require physical interactions between the donor and acceptor chromophores, RET is readily reversible once the distance between

chromophores exceeds 10 nm. As a consequence, intermolecular RET represents an excellent means of detecting protein−protein interactions inside the cell (Figure 8a). To this end, both FRET- and BRET-based methods have been described to probe the assembly and disassembly of protein complexes inside the cell. For instance, FRET has been used to detect numerous dynamic protein−protein interactions in living cells, including the association/dissociation of heterotrimeric G-protein subunits,[408,409] the transient binding of nuclear receptors to coactivators,[410] the interaction between short-lived kinase-substrate pairs[356] and the formation of kinase-scaffold complexes.[411,412] Importantly, several FRET detection methods allow the apparent FRET efficiency, E_{app}, to be quantified within a heterogeneous population of donor−acceptor pairs. Using mathematical models generated from measured E_{app} values, important information can be gained about the structure and kinetics of protein−protein interaction networks (reviewed in ref 406). This approach has been particularly useful in defining the steps involved in the assembly and disassembly of signalosomes formed at the immune synapse.[406] Likewise, FRET-based techniques have provided insights into the assembly of other signaling complexes designed to coordinate the activities of several signaling molecules in space and time. For example, by measuring FRET between CFP- and YFP-tagged versions of CaN and the RII subunit of PKA, respectively, Oliveria et al. demonstrated that the molecular scaffold, AKAP79, organizes a kinase-scaffold-phosphatase ternary complex involved in the regulation of synaptic plasticity.[413] According to this study, which was the first to detect such a ternary complex in living cells, PKA and CaN reside in close proximity (estimated to be less than 50 Å) to one another in the context of the signaling complex.[413] Since CaN and PKA share many of the same substrates inside the cell, their close proximity on AKAP79 may have important implications during the propagation and attenuation of intracellular signals.

It is important to note that, when measuring protein−protein interactions, the maximum FRET efficiency between FP FRET pairs is only ∼40%.[403] This is largely because the dimensions of the FPs themselves (4.2 nm in length and 2.4 nm in diameter) occupies much of the useful FRET distance between the chromophores (Figure 1).[9] As a consequence, FP variants have sometimes been paired with the much smaller tetracysteine/biarsenical system to measure protein−protein interactions, especially in cases where the size of the FPs is limiting.[74,135] Though the relatively broad excitation spectrum of ReAsH allows it to function as a FRET acceptor for GFP,[135] the CFP-FlAsH FRET pair generally offers more efficient energy transfer.[74]

Interestingly, since the calculated R_0 for FlAsH and ReAsH is 39 Å, these dyes are predicted to be a relatively good FRET pair in and of themselves. However, because the tetracysteine motif cannot distinguish between the two ligands when they are administered at the same time, it is difficult to ensure that the majority of excited FlAsH molecules will actually induce FRET. This limitation can be overcome by adding a molar excess of ReAsH relative to FlAsH, thereby generating an excess of acceptor compared to fluorescence donor.[414] This approach was the key to detecting the aggregation of α-synuclein, a major component of intraneuronal plaques implicated in the etiology of Parkinson disease. Previous attempts at labeling α-synuclein with GFP variants had produced only nonfluorescent aggregates, presumably because the relatively large size of the FPs (∼27 kDa) prevented the aggregation of the smaller α-synuclein molecules (∼15 kDa). In contrast, when α-synuclein was tagged with a short tetracysteine motif and ReAsH and FlAsH were added at a 4:1 molar ratio, the aggregation of tagged α-synuclein molecules was readily detected by FRET. This approach, which allowed α-synuclein aggregation to be followed in real time, holds great promise as a tool for the development of drugs to combat Parkinson's disease.

Like FRET, BRET-based assays have also been instrumental in probing the protein−protein interactions that underlie many important intracellular signaling events.[415−417] In fact, this was one of the earliest applications of BRET in live cells.[418] During these studies, which were designed to monitor receptor dimerization following agonist addition, the β_2-adrenergic receptor (β_2-AR) was fused to either *Renilla* luciferase or EYFP. Following the addition of the coelentrazine substrate, changes in receptor dimerization caused by the agonist isoproterenol could be translated into changes in BRET. Surprisingly, these studies demonstrated that isoproterenol binds to constitutively dimerized β_2-ARs rather than monomeric receptor molecules, as had been predicted by the classical model of agonist-induced GPCR activation.[418] These data suggest that, rather than promoting the dimerization of β_2-AR monomers on the cell surface, β_2-AR agonists actually associate with preformed dimers and induce conformational changes in the dimer that lead to receptor activation. Presumably, these conformational changes reorient the chromophores, resulting in a change in BRET. Similar studies have since been conducted to measure both homo- and heterodimerization of several GPCR family members in the presence and the absence of a large number of agonists (reviewed in ref 404). Aside from the initial steps in receptor activation, BRET has also been used to monitor events that occur further downstream, such as interactions between GPCRs and components of the G$\alpha\beta\gamma$-complex[415,419,420] and the GPCR attenuator, β-arrestin.[421,422] Together, these studies have not only offered important insights into the molecular parameters governing GPCR signaling in live cells, but they have also begun to reshape many of our notions about how GPCR activation is regulated inside the cell.

BRET-based assays have also proven useful for high-throughput screening (HTS) applications.[422,423] For instance, Hamdan et al. recently used BRET to screen over 26,000 potential antagonists of CCR5, the primary coreceptor utilized by the human immunodeficiency virus (HIV) during infection.[422,424] Previous studies have demonstrated that CCR5 antagonists, such as Maraviroc, prevent HIV infection by blocking the interaction between CCR5 and the T-cell receptor.[425] To identify other CCR5 antagonists which may be useful in this regard, the authors developed a BRET-based assay to measure agonist-induced activation of CCR5 in the presence or absence of candidate receptor antagonists. This HTS, which was conducted in 96-well format using HEK293 cells stably expressing Venus-tagged CCR5 and RLuc-tagged β-arrestin2, relied upon agonist-induced interactions between CCR5 and β-arrestin2 to gauge the extent of receptor activation.[422] Recall that β-arrestins, which are intracellular adaptor proteins involved in the desensitization of many GPCR family members following activation, function by binding to the active form of the receptor and causing its internalization. As a consequence, interactions between β-arrestin and CCR5, reported as an increase in BRET, could be correlated with receptor activation. By extension, those compounds that prevented increases in BRET following agonist addition could potentially function as CCR5 antagonists. Using

this approach, the authors identified 12 compounds that led to a reduction in BRET, which represent new drug candidates for chemoprevention of HIV infection.

It should be noted that, during the aforementioned studies, BRET was measured at the population level rather than inside single cells. In fact, although BRET-based techniques offer relatively large signal-to-noise ratios compared to FRET, until recently, the amount of light emission intrinsic to the luciferase donor has prevented BRET from being used to monitor the formation of protein complexes at the subcellular level. However, recent advances in the sensitivity of detection systems, coupled with improved bioluminescent probes, has allowed BRET-based imaging to be extended to the single-cell level.[416,417,426] These advances promise to greatly enhance the information content available from BRET-based studies in both high-throughput applications and more focused investigations.

3.3.2. Protein Fragment Complementation. Several proteins, including GFP family members, are amenable to protein fragmentation. If brought into close proximity with one another, these protein fragments can recombine to form a functional protein. This property, which is the basis for BiFC and several related protein fragment complementation assays (PCAs), has been exploited to detect protein−protein interactions in living cells and even whole animals.[427−430] The principle of BiFC was first described by Ghosh et al., who showed that when N- and C-terminal fragments of *A. victoria* GFP were fused to short, interacting peptide sequences, GFP fluorescence could be reconstituted in vitro (Figure 8b).[431] The Kerpola group later built upon these findings by demonstrating that fragmented GFP variants could be used to detect protein−protein interactions in living cells.[432] These studies, which sought to explore the interactions between various basic region leucine zipper (bZIP) and Rel transcription factors, employed protein chimeras composed of Fos, Jun or Rel family members fused to YFP fragments split between amino acids 154 and 155. Using these chimeras, the authors demonstrated that only certain combinations of fusion proteins resulted in nuclear fluorescence, suggesting that only specific pairs of transcription factors could dimerize inside the cell. More recently, these studies have been extended to study interactions between Fos and Jun at different stages of nematode development.[433] To this end, Fos and Jun proteins fused to separate halves of split Venus were expressed under the control of the heat shock promoter, *hsp16.41*, in *C. elegans*.[433] Though these studies were aimed primarily at demonstrating the feasibility of conducting BiFC experiments in live animals, the ability to detect specific interactions in vivo will have important implications for future investigations.

Unlike many of the methods currently used to detect protein−protein interactions in cells, the large dynamic range afforded by BiFC allows many protein−protein interactions to be detected at protein levels that do not dramatically alter the cellular context in which the interactions occur. This property makes BiFC extremely attractive for studying signaling enzymes such as kinases, phosphatases and proteases which, when overexpressed, may adversely affect cellular physiology. Moreover, the development of intensely fluorescent CFP and YFP variants that are amenable to fluorescence complementation, coupled with improvements in the sensitivity of fluorescence detection systems, should reduce the number of molecular interactions required to achieve a detectable signal.

Aside from its ability to detect protein−protein interactions within the endogenous environment, one of the greatest strengths of BiFC is its versatility. For instance, since several GFP color variants are amenable to protein fragmentation, multiple protein interactions can be monitored simultaneously in the same cell.[432] To this end, different members of the bZIP transcription factor family were fused to fragments of either YFP, CFP, GFP, or BFP.[434] Interestingly, when fragments from YFP and CFP were brought into close proximity with one another by protein−protein interactions, the resultant FP hybrid exhibited excitation and emission spectra that were intermediate between those characteristic of YFP and CFP. This serendipitous finding provides an additional level of discrimination using this approach, allowing multiple protein interactions to be detected within a single cell. For instance, to delineate the subcellular locations of bJun/bFos and Jun/bFos interactions, a fusion protein consisting of bFos and a C-terminal fragment of YFP (bFosYC155) was coexpressed with bJun- and Jun-chimeras containing N-terminal fragments of CFP (bJunCN173) and YFP (JunYN155), respectively. These studies demonstrated that, while bJunCN173 and bFosYC155 associate primarily in the nucleolus, JunYN155/bFosYC155 interactions are restricted to the nucleoplasm. While only two interactions were visualized simultaneously during these experiments, in theory, the number of interactions that can be probed simultaneously using BiFC is limited only by the number of spectrally distinct fluorescent species that can be formed and unequivocally imaged. Indeed, the recent development of BiFC-compatible protein fragments based on mRFP[435] and the mKate derivative, mLumin,[436] has further expanded the repertoire of FP fragments available for BiFC, making the simultaneous visualization of more than two protein interactions in a single cell feasible.

Importantly, because FP complementation is essentially irreversible, BiFC is able to detect weak and/or transient interactions inside cells. However, it should be noted that the exquisite sensitivity afforded by BiFC comes at a price. For instance, though fast maturing FP fragments have recently been described,[437] in general, because of the slow maturation of the chromophore once complementary FP fragments have been recombined, a given binding event cannot be detected for at least an hour after the initial interaction (Figure 8b). Therefore, since most protein−protein interactions occur within a matter of seconds, BiFC does not accurately report the temporal regulation of most interactions. Furthermore, BiFC contains little information about the dynamic nature of many binding events because of the irreversibility of the protein complementation assay. In those cases where kinetic analysis of complex formation is desired, RET-based techniques or reversible protein fragment complementation systems, such as those based on split luciferase,[438−444] may offer more relevant information about the rates of protein association and dissociation. Ideally, these approaches could be employed in a complementary manner to more fully characterize protein−protein interactions inside cells.

Finally, it is worth mentioning that, like the BRET-based techniques described above, protein fragment complementation technologies are amenable to high-throughput screens. This property is particularly important when identifying protein binding partners because a given protein may interact with hundreds or even thousands of proteins in the cellular milieu. In the postgenomic era, these data have been used to build so-called "interactomes" that can offer important insights into the biological function of an unknown protein or implicate a known protein in a novel cellular process. For instance, the protein kinase Akt is a central regulator of a number of cellular processes and, as such, is believed to transiently interact

with a wide variety of substrates in a context-specific manner. To identify new binding partners of Akt, researchers appended one-half of a split GFP molecule to Akt and screened the chimera against a library of 10^7-10^8 independent cDNAs which were fused to the other half of GFP.[445] To increase the throughput of the assay, fluorescent cells were screened by fluorescence activated cell sorting (FACS), allowing the cDNA of positive clones to be recovered and sequenced in a rapid fashion. From this screen, over 2,500 clones were identified, of which 22 were deemed to be strong candidates for binding Akt in vivo. In some cases, the biological function of the identified proteins was unknown. For instance, one protein, hFt1, which shared significant sequence homology with murine Ft1 but was itself uncharacterized, was recovered from three independent cDNA clones.[446] A more in-depth analysis demonstrated that, indeed, hFt1 is a novel Akt binding partner. Moreover, the Akt-hFt1 interaction was inhibited by pretreatment with either wortmannin or LY294002, each of which prevents Akt activation, suggesting that hFt1 associates preferentially with the active form of Akt.[446] These findings are consistent with subsequent studies which demonstrated that hFt1 enhances Akt activation mediated by the upstream kinase, 3-phosphoinositide-dependent kinase 1 (PDK1), and that this interaction has a strong impact on the susceptibility of T lymphocytes to undergo apoptosis in response to glucocorticoids.[446]

More recently, the Michnick lab described a genome-wide in vivo screen of protein−protein interactions in the yeast *Saccharomyces cerevisiae*.[398] During these studies, the authors used a PCA based on murine dihydrofolate reductase (DHFR) to identify 2,770 protein−protein interactions among 1,124 endogenously expressed proteins.[398] These data, which provided a global view of protein−protein interactions under the experimental conditions, promise to generate new insights into the organization and function of protein interaction networks in yeast. Unfortunately, since the screen used during these studies was based on a survival-selection end point that is specific to yeast, this approach cannot be used to construct interaction maps in mammalian cell types. BiFC may be a logical alternative. Indeed, the recent development of HTS methods that couple the sensitivity of BiFC with the throughput of FACS opens the door for such studies in mammalian cell types.[445,447]

4. CONCLUSIONS AND FUTURE PERSPECTIVES

To date, genetically encoded fluorescent probes have provided critical insights into the molecular mechanisms underlying the regulation of several intracellular signal transduction pathways. Importantly, in addition to offering rich biological information about the cellular system under study, these studies have also taught us valuable lessons about the design of biosensors, themselves. This information, coupled with parallel studies aimed at (1) improving the photophysical characteristics of existing FP family members for live cell imaging and (2) identifying new FP variants and complementary labeling technologies capable of visualizing cellular events,[66,68] will aid in the development of novel biosensors designed to image signal transduction in a variety of biological contexts, including truly in vivo settings. The development of new biosensors will also allow a wider range of signaling parameters to be measured within the cellular environment, providing the experimental information required to build detailed computational models of signal transduction inside the cell. Such an approach will be necessary if we are to gain a quantitative understanding of the complex interactions that occur between signaling molecules at the systems level. Finally, by combining the reporting power of fluorescent biosensors with novel molecular tools designed to manipulate biological systems in a spatially and temporally restricted manner, researchers will be able to probe the biochemical properties of signaling enzymes within the endogenous cellular environment, promoting a type of "native biochemistry" that promises to yield important information about the regulation of signaling proteins in the presence of endogenous levels of their regulatory elements. Recently, several significant steps have been made toward realizing these goals.

4.1. Tracking Signaling Dynamics in Vivo

To better understand how cellular signaling pathways are regulated under physiological conditions, several groups have described methods to monitor dynamic signaling processes in transgenic animals.[246,249,250,253,448−453] Aside from GECIs, which have been used extensively to measure Ca^{2+} transients within defined populations of neurons[246,249,250,253,448,451] and cardiomyocytes[253] in both mice and fruit flies, fluorescent biosensors of other important signaling molecules have recently been applied to the study of signaling dynamics in the context of live animals.[293,449,452,453] For instance, cAMP signaling pathways are believed to play important roles during neuronal development as well as in learning and memory processes. Therefore, to monitor cAMP dynamics in both developing and mature fruit flies, the Zaccolo laboratory created transgenic animals that express the bimolecular PKA-based FRET biosensor, PKA-GFP, in a tissue-specific manner.[453] To ensure that both components of the reporter (i.e., RII-CFP and PKA^{cat}-YFP) were expressed at similar levels, each chimera was placed under the control of an independent upstream activating sequence (UAS) contained within a single transformation vector. As a proof-of-principle, the authors used two-photon confocal microscopy to measure forskolin-induced increases in $[cAMP]_i$ (corresponding to a decrease in FRET efficiency between CFP and YFP) in the horizontal lobes of mushroom body neurons of live animals.[453] Though this system has not yet been used to measure cAMP signals evoked by physiologically relevant stimuli, it provides a platform for measuring cAMP dynamics in intact animals.

More recently, Kamiyama and Chiba used a FRET-based activation reporter, termed A-probe.1, to measure the endogenous activation patterns of the Rho GTPase, Cdc42, during *Drosophila* embryogenesis.[452] These studies, which tracked Cdc42 activation both in individual cells and in entire cell populations in the context of intact *Drosophila* embryos, demonstrated that Cdc42 activation coincides both spatially and temporally with the onset of dendrogenesis during the final stages of embryogenesis.[452] For example, when the probe was expressed exclusively in the anterior corner cell (aCC) motorneuron, which is one of the first neurons to develop complex cellular morphologies in the CNS of *Drosophila*, highly restricted Cdc42 activation patterns were observed in the proximal region of the axon from which dendrites emerge.[452] These data suggest that Cdc42 activation not only coincides temporally with the onset of dendrogenesis in the aCC motorneuron, but that it is also spatially restricted to the compartment responsible for dendrite outgrowth.[452] Indeed, based upon these data and those obtained from complementary genetic experiments, the authors concluded that, though Cdc42 is ubiquitously expressed

throughout embryogenesis, its activation is restricted to the final stages of development, where it plays an essential role in normal neuronal development.[452]

4.2. Computational Modeling Based on Live Cell Imaging Data

Recently, several groups have begun to incorporate quantitative fluorescence imaging data into mathematical models in order to gain insights into the molecular events underlying complex cellular behaviors. Not only does this approach have the potential to uncover details about the behavior of individual components within a signaling network, but it can also provide crucial insights into how information is propagated through the system, as a whole. Because these types of questions are difficult (if not impossible) to answer using experimental approaches alone, computational methods can provide a more comprehensive view of signaling networks that will ultimately promote a better understanding of cellular signaling at the systems level.

To this end, computational models have recently been developed to better understand the impact of PKA-mediated phosphorylation gradients in cardiomyocytes[454] and hippocampal neurons.[455] They have also been used to decifer the mechanisms by which the activities of Ca^{2+}/CaM-dependent signaling enzymes are regulated in response to dynamic changes in $[Ca^{2+}]_i$[456] and to gain quantitative information about the kinetic parameters associated with each step in the M_1 muscarinic receptor signaling pathway, from ligand binding to PLC-mediated PIP_2 depletion.[457,458] One of the primary goals of this type of systems biology approach is to determine the relative contributions of multiple feedback and feed-forward loops in producing the tight spatiotemporal control exhibited by many signal transduction pathways. For instance, based upon data obtained from live cell imaging experiments using the FRET-based cAMP reporter, ICUE2, our lab recently constructed a model of β_2-AR-mediated cAMP signaling in conjunction with the Lefkowitz laboratory that has both descriptive and predictive power.[459] Using this model, we were able to better define the relative contributions of homologous and heterologous desensitization mechanisms during receptor inactivation. Interestingly, simulations suggest that while PKA plays a central role in determining the amplitude and duration of the cAMP signal by stimulating PDE4 activity, its direct contribution to receptor inactivation is minimal.[459] Instead, receptor inactivation appears to be controlled almost exclusively by homologous desensitization through the action of GRK6 and β-arrestins. Moreover, the model shows that receptor deactivation is surprisingly rapid, reaching half-maximal levels only 70 s after activation.[459] Together with PKA-dependent acceleration of PDE4 activity, such rapid receptor deactivation kinetics afford cells very strict control over cAMP dynamics. As illustrated by this and other similar studies,[514] when combined with live cell imaging, computational models can provide quantitative information about the relative contribution made by individual components in a signaling network during a given cellular response.

In much the same way, computational models derived from live cell imaging data have also begun to provide clues about the ways in which information is both stored and propagated throughout a cell in space and time. For instance, using an integrated approach based on computational modeling, live cell imaging and immunohistochemistry, Neves et al. recently demonstrated that several parameters, including cellular geometry, network topology and the biochemical activities of negative regulators, such as protein phosphatases and PDEs, lead to the formation of spatially restricted microdomains that play an important role in regulating the β-AR/cAMP/PKA/B-Raf/MAPK1,2 signaling axis in rat hippocampal neurons.[455] Importantly, with continued advances in biosensor development, the quality and depth of information that can be incorporated into models of signal transduction will continue to increase, promoting a more quantitative understanding of the molecular mechanisms that influence signaling dynamics inside the cell. Such quantitative information will be critical if we are to truly understand the functional interactions that occur between individual signaling molecules to drive complex cellular behaviors.

4.3. Manipulation of Cellular Signaling Pathways: Toward a Native Biochemistry

Finally, as we have seen throughout the course of this review, to achieve a specific cellular response, each component of a given signaling pathway must be precisely controlled in both space and time. However, within the highly connected environment of living cells, where any number of downstream effectors may feedback to reinforce/inhibit upstream signals, it is often difficult to determine unequivocally what impact a particular signaling factor has on an observed cellular response. One of the primary reasons for this gap in our understanding of intracellular signaling dynamics stems from the fact that, until recently, our ability to manipulate the activity of specific signaling factors in living cells with the spatial and/or temporal resolution required to dissect their relative contribution to a given cellular response has been limited. This point is illustrated by examining the cellular mechanisms responsible for PLC-mediated suppression of K^+ currents in neurons. Though the activation of PLC by muscarinic receptors had been shown to induce closure of KCNQ K^+ channels in response to several receptor agonists, the factors that actually controlled KCNQ channel closure remained controversial. Was PLC-mediated depletion of $PtdIns(4,5)P_2$ at the membrane sufficient to mediate this response or were additional downstream messengers, such as the PLC cleavage products diacylglycerol (DAG) and IP_3, also partly (or wholly) responsible for the observed effect?[460] To answer this question and others like it, researchers have developed a series of molecular tools designed to precisely manipulate signaling molecules in living cells.[461−470] When used in conjunction with genetically encodable fluorescent biosensors designed to measure changes in a specific cellular parameter, these tools allow researchers to conduct biochemical experiments, not in a test tube, but within the native cellular environment. Below we highlight two of these methods.

To resolve the controversy surrounding PLC-mediated suppression of KCNQ channels described above, researchers employed a chemical dimerizer strategy to specifically deplete $PtdIns(4,5)P_2$ at the plasma membrane without affecting the concentration of other second messengers, such as DAG, IP_3, or Ca^{2+}.[466] This system, which is based on the heterodimerization of protein domains from FK506 binding protein (FKBP) and mTOR (FRB) by the rapamycin analog, iRap,[464] enabled the authors to rapidly recruit a fusion protein composed of CFP, FKBP and the yeast inositol polyphosphate 5-phospatase (CF-Inp54p) to the plasma membrane through iRap-mediated interactions with Lyn_{11}-conjugated FRB molecules.[466] Because Inp54p specifically cleaves the 5-phosphate on $PtdIns(4,5)P_2$, this strategy allows $PtdIns(4,5)P_2$ levels to be modulated in a temporally restricted manner.[466] To confirm that iRap addition resulted solely in the depletion of $PtdIns(4,5)P_2$, a series of

YFP-conjugated PI probes were used to track changes in membrane lipid levels. Because IP_3 promotes the release of intracellular Ca^{2+}, changes in $[Ca^{2+}]_i$ were also measured using the Ca^{2+}-sensitive dye, Fura-2. As expected, CF-Inp54p recruitment only altered PtdIns(4,5)P_2 levels at the plasma membrane and not those of the other signaling molecules.[466] Importantly, iRap addition also led to the complete abolition of the K^+ current through KCNQ channels in a CF-Inp54p-dependent manner.[466] Likewise, the reciprocal experiment, in which Inp54p was replaced by a PtdIns(4)P kinase to increase PtdIns(4,5)P_2 levels at the plasma membrane, resulted in markedly slower suppression of KCNQ current following PLC activation.[466] Together, these data suggest that PtdIns(4,5)P_2, and not downstream signaling molecules, is the primary mediator of PLC-induced suppression of KCNQ K^+ currents.[466] Importantly, in addition to PI species, the versatility afforded by the FRB/FKBP/iRap dimerizer strategy has allowed researchers to modulate the activities of several different signaling molecules in live cells, including the G-proteins Rac1, Cdc42, and RhoA.[464]

Interestingly, Hahn and colleagues recently described a complementary method to modulate the activity of Rac1 in a highly controlled manner.[470] However, rather than relying upon a chemical inducer to alter the activity of Rac1 in cells, they did so using short pulses of 458 nm light. This was accomplished by fusing the photoreactive light oxygen voltage (LOV) domain from phototropin to a constitutively active form of Rac1 to create a photoactivatible analogue of Rac1 (PA-Rac1).[470] Because interactions between Rac1 and the LOV domain block the binding of Rac1 effectors such as RhoA in the uninduced state, Rac1 remains inactive in the dark. In contrast, exposure to 458 nm light drives a conformational change in the LOV domain that relieves this inhibition, causing an increase in Rac1 activity at the site of irradiation. As a proof-of-principle, the authors demonstrated that when MEFs stably expressing PA-Rac1 were irradiated with 20-μm spots of light at the cell edge, the cells generated large protrusions at the site of irradiation.[470] Interestingly, light-induced protrusions retracted once the light source was removed, suggesting that PA-Rac1 activity is reversible.[470] Next, to better understand how Rac regulates Rho activity in cells, PA-Rac1 was activated in the presence of a FRET-based RhoA biosensor.[350] These studies demonstrated that PA-Rac1 activation leads to immediate inhibition of RhoA at the site of irradiation, followed by further RhoA inhibition that spreads slowly outward from the point of PA-Rac1 activation.[470] Importantly, using tertiary structure predictions the authors were able to create a similar photoactivatible analog for the related GTPase, Cdc42 (PA-Cdc42), by introducing a single point mutation (F56W) on Cdc42.[470] These results suggest that this general strategy may be useful for creating other photoactivatible GTPases, and perhaps even other enzyme families, whose activities can be precisely controlled inside the cell using focused laser illumination and/or patterned light. Together with several other recently developed inducible enzyme systems, such as the photoswitchable "Phy-PIF" dimerizer system,[465] the channelrhodopsins,[516,517] a family of opsin-GPCR chimeras[462] and a series of "light-gated" receptor−ligand chimeras (reviewed in ref 471), the strategies outlined above provide the first steps toward a revolution in native cell biochemistry akin to the one ushered in by fluorescent biosensors nearly two decades ago.

4.4. Conclusions

Genetically encodable fluorescent biosensors represent versatile and potentially powerful tools for tracking signaling dynamics in living cells. These sensors have allowed researchers to observe the inner-workings of live cells in real time and with unprecedented spatial resolution. In so doing, they have sparked a revolution in the field of cell signaling that has helped refine and, in some cases, reshape our notions about how intracellular signaling networks are organized and controlled within the native cellular environment. At the heart of this revolution is *A. victoria* GFP and its ever-growing family tree. Indeed, GFP family members provide the foundation upon which most currently available fluorescent biosensors have been built. Due to their unique biochemical and photophysical properties, FPs have the potential to function not only as "passive" reporters of intracellular protein dynamics, but also as "active" probes whose fluorescence properties can be modulated in response to changes in the cellular environment. Moreover, the development of multicomponent FP-based reporter systems that exploit bio- and photophysical phenomena such as protein fragment complementation and RET to measure protein−protein interactions and enzyme activation within the cellular milieu has greatly expanded the number of intracellular events that can be monitored using fluorescence microscopy. In the future, the development and application of FP-based biosensors, along with complementary reporter systems based on several promising genetically targetable fluorescent tags, promises to yield new and unexpected information about the complex world of the cell.

ASSOCIATED CONTENT

Supporting Information

Comprehensive tables, describing many currently available FPs (Table S1), PI-FPs (Table S2), genetically targetable chemical labeling methods (Table S3), and genetically encodable fluorescent biosensors (Table S4). This information is available free of charge via the Internet at http://pubs.acs.org/.

AUTHOR INFORMATION

Corresponding Author

*Mailing address: 725 N. Wolfe St., Hunterian 307, Baltimore, MD 21205. E-mail: jzhang32@jhmi.edu.

BIOGRAPHIES

Rob Newman majored in biology and biochemistry at McDaniel College (B.A., 1999) before pursuing graduate work in the Department of Biochemistry and Molecular Biology at Johns Hopkins University (Ph.D., 2006). Under the direction of

Dr. Roger McMacken, Rob examined the molecular mechanisms underlying chaperone-mediated remodeling of a nucleoprotein complex involved in the initiation of lambda phage DNA replication. Following graduation, Rob joined the laboratory of Dr. Jin Zhang as a postdoctoral fellow, where he is using both live cell imaging and protein microarray technology to better understand the structure and regulation of intracellular signaling networks.

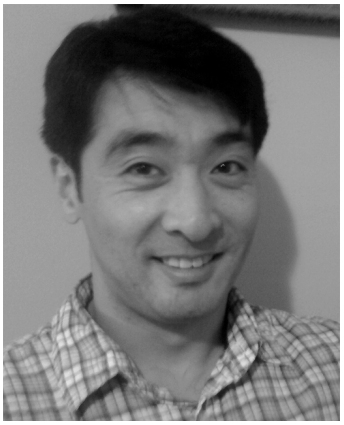

Matthew Fosbrink received a Bachelor of Science degree at the University of Maryland, Baltimore in Medical and Research Technology and pursued a Ph.D. in Toxicology at the same institution. His doctoral thesis focused on the signaling pathways and the novel gene RGC-32 on cell cycle activation by the complement C5b-9 membrane attack complex in the lab of Horea Rus. After completing his graduate work, he then joined Jin Zhang's lab at Johns Hopkins, School of Medicine as a postdoctoral fellow where he engineered FRET-based reporters for the detection of JNK activity in living cells. He is currently at SABiosciences, a subsidiary of Qiagen, developing tools to study miRNA function and expression.

Jin Zhang attended Tsinghua University for her undergraduate studies, and pursued her graduate studies in Chemistry at the U. Chicago. After completing her postdoctoral work at the U. California, San Diego, she joined the faculty of Johns Hopkins University School of Medicine, where she is currently an Associate Professor of Pharmacology, Neuroscience and Oncology, with a joint appointment in the Dept. of Chemical and Biomolecular Engineering in the Whiting School of Engineering. She received the American Heart Association National Scientist Development Award, the Biophysical Society Margaret Oakley Dayhoff Award, and the National Institutes of Health (NIH) Director's Pioneer Award.

ACKNOWLEDGMENT

The authors thank Charlene Depry, Sohum Mehta, Qiang Ni, and Xinxin Gao for critical reading of the manuscript. Work in the lab is funded by NIH (DK073368 and DP1OD006419) and 3M (to J.Z.).

REFERENCES

(1) Coons, A. H.; Creech, H. J.; Jones, R. N.; Berliner, E. *J. Immunol.* **1942**, *45*, 159.
(2) Trask, B. J. *Nat. Rev. Genet.* **2002**, *3*, 769.
(3) Tsien, R. Y. *Annu. Rev. Biochem.* **1998**, *67*, 509.
(4) Zimmer, M. *Chem. Rev.* **2002**, *102*, 759.
(5) Chalfie, M.; Tu, Y.; Euskirchen, G.; Ward, W. W.; Prasher, D. C. *Science* **1994**, *263*, 802.
(6) Cubitt, A. B.; Heim, R.; Adams, S. R.; Boyd, A. E.; Gross, L. A.; Tsien, R. Y. *Trends Biochem. Sci.* **1995**, *20*, 448.
(7) Chudakov, D. M.; Lukyanov, S.; Lukyanov, K. A. *Trends Biotechnol.* **2005**, *23*, 605.
(8) Yang, F.; Moss, L. G.; Phillips, G. N., Jr. *Nat. Biotechnol.* **1996**, *14*, 1246.
(9) Ormo, M.; Cubitt, A. B.; Kallio, K.; Gross, L. A.; Tsien, R. Y.; Remington, S. J. *Science* **1996**, *273*, 1392.
(10) Remington, S. J. *Curr. Opin. Struct. Biol.* **2006**, *16*, 714.
(11) Wachter, R. M. *Acc. Chem. Res.* **2007**, *40*, 120.
(12) Barondeau, D. P.; Putnam, C. D.; Kassmann, C. J.; Tainer, J. A.; Getzoff, E. D. *Proc. Natl. Acad. Sci. U.S.A.* **2003**, *100*, 12111.
(13) Niwa, H.; Inouye, S.; Hirano, T.; Matsuno, T.; Kojima, S.; Kubota, M.; Ohashi, M.; Tsuji, F. I. *Proc. Natl. Acad. Sci. U.S.A.* **1996**, *93*, 13617.
(14) For an in-depth analysis of the mechanistic details of GFP chromophore maturation, the interested reader is referred to refs 14−20.
(15) Pouwels, L. J.; Zhang, L.; Chan, N. H.; Dorrestein, P. C.; Wachter, R. M. *Biochemistry* **2008**, *47*, 10111.
(16) Zhang, L.; Patel, H. N.; Lappe, J. W.; Wachter, R. M. *J. Am. Chem. Soc.* **2006**, *128*, 4766.
(17) Verkhusha, V. V.; Lukyanov, K. A. *Nat. Biotechnol.* **2004**, *22*, 289.
(18) Shu, X.; Shaner, N. C.; Yarbrough, C. A.; Tsien, R. Y.; Remington, S. J. *Biochemistry* **2006**, *45*, 9639.
(19) Barondeau, D. P.; Putnam, C. D.; Kassmann, C. J.; Tainer, J. A.; Getzoff, E. D. *Proc. Natl. Acad. Sci. U.S.A.* **2003**, *100*, 12111.
(20) Rao, B. D.; Kemple, M. D.; Prendergast, F. G. *Biophys. J.* **1980**, *32*, 630.
(21) Ward, W. W.; Bokman, S. H. *Biochemistry* **1982**, *21*, 4535.
(22) Merzlyak, E. M.; Goedhart, J.; Shcherbo, D.; Bulina, M. E.; Shcheglov, A. S.; Fradkov, A. F.; Gaintzeva, A.; Lukyanov, K. A.; Lukyanov, S.; Gadella, T. W.; Chudakov, D. M. *Nat. Methods* **2007**, *4*, 555.
(23) Shcherbo, D.; Merzlyak, E. M.; Chepurnykh, T. V.; Fradkov, A. F.; Ermakova, G. V.; Solovieva, E. A.; Lukyanov, K. A.; Bogdanova, E. A.; Zaraisky, A. G.; Lukyanov, S.; Chudakov, D. M. *Nat. Methods* **2007**, *4*, 741.
(24) Follenius-Wund, A.; Bourotte, M.; Schmitt, M.; Iyice, F.; Lami, H.; Bourguignon, J. J.; Haiech, J.; Pigault, C. *Biophys. J.* **2003**, *85*, 1839.
(25) Brejc, K.; Sixma, T. K.; Kitts, P. A.; Kain, S. R.; Tsien, R. Y.; Ormo, M.; Remington, S. J. *Proc. Natl. Acad. Sci. U.S.A.* **1997**, *94*, 2306.
(26) Chattoraj, M.; King, B. A.; Bublitz, G. U.; Boxer, S. G. *Proc. Natl. Acad. Sci. U.S.A.* **1996**, *93*, 8362.
(27) Cormack, B. P.; Valdivia, R. H.; Falkow, S. *Gene* **1996**, *173*, 33.
(28) Baird, G. S.; Zacharias, D. A.; Tsien, R. Y. *Proc. Natl. Acad. Sci. U.S.A.* **2000**, *97*, 11984.
(29) Henderson, J. N.; Remington, S. J. *Proc. Natl. Acad. Sci. U.S.A.* **2005**, *102*, 12712.
(30) Day, R. N.; Davidson, M. W. *Chem. Soc. Rev.* **2009**, *38*, 2887.

(31) Sample, V.; Newman, R. H.; Zhang, J. *Chem. Soc. Rev.* **2009**, *38*, 2852.
(32) Shaner, N. C.; Patterson, G. H.; Davidson, M. W. *J. Cell Sci.* **2007**, *120*, 4247.
(33) Zolotukhin, S.; Potter, M.; Hauswirth, W. W.; Guy, J.; Muzyczka, N. *J. Virol.* **1996**, *70*, 4646.
(34) Yang, T. T.; Cheng, L.; Kain, S. R. *Nucleic Acids Res.* **1996**, *24*, 4592.
(35) Kozak, M. *J. Cell Biol.* **1989**, *108*, 229.
(36) Heim, R.; Tsien, R. Y. *Curr. Biol.* **1996**, *6*, 178.
(37) Pedelacq, J. D.; Cabantous, S.; Tran, T.; Terwilliger, T. C.; Waldo, G. S. *Nat. Biotechnol.* **2006**, *24*, 79.
(38) Kremers, G. J.; Goedhart, J.; van den Heuvel, D. J.; Gerritsen, H. C.; Gadella, T. W., Jr. *Biochemistry* **2007**, *46*, 3775.
(39) Nagai, T.; Yamada, S.; Tominaga, T.; Ichikawa, M.; Miyawaki, A. *Proc. Natl. Acad. Sci. U.S.A.* **2004**, *101*, 10554.
(40) Shaner, N. C.; Steinbach, P. A.; Tsien, R. Y. *Nat. Methods* **2005**, *2*, 905.
(41) Rizzo, M. A.; Springer, G. H.; Granada, B.; Piston, D. W. *Nat. Biotechnol.* **2004**, *22*, 445.
(42) Stauber, R. H.; Horie, K.; Carney, P.; Hudson, E. A.; Tarasova, N. I.; Gaitanaris, G. A.; Pavlakis, G. N. *Biotechniques* **1998**, *24*, 462.
(43) Ai, H. W.; Henderson, J. N.; Remington, S. J.; Campbell, R. E. *Biochem. J.* **2006**, *400*, 531.
(44) Matz, M. V.; Fradkov, A. F.; Labas, Y. A.; Savitsky, A. P.; Zaraisky, A. G.; Markelov, M. L.; Lukyanov, S. A. *Nat. Biotechnol.* **1999**, *17*, 969.
(45) Greenbaum, L.; Rothmann, C.; Lavie, R.; Malik, Z. *Biol. Chem.* **2000**, *381*, 1251.
(46) Fischer, J. R.; Julian, G. R.; Rogers, S. J. *Physiol. Chem. Phys.* **1974**, *6*, 179.
(47) Tsai, C. S.; Godin, J. R.; Wand, A. J. *Biochem. J.* **1985**, *225*, 203.
(48) Mena, M. A.; Treynor, T. P.; Mayo, S. L.; Daugherty, P. S. *Nat. Biotechnol.* **2006**, *24*, 1569.
(49) Ai, H. W.; Shaner, N. C.; Cheng, Z.; Tsien, R. Y.; Campbell, R. E. *Biochemistry* **2007**, *46*, 5904.
(50) Subach, O. M.; Gundorov, I. S.; Yoshimura, M.; Subach, F. V.; Zhang, J.; Gruenwald, D.; Souslova, E. A.; Chudakov, D. M.; Verkhusha, V. V. *Chem. Biol.* **2008**, *15*, 1116.
(51) Kummer, A. D.; Wiehler, J.; Schuttrigkeit, T. A.; Berger, B. W.; Steipe, B.; Michel-Beyerle, M. E. *ChemBiochem* **2002**, *3*, 659.
(52) Mauring, K.; Deich, J.; Rosell, F. I.; McAnaney, T. B.; Moerner, W. E.; Boxer, S. G. *J. Phys. Chem. B* **2005**, *109*, 12976.
(53) Pletnev, S.; Subach, F. V.; Dauter, Z.; Wlodawer, A.; Verkhusha, V. V. *J. Am. Chem. Soc.* **2010**, *132*, 2243.
(54) Shaner, N. C.; Lin, M. Z.; McKeown, M. R.; Steinbach, P. A.; Hazelwood, K. L.; Davidson, M. W.; Tsien, R. Y. *Nat. Methods* **2008**, *5*, 545.
(55) Wachter, R. M.; Elsliger, M. A.; Kallio, K.; Hanson, G. T.; Remington, S. J. *Structure* **1998**, *6*, 1267.
(56) Miyawaki, A.; Llopis, J.; Heim, R.; McCaffery, J. M.; Adams, J. A.; Ikura, M.; Tsien, R. Y. *Nature* **1997**, *388*, 882.
(57) Miyawaki, A.; Griesbeck, O.; Heim, R.; Tsien, R. Y. *Proc. Natl. Acad. Sci. U.S.A.* **1999**, *96*, 2135.
(58) Griesbeck, O.; Baird, G. S.; Campbell, R. E.; Zacharias, D. A.; Tsien, R. Y. *J. Biol. Chem.* **2001**, *276*, 29188.
(59) Nagai, T.; Ibata, K.; Park, E. S.; Kubota, M.; Mikoshiba, K.; Miyawaki, A. *Nat. Biotechnol.* **2002**, *20*, 87.
(60) Rekas, A.; Alattia, J. R.; Nagai, T.; Miyawaki, A.; Ikura, M. *J. Biol. Chem.* **2002**, *277*, 50573.
(61) Wachter, R. M.; Yarbrough, D.; Kallio, K.; Remington, S. J. *J. Mol. Biol.* **2000**, *301*, 157.
(62) He, Y. Y.; Huang, J. L.; Chignell, C. F. *J. Biol. Chem.* **2004**, *279*, 53867.
(63) Provost, N.; Moreau, M.; Leturque, A.; Nizard, C. *Am. J. Physiol. Cell Physiol.* **2003**, *284*, C51.
(64) Benson, R. C.; Meyer, R. A.; Zaruba, M. E.; McKhann, G. M. *J. Histochem. Cytochem.* **1979**, *27*, 44.
(65) Shaner, N. C.; Campbell, R. E.; Steinbach, P. A.; Giepmans, B. N.; Palmer, A. E.; Tsien, R. Y. *Nat. Biotechnol.* **2004**, *22*, 1567.
(66) Shcherbo, D.; Murphy, C. S.; Ermakova, G. V.; Solovieva, E. A.; Chepurnykh, T. V.; Shcheglov, A. S.; Verkhusha, V. V.; Pletnev, V. Z.; Hazelwood, K. L.; Roche, P. M.; Lukyanov, S.; Zaraisky, A. G.; Davidson, M. W.; Chudakov, D. M. *Biochem. J.* **2009**, *418*, 567.
(67) Lin, M. Z.; McKeown, M. R.; Ng, H. L.; Aguilera, T. A.; Shaner, N. C.; Campbell, R. E.; Adams, S. R.; Gross, L. A.; Ma, W.; Alber, T.; Tsien, R. Y. *Chem. Biol.* **2009**, *16*, 1169.
(68) Shu, X.; Royant, A.; Lin, M. Z.; Aguilera, T. A.; Lev-Ram, V.; Steinbach, P. A.; Tsien, R. Y. *Science* **2009**, *324*, 804.
(69) Shimomura, O.; Johnson, F. H.; Saiga, Y. *J. Cell Comp. Physiol.* **1962**, *59*, 223.
(70) Prendergast, F. G.; Mann, K. G. *Biochemistry* **1978**, *17*, 3448.
(71) Hink, M. A.; Griep, R. A.; Borst, J. W.; van Hoek, A.; Eppink, M. H.; Schots, A.; Visser, A. J. *J. Biol. Chem.* **2000**, *275*, 17556.
(72) Dyachok, O.; Isakov, Y.; Sagetorp, J.; Tengholm, A. *Nature* **2006**, *439*, 349.
(73) Enninga, J.; Mounier, J.; Sansonetti, P.; Tran, V. N. *Nat. Methods* **2005**, *2*, 959.
(74) Hoffmann, C.; Gaietta, G.; Bunemann, M.; Adams, S. R.; Oberdorff-Maass, S.; Behr, B.; Vilardaga, J. P.; Tsien, R. Y.; Ellisman, M. H.; Lohse, M. J. *Nat. Methods* **2005**, *2*, 171.
(75) Phillips, G. N., Jr. *Curr. Opin. Struct. Biol.* **1997**, *7*, 821.
(76) Campbell, R. E.; Tour, O.; Palmer, A. E.; Steinbach, P. A.; Baird, G. S.; Zacharias, D. A.; Tsien, R. Y. *Proc. Natl. Acad. Sci. U.S.A.* **2002**, *99*, 7877.
(77) Forster, T. *Annal. Phys.* **1948**, *2*, 55.
(78) Bacart, J.; Corbel, C.; Jockers, R.; Bach, S.; Couturier, C. *Biotechnol. J.* **2008**, *3*, 311.
(79) Patterson, G. H.; Piston, D. W.; Barisas, B. G. *Anal. Biochem.* **2000**, *284*, 438.
(80) Arai, R.; Nakagawa, H.; Kitayama, A.; Ueda, H.; Nagamune, T. *J. Biosci. Bioeng.* **2002**, *94*, 362.
(81) Yamakawa, Y.; Ueda, H.; Kitayama, A.; Nagamune, T. *J. Biosci. Bioeng.* **2002**, *93*, 537.
(82) Gammon, S. T.; Villalobos, V. M.; Roshal, M.; Samrakandi, M.; Piwnica-Worms, D. *Biotechnol. Prog.* **2009**, *25*, 559.
(83) Tannous, B. A.; Kim, D. E.; Fernandez, J. L.; Weissleder, R.; Breakefield, X. O. *Mol. Ther.* **2005**, *11*, 435.
(84) De, A.; Loening, A. M.; Gambhir, S. S. *Cancer Res.* **2007**, *67*, 7175.
(85) Loening, A. M.; Fenn, T. D.; Wu, A. M.; Gambhir, S. S. *Protein Eng. Des. Sel.* **2006**, *19*, 391.
(86) Loening, A. M.; Wu, A. M.; Gambhir, S. S. *Nat. Methods* **2007**, *4*, 641.
(87) Pfleger, K. D.; Dromey, J. R.; Dalrymple, M. B.; Lim, E. M.; Thomas, W. G.; Eidne, K. A. *Cell Signal* **2006**, *18*, 1664.
(88) Levi, J.; De, A.; Cheng, Z.; Gambhir, S. S. *J. Am. Chem. Soc.* **2007**, *129*, 11900.
(89) Pfleger, K. D.; Eidne, K. A. *Nat. Methods* **2006**, *3*, 165.
(90) Issad, T.; Blanquart, C.; Gonzalez-Yanes, C. *Expert Opin. Ther. Targets* **2007**, *11*, 541.
(91) Wu, X.; Simone, J.; Hewgill, D.; Siegel, R.; Lipsky, P. E.; He, L. *Cytometry, Part A* **2006**, *69*, 477.
(92) Peyker, A.; Rocks, O.; Bastiaens, P. I. *ChemBioChem* **2005**, *6*, 78.
(93) Kawai, H.; Suzuki, T.; Kobayashi, T.; Sakurai, H.; Ohata, H.; Honda, K.; Momose, K.; Namekata, I.; Tanaka, H.; Shigenobu, K.; Nakamura, R.; Hayakawa, T.; Kawanishi, T. *J. Pharmacol. Sci.* **2005**, *97*, 361.
(94) Carlson, H. J.; Campbell, R. E. *Curr. Opin. Biotechnol.* **2009**, *20*, 19.
(95) Ai, H. W.; Hazelwood, K. L.; Davidson, M. W.; Campbell, R. E. *Nat. Methods* **2008**, *5*, 401.
(96) Shaner, N. C.; Campbell, R. E.; Steinbach, P. A.; Giepmans, B. N.; Palmer, A. E.; Tsien, R. Y. *Nat. Biotechnol.* **2004**, *22*, 1567.
(97) Lippincott-Schwartz, J.; Patterson, G. H. *Methods Cell Biol.* **2008**, *85*, 45.

(98) Patterson, G. H. *Curr. Protoc. Cell Biol.* **2008**, *21.6*, 1.
(99) Lukyanov, K. A.; Chudakov, D. M.; Lukyanov, S.; Verkhusha, V. V. *Nat. Rev. Mol. Cell Biol.* **2005**, *6*, 885.
(100) Patterson, G. H.; Lippincott-Schwartz, J. *Science* **2002**, *297*, 1873.
(101) Subach, F. V.; Patterson, G. H.; Manley, S.; Gillette, J. M.; Lippincott-Schwartz, J.; Verkhusha, V. V. *Nat. Methods* **2009**, *6*, 153.
(102) Chudakov, D. M.; Verkhusha, V. V.; Staroverov, D. B.; Souslova, E. A.; Lukyanov, S.; Lukyanov, K. A. *Nat. Biotechnol.* **2004**, *22*, 1435.
(103) van Thor, J. J.; Gensch, T.; Hellingwerf, K. J.; Johnson, L. N. *Nat. Struct. Biol.* **2002**, *9*, 37.
(104) Henderson, J. N.; Gepshtein, R.; Heenan, J. R.; Kallio, K.; Huppert, D.; Remington, S. J. *J. Am. Chem. Soc.* **2009**, *131*, 4176.
(105) Heim, R.; Prasher, D. C.; Tsien, R. Y. *Proc. Natl. Acad. Sci. U.S.A.* **1994**, *91*, 12501.
(106) Ehrig, T.; O'Kane, D. J.; Prendergast, F. G. *FEBS Lett.* **1995**, *367*, 163.
(107) Ando, R.; Hama, H.; Yamamoto-Hino, M.; Mizuno, H.; Miyawaki, A. *Proc. Natl. Acad. Sci. U.S.A.* **2002**, *99*, 12651.
(108) Mizuno, H.; Mal, T. K.; Tong, K. I.; Ando, R.; Furuta, T.; Ikura, M.; Miyawaki, A. *Mol. Cell* **2003**, *12*, 1051.
(109) Wiedenmann, J.; Ivanchenko, S.; Oswald, F.; Schmitt, F.; Rocker, C.; Salih, A.; Spindler, K. D.; Nienhaus, G. U. *Proc. Natl. Acad. Sci. U.S.A.* **2004**, *101*, 15905.
(110) McKinney, S. A.; Murphy, C. S.; Hazelwood, K. L.; Davidson, M. W.; Looger, L. L. *Nat. Methods* **2009**, *6*, 131.
(111) Gurskaya, N. G.; Verkhusha, V. V.; Shcheglov, A. S.; Staroverov, D. B.; Chepurnykh, T. V.; Fradkov, A. F.; Lukyanov, S.; Lukyanov, K. A. *Nat. Biotechnol.* **2006**, *24*, 461.
(112) Chudakov, D. M.; Lukyanov, S.; Lukyanov, K. A. *Biotechniques* **2007**, *42*, 553; 555; 557.
(113) Chudakov, D. M.; Belousov, V. V.; Zaraisky, A. G.; Novoselov, V. V.; Staroverov, D. B.; Zorov, D. B.; Lukyanov, S.; Lukyanov, K. A. *Nat. Biotechnol.* **2003**, *21*, 191.
(114) Verkhusha, V. V.; Sorkin, A. *Chem. Biol.* **2005**, *12*, 279.
(115) Henderson, J. N.; Ai, H. W.; Campbell, R. E.; Remington, S. J. *Proc. Natl. Acad. Sci. U.S.A.* **2007**, *104*, 6672.
(116) Stiel, A. C.; Andresen, M.; Bock, H.; Hilbert, M.; Schilde, J.; Schonle, A.; Eggeling, C.; Egner, A.; Hell, S. W.; Jakobs, S. *Biophys. J.* **2008**, *95*, 2989.
(117) Ando, R.; Mizuno, H.; Miyawaki, A. *Science* **2004**, *306*, 1370.
(118) Flors, C.; Hotta, J.; Uji-i, H; Dedecker, P.; Ando, R.; Mizuno, H.; Miyawaki, A.; Hofkens, J. *J. Am. Chem. Soc.* **2007**, *129*, 13970.
(119) Stiel, A. C.; Trowitzsch, S.; Weber, G.; Andresen, M.; Eggeling, C.; Hell, S. W.; Jakobs, S.; Wahl, M. C. *Biochem. J.* **2007**, *402*, 35.
(120) Andresen, M.; Stiel, A. C.; Folling, J.; Wenzel, D.; Schonle, A.; Egner, A.; Eggeling, C.; Hell, S. W.; Jakobs, S. *Nat. Biotechnol.* **2008**, *26*, 1035.
(121) Quillin, M. L.; Anstrom, D. M.; Shu, X.; O'Leary, S.; Kallio, K.; Chudakov, D. M.; Remington, S. J. *Biochemistry* **2005**, *44*, 5774.
(122) Andresen, M.; Wahl, M. C.; Stiel, A. C.; Grater, F.; Schafer, L. V.; Trowitzsch, S.; Weber, G.; Eggeling, C.; Grubmuller, H.; Hell, S. W.; Jakobs, S. *Proc. Natl. Acad. Sci. U.S.A.* **2005**, *102*, 13070.
(123) Wilmann, P. G.; Turcic, K.; Battad, J. M.; Wilce, M. C.; Devenish, R. J.; Prescott, M.; Rossjohn, J. *J. Mol. Biol.* **2006**, *364*, 213.
(124) Andresen, M.; Stiel, A. C.; Trowitzsch, S.; Weber, G.; Eggeling, C.; Wahl, M. C.; Hell, S. W.; Jakobs, S. *Proc. Natl. Acad. Sci. U.S.A.* **2007**, *104*, 13005.
(125) Mizuno, H.; Mal, T. K.; Walchli, M.; Kikuchi, A.; Fukano, T.; Ando, R.; Jeyakanthan, J.; Taka, J.; Shiro, Y.; Ikura, M.; Miyawaki, A. *Proc. Natl. Acad. Sci. U.S.A.* **2008**, *105*, 9227.
(126) Donnert, G.; Eggeling, C.; Hell, S. W. *Nat. Methods* **2007**, *4*, 81.
(127) Sinnecker, D.; Voigt, P.; Hellwig, N.; Schaefer, M. *Biochemistry* **2005**, *44*, 7085.
(128) Carminati, J. L.; Stearns, T. *J. Cell Biol.* **1997**, *138*, 629.
(129) Vilardaga, J. P.; Bunemann, M.; Krasel, C.; Castro, M.; Lohse, M. J. *Nat. Biotechnol.* **2003**, *21*, 807.
(130) Andresen, M.; Schmitz-Salue, R.; Jakobs, S. *Mol. Biol. Cell* **2004**, *15*, 5616.
(131) Ozhalici-Unal, H.; Pow, C. L.; Marks, S. A.; Jesper, L. D.; Silva, G. L.; Shank, N. I.; Jones, E. W.; Burnette, J. M., III; Berget, P. B.; Armitage, B. A. *J. Am. Chem. Soc.* **2008**, *130*, 12620.
(132) Chen, I.; Ting, A. Y. *Curr. Opin. Biotechnol.* **2005**, *16*, 35.
(133) O'Hare, H. M.; Johnsson, K.; Gautier, A. *Curr. Opin. Struct. Biol.* **2007**, *17*, 488.
(134) Martin, B. R.; Giepmans, B. N.; Adams, S. R.; Tsien, R. Y. *Nat. Biotechnol.* **2005**, *23*, 1308.
(135) Adams, S. R.; Campbell, R. E.; Gross, L. A.; Martin, B. R.; Walkup, G. K.; Yao, Y.; Llopis, J.; Tsien, R. Y. *J. Am. Chem. Soc.* **2002**, *124*, 6063.
(136) Madani, F.; Lind, J.; Damberg, P.; Adams, S. R.; Tsien, R. Y.; Graslund, A. O. *J. Am. Chem. Soc.* **2009**, *131*, 4613.
(137) Gaietta, G.; Deerinck, T. J.; Adams, S. R.; Bouwer, J.; Tour, O.; Laird, D. W.; Sosinsky, G. E.; Tsien, R. Y.; Ellisman, M. H. *Science* **2002**, *296*, 503.
(138) Tour, O.; Adams, S. R.; Kerr, R. A.; Meijer, R. M.; Sejnowski, T. J.; Tsien, R. W.; Tsien, R. Y. *Nat. Chem. Biol.* **2007**, *3*, 423.
(139) Giepmans, B. N.; Adams, S. R.; Ellisman, M. H.; Tsien, R. Y. *Science* **2006**, *312*, 217.
(140) Szent-Gyorgyi, C.; Schmidt, B. F.; Creeger, Y.; Fisher, G. W.; Zakel, K. L.; Adler, S.; Fitzpatrick, J. A.; Woolford, C. A.; Yan, Q.; Vasilev, K. V.; Berget, P. B.; Bruchez, M. P.; Jarvik, J. W.; Waggoner, A. *Nat. Biotechnol.* **2008**, *26*, 235.
(141) Colby, D. W.; Garg, P.; Holden, T.; Chao, G.; Webster, J. M.; Messer, A.; Ingram, V. M.; Wittrup, K. D. *J. Mol. Biol.* **2004**, *342*, 901.
(142) Tanaka, T.; Lobato, M. N.; Rabbitts, T. H. *J. Mol. Biol.* **2003**, *331*, 1109.
(143) Proba, K.; Worn, A.; Honegger, A.; Pluckthun, A. *J. Mol. Biol.* **1998**, *275*, 245.
(144) Janssen, D. B. *Curr. Opin. Chem. Biol.* **2004**, *8*, 150.
(145) Miller, L. W.; Cai, Y.; Sheetz, M. P.; Cornish, V. W. *Nat. Methods* **2005**, *2*, 255.
(146) Gronemeyer, T.; Chidley, C.; Juillerat, A.; Heinis, C.; Johnsson, K. *Protein Eng. Des. Sel.* **2006**, *19*, 309.
(147) Keppler, A.; Gendreizig, S.; Gronemeyer, T.; Pick, H.; Vogel, H.; Johnsson, K. *Nat. Biotechnol.* **2003**, *21*, 86.
(148) Los, G. V.; Encell, L. P.; McDougall, M. G.; Hartzell, D. D.; Karassina, N.; Zimprich, C.; Wood, M. G.; Learish, R.; Ohana, R. F.; Urh, M.; Simpson, D.; Mendez, J.; Zimmerman, K.; Otto, P.; Vidugiris, G.; Zhu, J.; Darzins, A.; Klaubert, D. H.; Bulleit, R. F.; Wood, K. V. *ACS Chem. Biol.* **2008**, *3*, 373.
(149) Juillerat, A.; Gronemeyer, T.; Keppler, A.; Gendreizig, S.; Pick, H.; Vogel, H.; Johnsson, K. *Chem. Biol.* **2003**, *10*, 313.
(150) Los, G. V.; Wood, K. *Methods Mol. Biol.* **2007**, *356*, 195.
(151) Keppler, A.; Pick, H.; Arrivoli, C.; Vogel, H.; Johnsson, K. *Proc. Natl. Acad. Sci. U.S.A.* **2004**, *101*, 9955.
(152) Gronemeyer, T.; Godin, G.; Johnsson, K. *Curr. Opin. Biotechnol.* **2005**, *16*, 453.
(153) Keppler, A.; Kindermann, M.; Gendreizig, S.; Pick, H.; Vogel, H.; Johnsson, K. *Methods* **2004**, *32*, 437.
(154) Kindermann, M.; Sielaff, I.; Johnsson, K. *Bioorg. Med. Chem. Lett.* **2004**, *14*, 2725.
(155) Chapman, S.; Oparka, K. J.; Roberts, A. G. *Curr. Opin. Plant Biol.* **2005**, *8*, 565.
(156) Giepmans, B. N.; Deerinck, T. J.; Smarr, B. L.; Jones, Y. Z.; Ellisman, M. H. *Nat. Methods* **2005**, *2*, 743.
(157) Howarth, M.; Takao, K.; Hayashi, Y.; Ting, A. Y. *Proc. Natl. Acad. Sci. U.S.A.* **2005**, *102*, 7583.
(158) Zurn, A.; Zabel, U.; Vilardaga, J. P.; Schindelin, H.; Lohse, M. J.; Hoffmann, C. *Mol. Pharmacol.* **2009**, *75*, 534.
(159) Bannwarth, M.; Correa, I. R.; Sztretye, M.; Pouvreau, S.; Fellay, C.; Aebischer, A.; Royer, L.; Rois, E.; Johnsson, K. *ACS Chem. Biol.* **2009**, *4*, 179.
(160) Brun, M. A.; Tan, K. T.; Nakata, E.; Hinner, M. J.; Johnsson, K. *J. Am. Chem. Soc.* **2009**, *131*, 5873.

(161) Balla, T. *Trends Cell Biol.* **2009**, *19*, 575.
(162) Corish, P.; Tyler-Smith, C. *Protein Eng.* **1999**, *12*, 1035.
(163) Verkhusha, V. V.; Kuznetsova, I. M.; Stepanenko, O. V.; Zaraisky, A. G.; Shavlovsky, M. M.; Turoverov, K. K.; Uversky, V. N. *Biochemistry* **2003**, *42*, 7879.
(164) Li, X.; Zhao, X.; Fang, Y.; Jiang, X.; Duong, T.; Fan, C.; Huang, C. C.; Kain, S. R. *J. Biol. Chem.* **1998**, *273*, 34970.
(165) Strack, R. L.; Strongin, D. E.; Bhattacharyya, D.; Tao, W.; Berman, A.; Broxmeyer, H. E.; Keenan, R. J.; Glick, B. S. *Nat. Methods* **2008**, *5*, 955.
(166) Terskikh, A.; Fradkov, A.; Ermakova, G.; Zaraisky, A.; Tan, P.; Kajava, A. V.; Zhao, X.; Lukyanov, S.; Matz, M.; Kim, S.; Weissman, I.; Siebert, P. *Science* **2000**, *290*, 1585.
(167) Subach, F. V.; Subach, O. M.; Gundorov, I. S.; Morozova, K. S.; Piatkevich, K. D.; Cuervo, A. M.; Verkhusha, V. V. *Nat. Chem. Biol.* **2009**, *5*, 118.
(168) Li, X.; Fang, Y.; Zhao, X.; Jiang, X.; Duong, T.; Kain, S. R. *J. Biol. Chem.* **1999**, *274*, 21244.
(169) Chang, H. Y.; Levasseur, M.; Jones, K. T. *J. Cell Sci.* **2004**, *117*, 6289.
(170) Marangos, P.; Verschuren, E. W.; Chen, R.; Jackson, P. K.; Carroll, J. *J. Cell Biol.* **2007**, *176*, 65.
(171) Zhang, L.; Gurskaya, N. G.; Merzlyak, E. M.; Staroverov, D. B.; Mudrik, N. N.; Samarkina, O. N.; Vinokurov, L. M.; Lukyanov, S.; Lukyanov, K. A. *Biotechniques* **2007**, *42*, 446; 448; 450.
(172) Lauf, U.; Giepmans, B. N.; Lopez, P.; Braconnot, S.; Chen, S. C.; Falk, M. M. *Proc. Natl. Acad. Sci. U.S.A.* **2002**, *99*, 10446.
(173) Ananthanarayanan, B.; Fosbrink, M.; Rahdar, M.; Zhang, J. *J. Biol. Chem.* **2007**, *282*, 36634.
(174) Astoul, E.; Watton, S.; Cantrell, D. *J. Cell Biol.* **1999**, *145*, 1511.
(175) Meili, R.; Ellsworth, C.; Lee, S.; Reddy, T. B.; Ma, H.; Firtel, R. A. *EMBO J.* **1999**, *18*, 2092.
(176) Watton, S. J.; Downward, J. *Curr. Biol.* **1999**, *9*, 433.
(177) Wang, Q. J.; Bhattacharyya, D.; Garfield, S.; Nacro, K.; Marquez, V. E.; Blumberg, P. M. *J. Biol. Chem.* **1999**, *274*, 37233.
(178) Sakai, N.; Sasaki, K.; Ikegaki, N.; Shirai, Y.; Ono, Y.; Saito, N. *J. Cell Biol.* **1997**, *139*, 1465.
(179) Shirai, Y.; Kashiwagi, K.; Yagi, K.; Sakai, N.; Saito, N. *J. Cell Biol.* **1998**, *143*, 511.
(180) Wagner, S.; Harteneck, C.; Hucho, F.; Buchner, K. *Exp. Cell Res.* **2000**, *258*, 204.
(181) Kazi, J. U.; Soh, J. W. *Biochem. Biophys. Res. Commun.* **2007**, *364*, 231.
(182) Bartfeld, S.; Engels, C.; Bauer, B.; Aurass, P.; Flieger, A.; Bruggemann, H.; Meyer, T. F. *Cell Microbiol.* **2009**, *11*, 1638.
(183) Chikamatsu, S.; Furuno, T.; Kinoshita, Y.; Inoh, Y.; Hirashima, N.; Teshima, R.; Nakanishi, M. *Mol. Immunol.* **2007**, *44*, 1490.
(184) Sung, M. H.; Salvatore, L.; De Lorenzi, R.; Indrawan, A.; Pasparakis, M.; Hager, G. L.; Bianchi, M. E.; Agresti, A. *PLoS One* **2009**, *4*, No. e7163.
(185) Aramburu, J.; Garcia-Cozar, F.; Raghavan, A.; Okamura, H.; Rao, A.; Hogan, P. G. *Mol. Cell* **1998**, *1*, 627.
(186) Zhu, J.; Shibasaki, F.; Price, R.; Guillemot, J. C.; Yano, T.; Dotsch, V.; Wagner, G.; Ferrara, P.; McKeon, F. *Cell* **1998**, *93*, 851.
(187) Okamura, H.; Garcia-Rodriguez, C.; Martinson, H.; Qin, J.; Virshup, D. M.; Rao, A. *Mol. Cell. Biol.* **2004**, *24*, 4184.
(188) Shen, T.; Cseresnyes, Z.; Liu, Y.; Randall, W. R.; Schneider, M. F. *J. Physiol.* **2007**, *579*, 535.
(189) Fernandez-Suarez, M.; Ting, A. Y. *Nat. Rev. Mol. Cell Biol.* **2008**, *9*, 929.
(190) Hess, S. T.; Gould, T. J.; Gudheti, M. V.; Maas, S. A.; Mills, K. D.; Zimmerberg, J. *Proc. Natl. Acad. Sci. U.S.A.* **2007**, *104*, 17370.
(191) Manley, S.; Gillette, J. M.; Patterson, G. H.; Shroff, H.; Hess, H. F.; Betzig, E.; Lippincott-Schwartz, J. *Nat. Methods* **2008**, *5*, 155.
(192) Shroff, H.; Galbraith, C. G.; Galbraith, J. A.; Betzig, E. *Nat. Methods* **2008**, *5*, 417.
(193) Biteen, J. S.; Thompson, M. A.; Tselentis, N. K.; Bowman, G. R.; Shapiro, L.; Moerner, W. E. *Nat. Methods* **2008**, *5*, 947.
(194) Huang, B.; Bates, M.; Zhuang, X. *Annu. Rev. Biochem.* **2009**, *78*, 993.
(195) Tulu, U. S.; Rusan, N. M.; Wadsworth, P. *Curr. Biol.* **2003**, *13*, 1894.
(196) Kwon, O. Y.; Kwon, I. C.; Song, H. K.; Jeon, H. *Biochim. Biophys. Acta* **2008**, *1780*, 1403.
(197) Fuchs, J.; Bohme, S.; Oswald, F.; Hedde, P. N.; Krause, M.; Wiedenmann, J.; Nienhaus, G. U. *Nat. Methods* **2010**, *7*, 627.
(198) Effector domains commonly used for PI probes include (i) pleckstrin homology(PH) domains, (ii) epsin N-terminal homology-(ENTH) domains, and (iii) a PI-binding domain, termed FYVE, which was first identified in the proteins Fab1p, YOPB, Vps27p, and EEA1.
(199) Downes, C. P.; Gray, A.; Lucocq, J. M. *Trends Cell Biol.* **2005**, *15*, 259.
(200) Varnai, P.; Balla, T. *Biochim. Biophys. Acta* **2006**, *1761*, 957.
(201) Servant, G.; Weiner, O. D.; Herzmark, P.; Balla, T.; Sedat, J. W.; Bourne, H. R. *Science* **2000**, *287*, 1037.
(202) Yeung, T.; Heit, B.; Dubuisson, J. F.; Fairn, G. D.; Chiu, B.; Inman, R.; Kapus, A.; Swanson, M.; Grinstein, S. *J. Cell Biol.* **2009**, *185*, 917.
(203) Yeung, T.; Gilbert, G. E.; Shi, J.; Silvius, J.; Kapus, A.; Grinstein, S. *Science* **2008**, *319*, 210.
(204) Jayaraman, S.; Haggie, P.; Wachter, R. M.; Remington, S. J.; Verkman, A. S. *J. Biol. Chem.* **2000**, *275*, 6047.
(205) Galietta, L. J.; Haggie, P. M.; Verkman, A. S. *FEBS Lett.* **2001**, *499*, 220.
(206) Rhoden, K. J.; Cianchetta, S.; Stivani, V.; Portulano, C.; Galietta, L. J.; Romeo, G. *Am. J. Physiol. Cell Physiol.* **2007**, *292*, C814.
(207) Kuner, T.; Augustine, G. J. *Neuron* **2000**, *27*, 447.
(208) Markova, O.; Mukhtarov, M.; Real, E.; Jacob, Y.; Bregestovski, P. *J. Neurosci. Methods* **2008**, *170*, 67.
(209) Berglund, K.; Schleich, W.; Wang, H.; Feng, G.; Hall, W. C.; Kuner, T.; Augustine, G. J. *Brain Cell Biol.* **2008**, *36*, 101.
(210) Haverkamp, S.; Wassle, H.; Duebel, J.; Kuner, T.; Augustine, G. J.; Feng, G.; Euler, T. *J. Neurosci.* **2005**, *25*, 5438.
(211) Duebel, J.; Haverkamp, S.; Schleich, W.; Feng, G.; Augustine, G. J.; Kuner, T.; Euler, T. *Neuron* **2006**, *49*, 81.
(212) Wassle, H.; Puller, C.; Muller, F.; Haverkamp, S. *J. Neurosci.* **2009**, *29*, 106.
(213) Bizzarri, R.; Serresi, M.; Luin, S.; Beltram, F. *Anal. Bioanal. Chem.* **2009**, *393*, 1107.
(214) Bizzarri, R.; Arcangeli, C.; Arosio, D.; Ricci, F.; Faraci, P.; Cardarelli, F.; Beltram, F. *Biophys. J.* **2006**, *90*, 3300.
(215) Arosio, D.; Garau, G.; Ricci, F.; Marchetti, L.; Bizzarri, R.; Nifosi, R.; Beltram, F. *Biophys. J.* **2007**, *93*, 232.
(216) Hanson, G. T.; McAnaney, T. B.; Park, E. S.; Rendell, M. E.; Yarbrough, D. K.; Chu, S.; Xi, L.; Boxer, S. G.; Montrose, M. H.; Remington, S. J. *Biochemistry* **2002**, *41*, 15477.
(217) Miesenbock, G.; De Angelis, D. A.; Rothman, J. E. *Nature* **1998**, *394*, 192.
(218) Sankaranarayanan, S.; De Angelis, D.; Rothman, J. E.; Ryan, T. A. *Biophys. J.* **2000**, *79*, 2199.
(219) Kneen, M.; Farinas, J.; Li, Y.; Verkman, A. S. *Biophys. J.* **1998**, *74*, 1591.
(220) Llopis, J.; McCaffery, J. M.; Miyawaki, A.; Farquhar, M. G.; Tsien, R. Y. *Proc. Natl. Acad. Sci. U.S.A.* **1998**, *95*, 6803.
(221) Abad, M. F.; Di Benedetto, G.; Magalhaes, P. J.; Filippin, L.; Pozzan, T. *J. Biol. Chem.* **2004**, *279*, 11521.
(222) Porcelli, A. M.; Ghelli, A.; Zanna, C.; Pinton, P.; Rizzuto, R.; Rugolo, M. *Biochem. Biophys. Res. Commun.* **2005**, *326*, 799.
(223) Kneen, M.; Farinas, J.; Li, Y.; Verkman, A. S. *Biophys. J.* **1998**, *74*, 1591.
(224) Miesenbock, G.; De Angelis, D. A.; Rothman, J. E. *Nature* **1998**, *394*, 192.
(225) Hanson, G. T.; Aggeler, R.; Oglesbee, D.; Cannon, M.; Capaldi, R. A.; Tsien, R. Y.; Remington, S. J. *J. Biol. Chem.* **2004**, *279*, 13044.
(226) Lohman, J. R.; Remington, S. J. *Biochemistry* **2008**, *47*, 8678.
(227) Cannon, M. B.; Remington, S. J. *Protein Sci.* **2006**, *15*, 45.

(228) Cannon, M. B.; Remington, S. J. *Methods Mol. Biol.* **2008**, *476*, 51.
(229) Ostergaard, H.; Henriksen, A.; Hansen, F. G.; Winther, J. R. *EMBO J.* **2001**, *20*, 5853.
(230) Merksamer, P. I.; Trusina, A.; Papa, F. R. *Cell* **2008**, *135*, 933.
(231) Austin, C. D.; De Maziere, A. M.; Pisacane, P. I.; van Dijk, S. M.; Eigenbrot, C.; Sliwkowski, M. X.; Klumperman, J.; Scheller, R. H. *Mol. Biol. Cell* **2004**, *15*, 5268.
(232) Miyawaki, A.; Llopis, J.; Heim, R.; McCaffery, J. M.; Adams, J. A.; Ikura, M.; Tsien, R. Y. *Nature* **1997**, *388*, 882.
(233) Porumb, T.; Yau, P.; Harvey, T. S.; Ikura, M. *Protein Eng.* **1994**, *7*, 109.
(234) Tallini, Y. N.; Ohkura, M.; Choi, B. R.; Ji, G.; Imoto, K.; Doran, R.; Lee, J.; Plan, P.; Wilson, J.; Xin, H. B.; Sanbe, A.; Gulick, J.; Mathai, J.; Robbins, J.; Salama, G.; Nakai, J.; Kotlikoff, M. I. *Proc. Natl. Acad. Sci. U.S.A.* **2006**, *103*, 4753.
(235) Ohkura, M.; Matsuzaki, M.; Kasai, H.; Imoto, K.; Nakai, J. *Anal. Chem.* **2005**, *77*, 5861.
(236) Nakai, J.; Ohkura, M.; Imoto, K. *Nat. Biotechnol.* **2001**, *19*, 137.
(237) Nagai, T.; Sawano, A.; Park, E. S.; Miyawaki, A. *Proc. Natl. Acad. Sci. U.S.A.* **2001**, *98*, 3197.
(238) Emmanouilidou, E.; Teschemacher, A. G.; Pouli, A. E.; Nicholls, L. I.; Seward, E. P.; Rutter, G. A. *Curr. Biol.* **1999**, *9*, 915.
(239) Isshiki, M.; Ying, Y. S.; Fujita, T.; Anderson, R. G. *J. Biol. Chem.* **2002**, *277*, 43389.
(240) Foyouzi-Youssefi, R.; Arnaudeau, S.; Borner, C.; Kelley, W. L.; Tschopp, J.; Lew, D. P.; Demaurex, N.; Krause, K. H. *Proc. Natl. Acad. Sci. U.S.A.* **2000**, *97*, 5723.
(241) Yu, R.; Hinkle, P. M. *J. Biol. Chem.* **2000**, *275*, 23648.
(242) Kasai, H.; Yao, A.; Oyama, T.; Hasegawa, H.; Akazawa, H.; Toko, H.; Nagai, T.; Kinugawa, K.; Kohmoto, O.; Maruyama, K.; Takahashi, T.; Nagai, R.; Miyawaki, A.; Komuro, I. *Biochem. Biophys. Res. Commun.* **2004**, *314*, 1014.
(243) Heim, N.; Griesbeck, O. *J. Biol. Chem.* **2004**, *279*, 14280.
(244) Palmer, A. E.; Giacomello, M.; Kortemme, T.; Hires, S. A.; Lev-Ram, V.; Baker, D.; Tsien, R. Y. *Chem. Biol.* **2006**, *13*, 521.
(245) Mank, M.; Reiff, D. F.; Heim, N.; Friedrich, M. W.; Borst, A.; Griesbeck, O. *Biophys. J.* **2006**, *90*, 1790.
(246) Mank, M.; Griesbeck, O. *Chem. Rev.* **2008**, *108*, 1550.
(247) Tay, L. H.; Griesbeck, O.; Yue, D. T. *Biophys. J.* **2007**, *93*, 4031.
(248) Heim, N.; Garaschuk, O.; Friedrich, M. W.; Mank, M.; Milos, R. I.; Kovalchuk, Y.; Konnerth, A.; Griesbeck, O. *Nat. Methods* **2007**, *4*, 127.
(249) Wallace, D. J.; Meyer zum Alten, B. S.; Astori, S.; Yang, Y.; Bausen, M.; Kugler, S.; Palmer, A. E.; Tsien, R. Y.; Sprengel, R.; Kerr, J. N.; Denk, W.; Hasan, M. T. *Nat. Methods* **2008**, *5*, 797.
(250) Tian, L.; Hires, S. A.; Mao, T.; Huber, D.; Chiappe, M. E.; Chalasani, S. H.; Petreanu, L.; Akerboom, J.; McKinney, S. A.; Schreiter, E. R.; Bargmann, C. I.; Jayaraman, V.; Svoboda, K.; Looger, L. L. *Nat. Methods* **2009**, *6*, 875.
(251) Wang, Q.; Shui, B.; Kotlikoff, M. I.; Sondermann, H. *Structure* **2008**, *16*, 1817.
(252) Akerboom, J.; Rivera, J. D.; Guilbe, M. M.; Malave, E. C.; Hernandez, H. H.; Tian, L.; Hires, S. A.; Marvin, J. S.; Looger, L. L.; Schreiter, E. R. *J. Biol. Chem.* **2009**, *284*, 6455.
(253) Fletcher, M. L.; Masurkar, A. V.; Xing, J.; Imamura, F.; Xiong, W.; Nagayama, S.; Mutoh, H.; Greer, C. A.; Knopfel, T.; Chen, W. R. *J. Neurophysiol.* **2009**, *102*, 817.
(254) Lee, M. Y.; Song, H.; Nakai, J.; Ohkura, M.; Kotlikoff, M. I.; Kinsey, S. P.; Golovina, V. A.; Blaustein, M. P. *Proc. Natl. Acad. Sci. U.S.A.* **2006**, *103*, 13232.
(255) Fukano, T.; Shimozono, S.; Miyawaki, A. *Brain Cell Biol.* **2008**, *36*, 43.
(256) Young, K. W.; Bampton, E. T.; Pinon, L.; Bano, D.; Nicotera, P. *Cell Calcium* **2008**, *43*, 296.
(257) Frieden, M.; James, D.; Castelbou, C.; Danckaert, A.; Martinou, J. C.; Demaurex, N. *J. Biol. Chem.* **2004**, *279*, 22704.
(258) Francis, S. H.; Blount, M. A.; Zoraghi, R.; Corbin, J. D. *Front. Biosci.* **2005**, *10*, 2097.
(259) Nausch, L. W.; Ledoux, J.; Bonev, A. D.; Nelson, M. T.; Dostmann, W. R. *Proc. Natl. Acad. Sci. U.S.A.* **2008**, *105*, 365.
(260) Honda, A.; Adams, S. R.; Sawyer, C. L.; Lev-Ram, V.; Tsien, R. Y.; Dostmann, W. R. *Proc. Natl. Acad. Sci. U.S.A.* **2001**, *98*, 2437.
(261) Honda, A.; Sawyer, C. L.; Cawley, S. M.; Dostmann, W. R. *Methods Mol. Biol.* **2005**, *307*, 27.
(262) Wang, W.; Fang, H.; Groom, L.; Cheng, A.; Zhang, W.; Liu, J.; Wang, X.; Li, K.; Han, P.; Zheng, M.; Yin, J.; Wang, W.; Mattson, M. P.; Kao, J. P.; Lakatta, E. G.; Sheu, S. S.; Ouyang, K.; Chen, J.; Dirksen, R. T.; Cheng, H. *Cell* **2008**, *134*, 279.
(263) Belousov, V. V.; Fradkov, A. F.; Lukyanov, K. A.; Staroverov, D. B.; Shakhbazov, K. S.; Terskikh, A. V.; Lukyanov, S. *Nat. Methods* **2006**, *3*, 281.
(264) Ashcroft, F. M.; Gribble, F. M. *Diabetologia* **1999**, *42*, 903.
(265) Dennis, P. B.; Jaeschke, A.; Saitoh, M.; Fowler, B.; Kozma, S. C.; Thomas, G. *Science* **2001**, *294*, 1102.
(266) Berg, J.; Hung, Y. P.; Yellen, G. *Nat. Methods* **2009**, *6*, 161.
(267) Baird, G. S.; Zacharias, D. A.; Tsien, R. Y. *Proc. Natl. Acad. Sci. U.S.A.* **1999**, *96*, 11241.
(268) Yildiz, O.; Kalthoff, C.; Raunser, S.; Kuhlbrandt, W. *EMBO J.* **2007**, *26*, 589.
(269) Baker, B. J.; Mutoh, H.; Dimitrov, D.; Akemann, W.; Perron, A.; Iwamoto, Y.; Jin, L.; Cohen, L. B.; Isacoff, E. Y.; Pieribone, V. A.; Hughes, T.; Knopfel, T. *Brain Cell Biol.* **2008**, *36*, 53.
(270) Siegel, M. S.; Isacoff, E. Y. *Neuron* **1997**, *19*, 735.
(271) Guerrero, G.; Siegel, M. S.; Roska, B.; Loots, E.; Isacoff, E. Y. *Biophys. J.* **2002**, *83*, 3607.
(272) Sakai, R.; Repunte-Canonigo, V.; Raj, C. D.; Knopfel, T. *Eur. J. Neurosci.* **2001**, *13*, 2314.
(273) Knopfel, T.; Tomita, K.; Shimazaki, R.; Sakai, R. *Methods* **2003**, *30*, 42.
(274) Ataka, K.; Pieribone, V. A. *Biophys. J.* **2002**, *82*, 509.
(275) Lundby, A.; Mutoh, H.; Dimitrov, D.; Akemann, W.; Knopfel, T. *PLoS One* **2008**, *3*, e2514.
(276) Tsutsui, H.; Karasawa, S.; Okamura, Y.; Miyawaki, A. *Nat. Methods* **2008**, *5*, 683.
(277) Akemann, W.; Mutoh, H.; Perron, A.; Rossier, J.; Knopfel, T. *Nat. Methods* **2010**, *7*, 643.
(278) Zhang, J.; Campbell, R. E.; Ting, A. Y.; Tsien, R. Y. *Nat. Rev. Mol. Cell Biol.* **2002**, *3*, 906.
(279) Hayes, J. S.; Brunton, L. L.; Mayer, S. E. *J. Biol. Chem.* **1980**, *255*, 5113.
(280) Brunton, L. L.; Hayes, J. S.; Mayer, S. E. *Adv. Cyclic Nucleotide Res.* **1981**, *14*, 391.
(281) Buxton, I. L.; Brunton, L. L. *J. Biol. Chem.* **1983**, *258*, 10233.
(282) Nikolaev, V. O.; Bunemann, M.; Hein, L.; Hannawacker, A.; Lohse, M. J. *J. Biol. Chem.* **2004**, *279*, 37215.
(283) Zaccolo, M.; De Giorgi, F.; Cho, C. Y.; Feng, L.; Knapp, T.; Negulescu, P. A.; Taylor, S. S.; Tsien, R. Y.; Pozzan, T. *Nat. Cell Biol.* **2000**, *2*, 25.
(284) Zaccolo, M.; Pozzan, T. *Science* **2002**, *295*, 1711.
(285) Jiang, L. I.; Collins, J.; Davis, R.; Lin, K. M.; DeCamp, D.; Roach, T.; Hsueh, R.; Rebres, R. A.; Ross, E. M.; Taussig, R.; Fraser, I.; Sternweis, P. C. *J. Biol. Chem.* **2007**, *282*, 10576.
(286) DiPilato, L. M.; Cheng, X.; Zhang, J. *Proc. Natl. Acad. Sci. U.S.A.* **2004**, *101*, 16513.
(287) Ponsioen, B.; Zhao, J.; Riedl, J.; Zwartkruis, F.; van der, K. G.; Zaccolo, M.; Moolenaar, W. H.; Bos, J. L.; Jalink, K. *EMBO Rep.* **2004**, *5*, 1176.
(288) Nikolaev, V. O.; Bunemann, M.; Hein, L.; Hannawacker, A.; Lohse, M. J. *J. Biol. Chem.* **2004**, *279*, 37215.
(289) Di Benedetto, G.; Zoccarato, A.; Lissandron, V.; Terrin, A.; Li, X.; Houslay, M. D.; Baillie, G. S.; Zaccolo, M. *Circ. Res.* **2008**, *103*, 836.
(290) Rehmann, H.; Rueppel, A.; Bos, J. L.; Wittinghofer, A. *J. Biol. Chem.* **2003**, *278*, 23508.

(291) Rehmann, H.; Prakash, B.; Wolf, E.; Rueppel, A.; de Rooij, J.; Bos, J. L.; Wittinghofer, A. *Nat. Struct. Biol.* **2003**, *10*, 26.
(292) DiPilato, L. M.; Zhang, J. *Mol. Biosyst.* **2009**, *5*, 832.
(293) Calebiro, D.; Nikolaev, V. O.; Gagliani, M. C.; de Filippis, T.; Dees, C.; Tacchetti, C.; Persani, L.; Lohse, M. J. *PLoS Biol.* **2009**, *7*, e1000172.
(294) Ferrandon, S.; Feinstein, T. N.; Castro, M.; Wang, B.; Bouley, R.; Potts, J. T.; Gardella, T. J.; Vilardaga, J. P. *Nat. Chem. Biol.* **2009**, *5*, 734.
(295) Masri, B.; Salahpour, A.; Didriksen, M.; Ghisi, V.; Beaulieu, J. M.; Gainetdinov, R. R.; Caron, M. G. *Proc. Natl. Acad. Sci. U.S.A.* **2008**, *105*, 13656.
(296) Saito, K.; Hatsugai, N.; Horikawa, K.; Kobayashi, K.; Matsu-ura, T.; Mikoshiba, K.; Nagai, T. *PLoS One* **2010**, *5*, e9935.
(297) Sato, M.; Hida, N.; Umezawa, Y. *Proc. Natl. Acad. Sci. U.S.A.* **2005**, *102*, 14515.
(298) Norris, R. P.; Ratzan, W. J.; Freudzon, M.; Mehlmann, L. M.; Krall, J.; Movsesian, M. A.; Wang, H.; Ke, H.; Nikolaev, V. O.; Jaffe, L. A. *Development* **2009**, *136*, 1869.
(299) Nikolaev, V. O.; Gambaryan, S.; Lohse, M. J. *Nat. Methods* **2006**, *3*, 23.
(300) Cawley, S. M.; Sawyer, C. L.; Brunelle, K. F.; van, d., V; Dostmann, W. R. *Cell Signal* **2007**, *19*, 1023.
(301) Russwurm, M.; Mullershausen, F.; Friebe, A.; Jager, R.; Russwurm, C.; Koesling, D. *Biochem. J.* **2007**, *407*, 69.
(302) GAF domains are named for their presence in cGMP-regulated PDEs, some adenylyl cyclases and the bacterial transcription factor, FhlA.
(303) Pearce, L. L.; Gandley, R. E.; Han, W.; Wasserloos, K.; Stitt, M.; Kanai, A. J.; McLaughlin, M. K.; Pitt, B. R.; Levitan, E. S. *Proc. Natl. Acad. Sci. U.S.A.* **2000**, *97*, 477.
(304) St Croix, C. M.; Stitt, M. S.; Leelavanichkul, K.; Wasserloos, K. J.; Pitt, B. R.; Watkins, S. C. *Free Radic. Biol. Med.* **2004**, *37*, 785.
(305) Zhang, L. M.; St Croix, C.; Cao, R.; Wasserloos, K.; Watkins, S. C.; Stevens, T.; Li, S.; Tyurin, V.; Kagan, V. E.; Pitt, B. R. *Exp. Biol. Med. (Maywood)* **2006**, *231*, 1507.
(306) Sato, M.; Ueda, Y.; Takagi, T.; Umezawa, Y. *Nat. Cell Biol.* **2003**, *5*, 1016.
(307) Ananthanarayanan, B.; Ni, Q.; Zhang, J. *Proc. Natl. Acad. Sci. U.S.A.* **2005**, *102*, 15081.
(308) van der, W. J.; Habets, R.; Varnai, P.; Balla, T.; Jalink, K. *J. Biol. Chem.* **2001**, *276*, 15337.
(309) Tanimura, A.; Nezu, A.; Morita, T.; Turner, R. J.; Tojyo, Y. *J. Biol. Chem.* **2004**, *279*, 38095.
(310) Remus, T. P.; Zima, A. V.; Bossuyt, J.; Bare, D. J.; Martin, J. L.; Blatter, L. A.; Bers, D. M.; Mignery, G. A. *J. Biol. Chem.* **2006**, *281*, 608.
(311) Matsu-ura, T.; Michikawa, T.; Inoue, T.; Miyawaki, A.; Yoshida, M.; Mikoshiba, K. *J. Cell Biol.* **2006**, *173*, 755.
(312) van Zeijl, L.; Ponsioen, B.; Giepmans, B. N.; Ariaens, A.; Postma, F. R.; Varnai, P.; Balla, T.; Divecha, N.; Jalink, K.; Moolenaar, W. H. *J. Cell Biol.* **2007**, *177*, 881.
(313) Imamura, H.; Nhat, K. P.; Togawa, H.; Saito, K.; Iino, R.; Kato-Yamada, Y.; Nagai, T.; Noji, H. *Proc. Natl. Acad. Sci. U.S.A.* **2009**, *106*, 15651.
(314) Kato-Yamada, Y.; Yoshida, M. *J. Biol. Chem.* **2003**, *278*, 36013.
(315) Iino, R.; Murakami, T.; Iizuka, S.; Kato-Yamada, Y.; Suzuki, T.; Yoshida, M. *J. Biol. Chem.* **2005**, *280*, 40130.
(316) Yagi, H.; Kajiwara, N.; Tanaka, H.; Tsukihara, T.; Kato-Yamada, Y.; Yoshida, M.; Akutsu, H. *Proc. Natl. Acad. Sci. U.S.A.* **2007**, *104*, 11233.
(317) Fehr, M.; Okumoto, S.; Deuschle, K.; Lager, I.; Looger, L. L.; Persson, J.; Kozhukh, L.; Lalonde, S.; Frommer, W. B. *Biochem. Soc. Trans.* **2005**, *33*, 287.
(318) Deuschle, K.; Okumoto, S.; Fehr, M.; Looger, L. L.; Kozhukh, L.; Frommer, W. B. *Protein Sci.* **2005**, *14*, 2304.
(319) Okumoto, S.; Looger, L. L.; Micheva, K. D.; Reimer, R. J.; Smith, S. J.; Frommer, W. B. *Proc. Natl. Acad. Sci. U.S.A.* **2005**, *102*, 8740.
(320) Tsien, R. Y. *FEBS Lett.* **2005**, *579*, 927.
(321) Hires, S. A.; Zhu, Y.; Tsien, R. Y. *Proc. Natl. Acad. Sci. U.S.A.* **2008**, *105*, 4411.
(322) Nagai, T.; Miyawaki, A. *Biochem. Biophys. Res. Commun.* **2004**, *319*, 72.
(323) Vinkenborg, J. L.; Nicolson, T. J.; Bellomo, E. A.; Koay, M. S.; Rutter, G. A.; Merkx, M. *Nat. Methods* **2009**, *6*, 737.
(324) van Dongen, E. M.; Evers, T. H.; Dekkers, L. M.; Meijer, E. W.; Klomp, L. W.; Merkx, M. *J. Am. Chem. Soc.* **2007**, *129*, 3494.
(325) Dittmer, P. J.; Miranda, J. G.; Gorski, J. A.; Palmer, A. E. *J. Biol. Chem.* **2009**, *284*, 16289.
(326) Hammer, M. M.; Wehrman, T. S.; Blau, H. M. *FASEB J.* **2007**, *21*, 3827.
(327) Lohse, M. J.; Nikolaev, V. O.; Hein, P.; Hoffmann, C.; Vilardaga, J. P.; Bunemann, M. *Trends Pharmacol. Sci.* **2008**, *29*, 159.
(328) Gilman, A. G. *Annu. Rev. Biochem.* **1987**, *56*, 615.
(329) Gether, U. *Endocr. Rev.* **2000**, *21*, 90.
(330) Rochais, F.; Vilardaga, J. P.; Nikolaev, V. O.; Bunemann, M.; Lohse, M. J.; Engelhardt, S. *J. Clin. Invest.* **2007**, *117*, 229.
(331) Vilardaga, J. P.; Bunemann, M.; Krasel, C.; Castro, M.; Lohse, M. J. *Nat. Biotechnol.* **2003**, *21*, 807.
(332) Chachisvilis, M.; Zhang, Y. L.; Frangos, J. A. *Proc. Natl. Acad. Sci. U.S.A.* **2006**, *103*, 15463.
(333) Nikolaev, V. O.; Hoffmann, C.; Bunemann, M.; Lohse, M. J.; Vilardaga, J. P. *J. Biol. Chem.* **2006**, *281*, 24506.
(334) Vilardaga, J. P.; Steinmeyer, R.; Harms, G. S.; Lohse, M. J. *Nat. Chem. Biol.* **2005**, *1*, 25.
(335) Yao, X.; Parnot, C.; Deupi, X.; Ratnala, V. R.; Swaminath, G.; Farrens, D.; Kobilka, B. *Nat. Chem. Biol.* **2006**, *2*, 417.
(336) Hein, P.; Frank, M.; Hoffmann, C.; Lohse, M. J.; Bunemann, M. *EMBO J.* **2005**, *24*, 4106.
(337) Gales, C.; Rebois, R. V.; Hogue, M.; Trieu, P.; Breit, A.; Hebert, T. E.; Bouvier, M. *Nat. Methods* **2005**, *2*, 177.
(338) Gales, C.; Van Durm, J. J.; Schaak, S.; Pontier, S.; Percherancier, Y.; Audet, M.; Paris, H.; Bouvier, M. *Nat. Struct. Mol. Biol.* **2006**, *13*, 778.
(339) Krasel, C.; Vilardaga, J. P.; Bunemann, M.; Lohse, M. J. *Biochem. Soc. Trans.* **2004**, *32*, 1029.
(340) Janetopoulos, C.; Devreotes, P. *Methods* **2002**, *27*, 366.
(341) Hein, P.; Rochais, F.; Hoffmann, C.; Dorsch, S.; Nikolaev, V. O.; Engelhardt, S.; Berlot, C. H.; Lohse, M. J.; Bunemann, M. *J. Biol. Chem.* **2006**, *281*, 33345.
(342) Lohse, M. J.; Bunemann, M.; Hoffmann, C.; Vilardaga, J. P.; Nikolaev, V. O. *Curr. Opin. Pharmacol.* **2007**, *7*, 547.
(343) Chiu, V. K.; Bivona, T.; Hach, A.; Sajous, J. B.; Silletti, J.; Wiener, H.; Johnson, R. L.; Cox, A. D.; Philips, M. R. *Nat. Cell Biol.* **2002**, *4*, 343.
(344) Apolloni, A.; Prior, I. A.; Lindsay, M.; Parton, R. G.; Hancock, J. F. *Mol. Cell. Biol.* **2000**, *20*, 2475.
(345) Choy, E.; Chiu, V. K.; Silletti, J.; Feoktistov, M.; Morimoto, T.; Michaelson, D.; Ivanov, I. E.; Philips, M. R. *Cell* **1999**, *98*, 69.
(346) Mochizuki, N.; Yamashita, S.; Kurokawa, K.; Ohba, Y.; Nagai, T.; Miyawaki, A.; Matsuda, M. *Nature* **2001**, *411*, 1065.
(347) Itoh, R. E.; Kurokawa, K.; Ohba, Y.; Yoshizaki, H.; Mochizuki, N.; Matsuda, M. *Mol. Cell. Biol.* **2002**, *22*, 6582.
(348) Yoshizaki, H.; Ohba, Y.; Kurokawa, K.; Itoh, R. E.; Nakamura, T.; Mochizuki, N.; Nagashima, K.; Matsuda, M. *J. Cell Biol.* **2003**, *162*, 223.
(349) Yoshizaki, H.; Aoki, K.; Nakamura, T.; Matsuda, M. *Biochem. Soc. Trans.* **2006**, *34*, 851.
(350) Pertz, O.; Hodgson, L.; Klemke, R. L.; Hahn, K. M. *Nature* **2006**, *440*, 1069.
(351) Machacek, M.; Hodgson, L.; Welch, C.; Elliott, H.; Pertz, O.; Nalbant, P.; Abell, A.; Johnson, G. L.; Hahn, K. M.; Danuser, G. *Nature* **2009**, *461*, 99.
(352) Fukano, T.; Sawano, A.; Ohba, Y.; Matsuda, M.; Miyawaki, A. *Cell Struct. Funct.* **2007**, *32*, 9.
(353) Johnson, S. A.; Hunter, T. *Nat. Methods* **2005**, *2*, 17.

(354) Fujioka, A.; Terai, K.; Itoh, R. E.; Aoki, K.; Nakamura, T.; Kuroda, S.; Nishida, E.; Matsuda, M. *J. Biol. Chem.* **2006**, *281*, 8917.
(355) Neininger, A.; Thielemann, H.; Gaestel, M. *EMBO Rep.* **2001**, *2*, 703.
(356) Calleja, V.; Alcor, D.; Laguerre, M.; Park, J.; Vojnovic, B.; Hemmings, B. A.; Downward, J.; Parker, P. J.; Larijani, B. *PLoS Biol.* **2007**, *5*, e95.
(357) Chang, L.; Karin, M. *Nature* **2001**, *410*, 37.
(358) Mitra, R. D.; Silva, C. M.; Youvan, D. C. *Gene* **1996**, *173*, 13.
(359) Xu, X.; Gerard, A. L.; Huang, B. C.; Anderson, D. C.; Payan, D. G.; Luo, Y. *Nucleic Acids Res.* **1998**, *26*, 2034.
(360) Wu, X.; Simone, J.; Hewgill, D.; Siegel, R.; Lipsky, P. E.; He, L. *Cytometry A* **2006**, *69*, 477.
(361) Allen, M. D.; Zhang, J. *Angew. Chem., Int. Ed. Engl.* **2008**, *47*, 500.
(362) Ni, Q.; Titov, D. V.; Zhang, J. *Methods* **2006**, *40*, 279.
(363) Zhang, J.; Allen, M. D. *Mol. Biosyst.* **2007**, *3*, 759.
(364) Zhang, J.; Ma, Y.; Taylor, S. S.; Tsien, R. Y. *Proc. Natl. Acad. Sci. U.S.A.* **2001**, *98*, 14997.
(365) Zhang, J.; Hupfeld, C. J.; Taylor, S. S.; Olefsky, J. M.; Tsien, R. Y. *Nature* **2005**, *437*, 569.
(366) Allen, M. D.; Zhang, J. *Biochem. Biophys. Res. Commun.* **2006**, *348*, 716.
(367) Violin, J. D.; Zhang, J.; Tsien, R. Y.; Newton, A. C. *J. Cell Biol.* **2003**, *161*, 899.
(368) Schleifenbaum, A.; Stier, G.; Gasch, A.; Sattler, M.; Schultz, C. *J. Am. Chem. Soc.* **2004**, *126*, 11786.
(369) Johnson, S. A.; You, Z.; Hunter, T. *DNA Repair* **2007**, *6*, 1277.
(370) Kunkel, M. T.; Ni, Q.; Tsien, R. Y.; Zhang, J.; Newton, A. C. *J. Biol. Chem.* **2005**, *280*, 5581.
(371) Sato, M.; Umezawa, Y. *Methods* **2004**, *32*, 451.
(372) Gao, X.; Zhang, J. *Mol. Biol. Cell* **2008**, *19*, 4366.
(373) Ting, A. Y.; Kain, K. H.; Klemke, R. L.; Tsien, R. Y. *Proc. Natl. Acad. Sci. U.S.A.* **2001**, *98*, 15003.
(374) Wang, Y.; Botvinick, E. L.; Zhao, Y.; Berns, M. W.; Usami, S.; Tsien, R. Y.; Chien, S. *Nature* **2005**, *434*, 1040.
(375) Fuller, B. G.; Lampson, M. A.; Foley, E. A.; Rosasco-Nitcher, S.; Le, K. V.; Tobelmann, P.; Brautigan, D. L.; Stukenberg, P. T.; Kapoor, T. M. *Nature* **2008**, *453*, 1132.
(376) Sato, M.; Kawai, Y.; Umezawa, Y. *Anal. Chem.* **2007**, *79*, 2570.
(377) Harvey, C. D.; Ehrhardt, A. G.; Cellurale, C.; Zhong, H.; Yasuda, R.; Davis, R. J.; Svoboda, K. *Proc. Natl. Acad. Sci. U.S.A.* **2008**, *105*, 19264.
(378) Fosbrink, M.; Aye-Han, N. N.; Cheong, R.; Levchenko, A.; Zhang, J. *Proc. Natl. Acad. Sci. U.S.A.* **2010**, *107*, 5459.
(379) Gavet, O.; Pines, J. *Dev. Cell* **2010**, *18*, 533.
(380) Itoh, R. E.; Kurokawa, K.; Fujioka, A.; Sharma, A.; Mayer, B. J.; Matsuda, M. *Exp. Cell Res.* **2005**, *307*, 142.
(381) Offterdinger, M.; Georget, V.; Girod, A.; Bastiaens, P. I. *J. Biol. Chem.* **2004**, *279*, 36972.
(382) Dunn, T. A.; Wang, C. T.; Colicos, M. A.; Zaccolo, M.; DiPilato, L. M.; Zhang, J.; Tsien, R. Y.; Feller, M. B. *J. Neurosci.* **2006**, *26*, 12807.
(383) Newman, R. H.; Zhang, J. *Mol. Biosyst.* **2008**, *4*, 496.
(384) Carrillo, L. D.; Krishnamoorthy, L.; Mahal, L. K. *J. Am. Chem. Soc.* **2006**, *128*, 14768.
(385) Felsenfeld, G.; Groudine, M. *Nature* **2003**, *421*, 448.
(386) Lin, C. W.; Jao, C. Y.; Ting, A. Y. *J. Am. Chem. Soc.* **2004**, *126*, 5982.
(387) Sasaki, K.; Ito, T.; Nishino, N.; Khochbin, S.; Yoshida, M. *Proc. Natl. Acad. Sci. U.S.A.* **2009**, *106*, 16257.
(388) Jones, D. O.; Cowell, I. G.; Singh, P. B. *Bioessays* **2000**, *22*, 124.
(389) Daniel, J. A.; Pray-Grant, M. G.; Grant, P. A. *Cell Cycle* **2005**, *4*, 919.
(390) Pivot-Pajot, C.; Caron, C.; Govin, J.; Vion, A.; Rousseaux, S.; Khochbin, S. *Mol. Cell. Biol.* **2003**, *23*, 5354.
(391) Nakajima, T.; Sato, M.; Akaza, N.; Umezawa, Y. *ACS Chem. Biol.* **2008**, *3*, 352.
(392) Sato, M.; Nakajima, T.; Goto, M.; Umezawa, Y. *Anal. Chem.* **2006**, *78*, 8175.
(393) Sakaue-Sawano, A.; Kurokawa, H.; Morimura, T.; Hanyu, A.; Hama, H.; Osawa, H.; Kashiwagi, S.; Fukami, K.; Miyata, T.; Miyoshi, H.; Imamura, T.; Ogawa, M.; Masai, H.; Miyawaki, A. *Cell* **2008**, *132*, 487.
(394) Sato, M.; Hida, N.; Ozawa, T.; Umezawa, Y. *Anal. Chem.* **2000**, *72*, 5918.
(395) Sasaki, E.; Kojima, H.; Nishimatsu, H.; Urano, Y.; Kikuchi, K.; Hirata, Y.; Nagano, T. *J. Am. Chem. Soc.* **2005**, *127*, 3684.
(396) Chautard, E.; Thierry-Mieg, N.; Ricard-Blum, S. *Pathol. Biol. (Paris)* **2009**, *57*, 324.
(397) Yamada, T.; Bork, P. *Nat. Rev. Mol. Cell Biol.* **2009**, *10*, 791.
(398) Tarassov, K.; Messier, V.; Landry, C. R.; Radinovic, S.; Serna Molina, M. M.; Shames, I.; Malitskaya, Y.; Vogel, J.; Bussey, H.; Michnick, S. W. *Science* **2008**, *320*, 1465.
(399) Bauman, A. L.; Michel, J. J.; Henson, E.; Dodge-Kafka, K. L.; Kapiloff, M. S. *IUBMB Life* **2007**, *59*, 163.
(400) Harwood, N. E.; Batista, F. D. *Immunity* **2008**, *28*, 609.
(401) Wei, N.; Serino, G.; Deng, X. W. *Trends Biochem. Sci.* **2008**, *33*, 592.
(402) Kerppola, T. K. *Methods Cell Biol.* **2008**, *85*, 431.
(403) Piston, D. W.; Kremers, G. J. *Trends Biochem. Sci.* **2007**, *32*, 407.
(404) Pfleger, K. D.; Eidne, K. A. *Nat. Methods* **2006**, *3*, 165.
(405) Ciruela, F. *Curr. Opin. Biotechnol.* **2008**, *19*, 338.
(406) Zal, T. *Adv. Exp. Med. Biol.* **2008**, *640*, 183.
(407) Stryer, L. *Annu. Rev. Biochem.* **1978**, *47*, 819.
(408) Azpiazu, I.; Gautam, N. *J. Biol. Chem.* **2004**, *279*, 27709.
(409) Janetopoulos, C.; Jin, T.; Devreotes, P. *Science* **2001**, *291*, 2408.
(410) Llopis, J.; Westin, S.; Ricote, M.; Wang, Z.; Cho, C. Y.; Kurokawa, R.; Mullen, T. M.; Rose, D. W.; Rosenfeld, M. G.; Tsien, R. Y.; Glass, C. K. *Proc. Natl. Acad. Sci. U.S.A.* **2000**, *97*, 4363.
(411) Uhlik, M. T.; Abell, A. N.; Johnson, N. L.; Sun, W.; Cuevas, B. D.; Lobel-Rice, K. E.; Horne, E. A.; Dell'Acqua, M. L.; Johnson, G. L. *Nat. Cell Biol.* **2003**, *5*, 1104.
(412) Ruehr, M. L.; Zakhary, D. R.; Damron, D. S.; Bond, M. *J. Biol. Chem.* **1999**, *274*, 33092.
(413) Oliveria, S. F.; Gomez, L. L.; Dell'Acqua, M. L. *J. Cell Biol.* **2003**, *160*, 101.
(414) Roberti, M. J.; Bertoncini, C. W.; Klement, R.; Jares-Erijman, E. A.; Jovin, T. M. *Nat. Methods* **2007**, *4*, 345.
(415) Pfleger, K. D.; Eidne, K. A. *Biochem. J.* **2005**, *385*, 625.
(416) Germain-Desprez, D.; Bazinet, M.; Bouvier, M.; Aubry, M. *J. Biol. Chem.* **2003**, *278*, 22367.
(417) Perroy, J.; Pontier, S.; Charest, P. G.; Aubry, M.; Bouvier, M. *Nat. Methods* **2004**, *1*, 203.
(418) Angers, S.; Salahpour, A.; Joly, E.; Hilairet, S.; Chelsky, D.; Dennis, M.; Bouvier, M. *Proc. Natl. Acad. Sci. U.S.A.* **2000**, *97*, 3684.
(419) Milligan, G.; Bouvier, M. *FEBS J.* **2005**, *272*, 2914.
(420) Gales, C.; Rebois, R. V.; Hogue, M.; Trieu, P.; Breit, A.; Hebert, T. E.; Bouvier, M. *Nat. Methods* **2005**, *2*, 177.
(421) Bertrand, L.; Parent, S.; Caron, M.; Legault, M.; Joly, E.; Angers, S.; Bouvier, M.; Brown, M.; Houle, B.; Menard, L. *J. Recept. Signal. Transduct. Res.* **2002**, *22*, 533.
(422) Hamdan, F. F.; Audet, M.; Garneau, P.; Pelletier, J.; Bouvier, M. *J. Biomol. Screen.* **2005**, *10*, 463.
(423) Boute, N.; Jockers, R.; Issad, T. *Trends Pharmacol. Sci.* **2002**, *23*, 351.
(424) Berger, E. A.; Murphy, P. M.; Farber, J. M. *Annu. Rev. Immunol.* **1999**, *17*, 657.
(425) Briz, V.; Poveda, E.; Soriano, V. *J. Antimicrob. Chemother.* **2006**, *57*, 619.
(426) Hoshino, H.; Nakajima, Y.; Ohmiya, Y. *Nat. Methods* **2007**, *4*, 637.
(427) Benton, R.; Sachse, S.; Michnick, S. W.; Vosshall, L. B. *PLoS Biol.* **2006**, *4*, e20.

(428) Saka, Y.; Hagemann, A. I.; Smith, J. C. *Methods* **2008**, *45*, 192.
(429) Chen, B.; Liu, Q.; Ge, Q.; Xie, J.; Wang, Z. W. *Curr. Biol.* **2007**, *17*, 1334.
(430) Shyu, Y. J.; Hiatt, S. M.; Duren, H. M.; Ellis, R. E.; Kerppola, T. K.; Hu, C. D. *Nat. Protoc.* **2008**, *3*, 588.
(431) Ghosh, I.; Hamilton, A. D.; Regan, L. *J. Am. Chem. Soc.* **2000**, *122*, 5658.
(432) Hu, C. D.; Chinenov, Y.; Kerppola, T. K. *Mol. Cell* **2002**, *9*, 789.
(433) Hiatt, S. M.; Shyu, Y. J.; Duren, H. M.; Hu, C. D. *Methods* **2008**, *45*, 185.
(434) Hu, C. D.; Kerppola, T. K. *Nat. Biotechnol.* **2003**, *21*, 539.
(435) Jach, G.; Pesch, M.; Richter, K.; Frings, S.; Uhrig, J. F. *Nat. Methods* **2006**, *3*, 597.
(436) Chu, J.; Zhang, Z.; Zheng, Y.; Yang, J.; Qin, L.; Lu, J.; Huang, Z. L.; Zeng, S.; Luo, Q. *Biosens. Bioelectron.* **2009**, *25*, 234.
(437) Demidov, V. V.; Dokholyan, N. V.; Witte-Hoffmann, C.; Chalasani, P.; Yiu, H. W.; Ding, F.; Yu, Y.; Cantor, C. R.; Broude, N. E. *Proc. Natl. Acad. Sci. U.S.A.* **2006**, *103*, 2052.
(438) Luker, K. E.; Smith, M. C.; Luker, G. D.; Gammon, S. T.; Piwnica-Worms, H.; Piwnica-Worms, D. *Proc. Natl. Acad. Sci. U.S.A.* **2004**, *101*, 12288.
(439) Paulmurugan, R.; Gambhir, S. S. *Anal. Chem.* **2003**, *75*, 1584.
(440) Paulmurugan, R.; Gambhir, S. S. *Anal. Chem.* **2005**, *77*, 1295.
(441) Remy, I.; Michnick, S. W. *Nat. Methods* **2006**, *3*, 977.
(442) Stefan, E.; Aquin, S.; Berger, N.; Landry, C. R.; Nyfeler, B.; Bouvier, M.; Michnick, S. W. *Proc. Natl. Acad. Sci. U.S.A.* **2007**, *104*, 16916.
(443) Luker, K. E.; Gupta, M.; Luker, G. D. *Anal. Chem.* **2008**, *80*, 5565.
(444) Luker, K. E.; Gupta, M.; Luker, G. D. *FASEB J.* **2009**, *23*, 823.
(445) Remy, I.; Michnick, S. W. *Methods* **2004**, *32*, 381.
(446) Remy, I.; Michnick, S. W. *Mol. Cell. Biol.* **2004**, *24*, 1493.
(447) Morell, M.; Espargaro, A.; Aviles, F. X.; Ventura, S. *Nat. Protoc.* **2008**, *3*, 22.
(448) Atkin, S. D.; Patel, S.; Kocharyan, A.; Holtzclaw, L. A.; Weerth, S. H.; Schram, V.; Pickel, J.; Russell, J. T. *J. Neurosci. Methods* **2009**, *181*, 212.
(449) Bozza, T.; McGann, J. P.; Mombaerts, P.; Wachowiak, M. *Neuron* **2004**, *42*, 9.
(450) Diegelmann, S.; Fiala, A.; Leibold, C.; Spall, T.; Buchner, E. *Genesis* **2002**, *34*, 95.
(451) Fiala, A.; Spall, T.; Diegelmann, S.; Eisermann, B.; Sachse, S.; Devaud, J. M.; Buchner, E.; Galizia, C. G. *Curr. Biol.* **2002**, *12*, 1877.
(452) Kamiyama, D.; Chiba, A. *Science* **2009**, *324*, 1338.
(453) Lissandron, V.; Rossetto, M. G.; Erbguth, K.; Fiala, A.; Daga, A.; Zaccolo, M. *Cell Signal* **2007**, *19*, 2296.
(454) Saucerman, J. J.; Zhang, J.; Martin, J. C.; Peng, L. X.; Stenbit, A. E.; Tsien, R. Y.; McCulloch, A. D. *Proc. Natl. Acad. Sci. U.S.A.* **2006**, *103*, 12923.
(455) Neves, S. R.; Tsokas, P.; Sarkar, A.; Grace, E. A.; Rangamani, P.; Taubenfeld, S. M.; Alberini, C. M.; Schaff, J. C.; Blitzer, R. D.; Moraru, I. I.; Iyengar, R. *Cell* **2008**, *133*, 666.
(456) Song, Q.; Saucerman, J. J.; Bossuyt, J.; Bers, D. M. *J. Biol. Chem.* **2008**, *283*, 31531.
(457) Falkenburger, B. H.; Jensen, J. B.; Hille, B. *J. Gen. Physiol.* **2010**, *135*, 81.
(458) Falkenburger, B. H.; Jensen, J. B.; Hille, B. *J. Gen. Physiol.* **2010**, *135*, 99.
(459) Violin, J. D.; DiPilato, L. M.; Yildirim, N.; Elston, T. C.; Zhang, J.; Lefkowitz, R. J. *J. Biol. Chem.* **2008**, *283*, 2949.
(460) Delmas, P.; Brown, D. A. *Nat. Rev. Neurosci.* **2005**, *6*, 850.
(461) Abe, N.; Inoue, T.; Galvez, T.; Klein, L.; Meyer, T. *J. Cell Sci.* **2008**, *121*, 1488.
(462) Airan, R. D.; Thompson, K. R.; Fenno, L. E.; Bernstein, H.; Deisseroth, K. *Nature* **2009**, *458*, 1025.
(463) Fili, N.; Calleja, V.; Woscholski, R.; Parker, P. J.; Larijani, B. *Proc. Natl. Acad. Sci. U.S.A.* **2006**, *103*, 15473.
(464) Inoue, T.; Heo, W. D.; Grimley, J. S.; Wandless, T. J.; Meyer, T. *Nat. Methods* **2005**, *2*, 415.
(465) Levskaya, A.; Weiner, O. D.; Lim, W. A.; Voigt, C. A. *Nature* **2009**, *461*, 997.
(466) Suh, B. C.; Inoue, T.; Meyer, T.; Hille, B. *Science* **2006**, *314*, 1454.
(467) Szobota, S.; Gorostiza, P.; Del Bene, F.; Wyart, C.; Fortin, D. L.; Kolstad, K. D.; Tulyathan, O.; Volgraf, M.; Numano, R.; Aaron, H. L.; Scott, E. K.; Kramer, R. H.; Flannery, J.; Baier, H.; Trauner, D.; Isacoff, E. Y. *Neuron* **2007**, *54*, 535.
(468) Varnai, P.; Toth, B.; Toth, D. J.; Hunyady, L.; Balla, T. *J. Biol. Chem.* **2007**, *282*, 29678.
(469) Volgraf, M.; Gorostiza, P.; Numano, R.; Kramer, R. H.; Isacoff, E. Y.; Trauner, D. *Nat. Chem. Biol.* **2006**, *2*, 47.
(470) Wu, Y. I.; Frey, D.; Lungu, O. I.; Jaehrig, A.; Schlichting, I.; Kuhlman, B.; Hahn, K. M. *Nature* **2009**, *461*, 104.
(471) Gorostiza, P.; Isacoff, E. Y. *Science* **2008**, *322*, 395.
(472) Tomosugi, W.; Matsuda, T.; Tani, T.; Nemoto, T.; Kotera, I.; Saito, K.; Horikawa, K.; Nagai, T. *Nat. Methods* **2009**, *6*, 351.
(473) Patterson, G. H.; Knobel, S. M.; Sharif, W. D.; Kain, S. R.; Piston, D. W. *Biophys. J.* **1997**, *73*, 2782.
(474) Kremers, G. J.; Goedhart, J.; van Munster, E. B.; Gadella, T. W., Jr. *Biochemistry* **2006**, *45*, 6570.
(475) Goedhart, J.; van Weeren, L.; Hink, M. A.; Vischer, N. O.; Jalink, K.; Gadella, T. W., Jr. *Nat. Methods* **2010**, *7*, 137.
(476) Matsuda, T.; Miyawaki, A.; Nagai, T. *Nat. Methods* **2008**, *5*, 339.
(477) Nguyen, A. W.; Daugherty, P. S. *Nat. Biotechnol.* **2005**, *23*, 355.
(478) Xia, N. S.; Luo, W. X.; Zhang, J.; Xie, X. Y.; Yang, H. J.; Li, S. W.; Chen, M.; Ng, M. H. *Mar. Biotechnol. (NY)* **2002**, *4*, 155.
(479) Karasawa, S.; Araki, T.; Nagai, T.; Mizuno, H.; Miyawaki, A. *Biochem. J.* **2004**, *381*, 307.
(480) Shagin, D. A.; Barsova, E. V.; Yanushevich, Y. G.; Fradkov, A. F.; Lukyanov, K. A.; Labas, Y. A.; Semenova, T. N.; Ugalde, J. A.; Meyers, A.; Nunez, J. M.; Widder, E. A.; Lukyanov, S. A.; Matz, M. V. *Mol. Biol. Evol.* **2004**, *21*, 841.
(481) Gurskaya, N. G.; Fradkov, A. F.; Pounkova, N. I.; Staroverov, D. B.; Bulina, M. E.; Yanushevich, Y. G.; Labas, Y. A.; Lukyanov, S.; Lukyanov, K. A. *Biochem. J.* **2003**, *373*, 403.
(482) Karasawa, S.; Araki, T.; Yamamoto-Hino, M.; Miyawaki, A. *J. Biol. Chem.* **2003**, *278*, 34167.
(483) Ai, H. W.; Olenych, S. G.; Wong, P.; Davidson, M. W.; Campbell, R. E. *BMC. Biol.* **2008**, *6*, 13.
(484) Cubitt, A. B.; Woollenweber, L. A.; Heim, R. *Methods Cell Biol.* **1999**, *58*, 19.
(485) Zapata-Hommer, O.; Griesbeck, O. *BMC. Biotechnol.* **2003**, *3*, 5.
(486) Ip, D. T.; Wong, K. B.; Wan, D. C. *Mar. Biotechnol. (NY)* **2007**, *9*, 469.
(487) Bevis, B. J.; Glick, B. S. *Nat. Biotechnol.* **2002**, *20*, 83.
(488) Kredel, S.; Oswald, F.; Nienhaus, K.; Deuschle, K.; Rocker, C.; Wolff, M.; Heilker, R.; Nienhaus, G. U.; Wiedenmann, J. *PLoS One* **2009**, *4*, e4391.
(489) Kredel, S.; Nienhaus, K.; Oswald, F.; Wolff, M.; Ivanchenko, S.; Cymer, F.; Jeromin, A.; Michel, F. J.; Spindler, K. D.; Heilker, R.; Nienhaus, G. U.; Wiedenmann, J. *Chem. Biol.* **2008**, *15*, 224.
(490) Kogure, T.; Karasawa, S.; Araki, T.; Saito, K.; Kinjo, M.; Miyawaki, A. *Nat. Biotechnol.* **2006**, *24*, 577.
(491) Wang, L.; Jackson, W. C.; Steinbach, P. A.; Tsien, R. Y. *Proc. Natl. Acad. Sci. U.S.A.* **2004**, *101*, 16745.
(492) Wang, L.; Tsien, R. Y. *Nat. Protoc.* **2006**, *1*, 1346.
(493) Shkrob, M. A.; Yanushevich, Y. G.; Chudakov, D. M.; Gurskaya, N. G.; Labas, Y. A.; Poponov, S. Y.; Mudrik, N. N.; Lukyanov, S.; Lukyanov, K. A. *Biochem. J.* **2005**, *392*, 649.
(494) Nishioka, T.; Aoki, K.; Hikake, K.; Yoshizaki, H.; Kiyokawa, E.; Matsuda, M. *Mol. Biol. Cell* **2008**, *19*, 4213.

(495) Cicchetti, G.; Biernacki, M.; Farquharson, J.; Allen, P. G. *Biochemistry* **2004**, *43*, 1939.
(496) Nishioka, T.; Frohman, M. A.; Matsuda, M.; Kiyokawa, E. *J. Biol. Chem.* **2010**, *285*, 35979.
(497) Awaji, T.; Hirasawa, A.; Shirakawa, H.; Tsujimoto, G.; Miyazaki, S. *Biochem. Biophys. Res. Commun.* **2001**, *289*, 457.
(498) Truong, K.; Sawano, A.; Mizuno, H.; Hama, H.; Tong, K. I.; Mal, T. K.; Miyawaki, A.; Ikura, M. *Nat. Struct. Biol.* **2001**, *8*, 1069.
(499) Allen, M. D.; DiPilato, L. M.; Rahdar, M.; Ren, Y. R.; Chong, C.; Liu, J. O.; Zhang, J. *ACS Chem. Biol.* **2006**, *1*, 371.
(500) Nikolaev, V. O.; Bunemann, M.; Schmitteckert, E.; Lohse, M. J.; Engelhardt, S. *Circ. Res.* **2006**, *99*, 1084.
(501) Fehr, M.; Lalonde, S.; Lager, I.; Wolff, M. W.; Frommer, W. B. *J. Biol. Chem.* **2003**, *278*, 19127.
(502) Fehr, M.; Frommer, W. B.; Lalonde, S. *Proc. Natl. Acad. Sci. U.S.A.* **2002**, *99*, 9846.
(503) Lager, I.; Fehr, M.; Frommer, W. B.; Lalonde, S. *FEBS Lett.* **2003**, *553*, 85.
(504) Dimitrov, D.; He, Y.; Mutoh, H.; Baker, B. J.; Cohen, L.; Akemann, W.; Knopfel, T. *PLoS One* **2007**, *2*, No. e440.
(505) Kunkel, M. T.; Toker, A.; Tsien, R. Y.; Newton, A. C. *J. Biol. Chem.* **2007**, *282*, 6733.
(506) Depry, C.; Zhang, J. *Current Protocols in Molecular Biology* 2010, 91:18.15.1.
(507) Kawai, Y.; Sato, M.; Umezawa, Y. *Anal. Chem.* **2004**, *76*, 6144.
(508) Kurokawa, K.; Mochizuki, N.; Ohba, Y.; Mizuno, H.; Miyawaki, A.; Matsuda, M. *J. Biol. Chem.* **2001**, *276*, 31305.
(509) Lin, C. W.; Ting, A. Y. *Angew. Chem., Int. Ed. Engl.* **2004**, *43*, 2940.
(510) Ouyang, M.; Lu, S.; Li, X. Y.; Xu, J.; Seong, J.; Giepmans, B. N.; Shyy, J. Y.; Weiss, S. J.; Wang, Y. *J. Biol. Chem.* **2008**, *283*, 17740.
(511) Grashoff, C.; Hoffman, B. D.; Brenner, M. D.; Zhou, R.; Parsons, M.; Yang, M. T.; McLean, M. A.; Sligar, S. G.; Chen, C. S.; Ha, T.; Schwartz, M. A. *Nature* **2010**, *466*, 263.
(512) Meng, F.; Suchyna, T. M.; Sachs, F. *FEBS J.* **2008**, *275*, 3072.
(513) Iwai, S.; Uyeda, T. Q. *Proc. Natl. Acad. Sci. U.S.A.* **2008**, *105*, 16882.
(514) Ni, Q.; Ganesan, A.; Aye-Han, N. N.; Gao, X.; Allen, M. D.; Levchenko, A.; Zhang, J. *Nat. Chem. Biol.* **2011**, *7*, 34.
(515) Shcherbo, D.; Shemiakina, I. I.; Ryabova, A. V.; Luker, K. E.; Schmidt, B. T.; Souslova, E. A.; Gorodnicheva, T. V.; Strukova, L.; Shidlovskiy, K. M.; Britanova, O. V.; Zaraisky, A. G.; Lukyanov, K. A.; Loschenov, V. B.; Luker, G. D.; Chudakov, D. M. *Nat. Methods* **2010**, *7*, 827.
(516) Lin, J. Y. *Exp. Physiol* **96**, *1*, 19.
(517) Zhang, F.; Wang, L. P.; Boyden, E. S.; Deisseroth, K. *Nat. Methods* **2006**, *3*, 785.
(518) Fitzpatrick, J. A. J.; Yan, Q.; Sieber, J. J.; Dyba, M.; Schwarz, U.; Szent-Gyorgyi, C.; Woolford, C. A.; Berget, P. B.; Waggoner, A. S.; Bruchez, M. P. *Bioconjugate Chem.* **2009**, *20*, 1843.